Journal of the Mechanics and Physics of Solids 134 (2020) 103771

Contents lists available at ScienceDirect

Journal of the Mechanics and Physics of Solids

journal homepage: www.elsevier.com/locate/jmps

Interacting charged elastic loops on a sphere

Vikash Chaurasia[a,b], Yi-Chao Chen[b], Eliot Fried[a,*]

[a] Mathematics, Mechanics, and Materials Unit, Okinawa Institute of Science and Technology Graduate University, Onna, Okinawa 904-0495 Japan

[b] Department of Mechanical Engineering, University of Houston, Houston, TX, USA

ARTICLE INFO

Article history:
Received 14 June 2019
Revised 4 October 2019
Accepted 23 October 2019
Available online 24 October 2019

ABSTRACT

A variational approach is used to study the behavior of two closed, inextensible, interacting elastic loops that are constrained to lie on a sphere. In addition to the bending energy of each loop, the total potential energy of the system includes nonlocal contributions that account for intraloop and interloop interactions. Euler–Lagrange equations and energy based stability conditions are derived using the first and second variations of the potential energy functional. As an illustrative application, a problem in which all the interaction potentials are Coulombic and both loops have the same length, bending rigidity, and positive charge density is considered. To ensure the existence of a trivial solution in which the loops are parallel and circular, the length of the loops are taken to be smaller than perimeter of the great circle of the sphere. Detailed bifurcation and linear stability analyses of the trivial solution are conducted. The stability of the trivial solution is governed by three dimensionless parameters a, ζ, and χ, where a is the ratio between of the radius of the loops to radius of the sphere and where ζ and χ encompass information about the ratio of intraloop interaction and interloop interaction to the bending rigidity. While the bending energy and the intraloop interaction energy stabilize the trivial solution, the interloop interaction has a destabilizing influence. Moreover, a cross-over phenomenon associated with the nature of the most destabilizing mode is discovered: for $0 < a < a_c$, the number of modes represented in the most destabilizing modes varies with ζ and χ; for $a_c < a < 1$, the most destabilizing mode is always the lowest mode in keeping with results for problems involving only bending energy.

1. Introduction

The adsorption of polyelectrolytes on oppositely charged curved surfaces is of central importance in colloidal science and biophysics. Sukhorukov et al. (1998) synthesized thin organic films by the stepwise deposition of polyelectrolyte chains on dissolvable spherical cores. Shells that remain after core dissolution have been used as containers for macromolecules, microcarriers, and microreactors. Hoogeveen et al. (1996) found that the charge density on the polyelectrolytes and the ionic strength of the surrounding medium are the primary factors in deciding the stability of multi-polyelectrolyte chain

* Corresponding author.
E-mail address: eliot.fried@oist.jp (E. Fried).

https://doi.org/10.1016/j.jmps.2019.103771

structures. A more detailed theoretical framework is needed to gain further insight into the various factors governing the shape and stability of these chains.

In biological structures like eukaryotic cells, it is widely agreed that the negatively charged DNA wraps around the positively charged histone-octamer (Nelson et al., 2008, Chapter 24). These complexes of DNA with histone proteins act as fundamental building blocks for the compactification of genetic material in chromatin (Khrapunov et al., 1997; Luger et al., 1997; Schiessel, 2003). Similar observations apply in the context of reverse cholesterol transport (RCT), a process during which high-density lipoprotein (HDL) particles scavenge cholesterol from the blood stream. In the late stage of this process, HDL particles adopt spheroidal shapes, with surfaces constituted by lipid headgroups. Huang et al. (2011); Silva et al. (2008, 2007), Mei and Atkinson (2011), and Gursky (2013) studied the crystal structure of thread-like peptides called apolipoprotein on the surface of HDL particles. Their work shows that multiple peptides wrap around the surfaces of HDL particles in various configurations. In type-2 diabetes, elevated levels of glucose cause glycosylation (Hermo et al., 2005; Khovidhunkit et al., 2004; Kontush and Chapman, 2008; O'Brien and Chait, 2006) of apo A-I proteins, profoundly modifying their conformation on the HDL surface. Hoang et al. (2007) adjudge that these modifications alter the functionality of HDL by about 70% in comparison to normal HDL.

Processes in which a single charged polymer is adsorbed onto a curved surface occur in a wide variety of applications and have been studied extensively. von Goeler and Muthukumar (1994) combined a variational procedure with a ground state dominance approximation to probe the adsorption of single polyelectrolytes on cylindrical and spherical surfaces. In their unified description for adsorption of polyelectrolyte chains onto planar and curved surfaces, Cherstvy and Winkler (2011) highlighted the role of surface curvature on scaling laws for adsorption. Comprensive lists of the theoretical literature on this topic appear in the review articles by Netz and Andelman (2003), Dobrynin and Rubinstein (2005), and Messina (2009). Monte-Carlo simulations conducted by Kong and Muthukumar (1998) confirm the theoretical predictions of scaling laws of adsorption. Results from other simulations are summarized in the review article by Messina et al. (2004). Cherstvy and Winkler (2004, 2005) investigated the adsorption of DNA molecules on cylindrical and spherical surfaces, considering the influence of the charged density of the DNA, the surface charge density of the curved surface, and the salt concentration of the suspending solution on wrapping and unwrapping transitions.

The majority of the existing literature on polyelectrolyte adsorption focuses on single chains because intrachain interactions dominate interchain interactions in most systems of importance (Dobrynin and Rubinstein, 2005). However, there is a growing interest in methods for fabricating coated nanoparticles and polyelectrolyte shells by the sequential deposition of polyelectrolyte chains on tailored surfaces. Decher and Hong (1991), Decher et al. (1992), Decher et al. (1994) and Decher (1997) devised techniques of depositing alternate layers of opposite charged polyelectrolytes on flat support. Caruso et al. (1998) and Gittins and Caruso (2001) fabricated polyelectrolyte shells by depositing the polyelectrolytes on dissolvable spherical core. Messina et al. (2003) used Monte–Carlo simulation to investigate the equilibrium structures arising from adsorption of multiple polyelectrolyte chains on a sphere but in so doing accounted only for electronic contributions to the energetics of the system. To our knowledge, the interactions between two or more polyelectrolytes that possess bending stiffness and are adsorbed on a single curved surface have not yet been studied.

In the present work, we consider a system consisting of two semiflexible, charged loops that are constrained to lie on a sphere. A polymer is semiflexible if its persistence length substantially exceeds the length of its constituent monomers. For such polymers, the energetics of bending decouples from the minutiae of the chemical structure and can thus be described to good accuracy by a continuum-level elastic model. The literature contains many relevant theoretical works on elastic curves constrained to spheres. In a pioneering work, Langer and Singer (1984) used a variational approach to study the shape of a closed, inextensible loop restricted to a spherical surface. They considered a simple model in which the bending energy per unit length of the loop is proportional to the square of its curvature. Working with a generalization of that energy, Arroyo et al. (2003, 2004, 2006, 2010) analyzed the existence and stability of curves on a spherical surface and determined the conditions under which an open curve closes into a loop.

In an effort to model a DNA molecule that exhibits non-local, long-range interactions between its base pairs, Biton et al. (2007) explored the three-dimensional equilibrium configurations of a electrically charged curve endowed with bending stiffness. They developed a numerical method that deals effectively with the full Jacobian of the equilibrium configuration that stems from the nonlocal intraloop interaction energy of the system. Hoffman and Manning (2009) studied the equilibrium shape and stability of an open curve that is constrained to lie in a plane an is endowed with bending stiffness and repulsive intraloop interaction energy, focusing on the challenges related to the singularity that is generated by the intraloop interaction energy of the curve.

The simplest mathematical expression for the intraloop interaction energy of a closed loop of length L with distributed charge density ρ and arclength parameterized position vector $\boldsymbol{r}$ is proportional, by Coulomb's constant, to the divergent double integral

$$\frac{1}{2}\int_0^L\int_0^L \frac{\rho(s)\rho(\bar{s})\,\mathrm{d}s\,\mathrm{d}\bar{s}}{|\boldsymbol{r}(s)-\boldsymbol{r}(\bar{s})|}. \tag{1}$$

Renormalization techniques have been used to circumvent the divergence. Fukuhara (1988) considered a discretized version of (1) that is bounded. Joan and Lomonaco (1983) replaced the distance $|\boldsymbol{r}(s)-\boldsymbol{r}(\bar{s})|$ in the denominator of the integrand in (1) by $|\boldsymbol{r}(s)-\boldsymbol{r}(\bar{s})|+\epsilon$, with $\epsilon>0$, to obtain a finite intraloop interaction energy. Other regularization approaches include subtracting from (1) an equally divergent term or multiplying the integrand of (1) by a factor that decays sufficiently rapidly

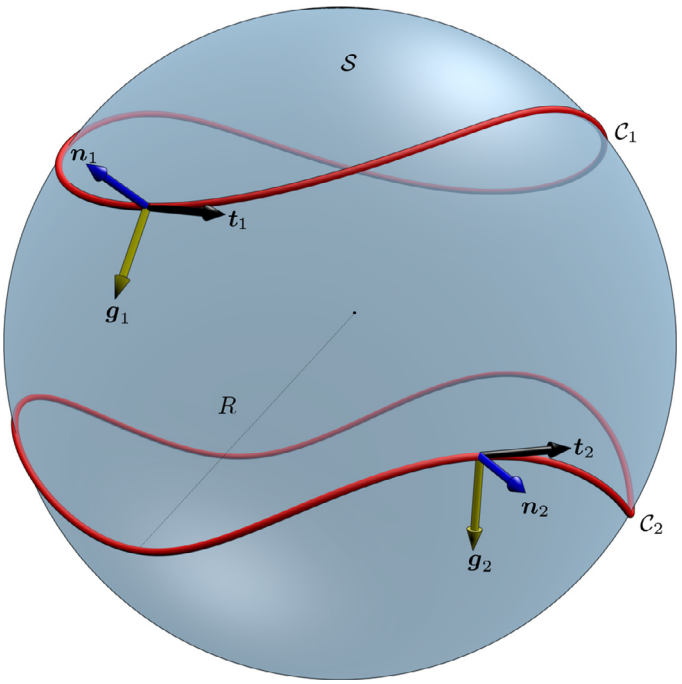

Fig. 1. Schematic of two inextensible loops (closed) $\mathcal{C}_1$ and $\mathcal{C}_2$ confined to a sphere $\mathcal{S}$ of radius R. Moving frames $\{\boldsymbol{t}_1, \boldsymbol{n}_1, \boldsymbol{g}_1\}$ of $\mathcal{C}_1$ and $\{\boldsymbol{t}_2, \boldsymbol{n}_2, \boldsymbol{g}_2\}$ of $\mathcal{C}_2$ are also depicted, where $\boldsymbol{n}_1$ and $\boldsymbol{n}_2$ are restriction of $\mathcal{C}_1$ and $\mathcal{C}_2$ to $\mathcal{S}$, $\boldsymbol{t}_1$ and $\boldsymbol{t}_2$ are unit tangents defined by $(8)_1$, and $\boldsymbol{g}_1$ and $\boldsymbol{g}_2$ are unit tangent-normal defined by $(8)_2$.

as $\bar{s} \to s$. In a series of papers, O'Hara (1991, 1992, 1994) used the subtractive approach to calculate the intraloop interaction energy of charged knots. Kusner and Sullivan (1994) used a multiplicative factor to regularize the inverse power-law that governs the intraloop interaction energy of a charged Möbius band. Hoffman and Manning (2009) used a mollifier with decay such that the intraloop interaction energy of a charged rod is regularized up the second variation of the energy functional.

Building on the works mentioned above, we present a variational framework for studying the interaction between two charged loops that are constrained to a sphere (Fig. 1). We restrict attention to inextensible loops. Moreover, for simplicity, we follow Langer and Singer (1984) by assuming that the bending energy density of each loop is proportional to the square of its curvature. We limit our study to situations in which the intraloop and interloop interaction energies of the loops are repulsive. Moreover, we use the multiplicative approach to regularize the intraloop interaction energy of the curves. On the basis of these simplifying assumptions, we explore the competition between bending resistance and repulsive interactions, in conjunction with the geometric constraints, to determine energetically preferred equilibrium configurations, the goal being to explain how these various effects influence the stability of equilibrium configurations and thereby provide insight on the equilibrium phenomena that occur subsequent to adsorption of polyelectrolyte on the curved surface. Although we do not study the equilibrium shape of a single charged polyelectrolyte deposited on a sphere, our framework can also be applied to such problems.

The remainder of the paper is organized as follows. The necessary geometrical quantities, notation, and assumptions are introduced in Section 2. The first and second variation conditions expressing the energy stability criterion are presented in Section 2.4. The framework developed in Section 2.4 is applied, in Section 3, to characterize the interaction of two uniformly charged loops that have the same length and material parameters. The trivial solution to that special problem is presented in Section 3.4. A stability condition for the trivial solution is identified in Section 3.5 and associated bifurcations are studied in Section 3.8. Explanation of how the geometric and material parameters effect the stability of the trivial solution are provided in Section 3.5. A synopsis of our findings appears in Section 4. For completeness, Section Appendix A contains detailed accounts of the calculations for the first and second variation conditions that underpin our analysis. Calculations leading to the second variation condition and the linear bifurcation analysis for the specialized problem that is described in Section 3 are collected in Appendix B and Appendix C, respectively.

2. Preliminaries

Consider (closed) inextensible loops $\mathcal{C}_1$ and $\mathcal{C}_2$ of respective lengths $L_1 = R\ell_1 > 0$ and $L_2 = R\ell_2 > 0$ confined to a sphere $\mathcal{S}$ of radius $R > 0$, as illustrated in Fig. 1. We suppose that each loop is endowed with a bending energy with density proportional to the square of its curvature and with a intraloop interaction energy with density dependent on the distance

between pairs of its points. Additionally, we assume that interactions between the loops are characterized by an energy with density dependent on the distance between pairs of their points.

2.1. Kinematics

Without loss of generality, we place the origin at the center of the sphere $\mathcal{S}$ and parameterize each loop $\mathcal{C}_i$ by

$$\mathcal{C}_i = \{\boldsymbol{r} : \boldsymbol{r} = R\boldsymbol{n}_i(s), 0 \le s \le \ell_i\}, \tag{2}$$

where s represents (dimensionless) arclength on $\mathcal{C}_i$, $i = 1, 2$, and $\boldsymbol{n}_i$ is normal to $\mathcal{S}$, directed away from the origin, and three-times continuously differentiable. As consequences of this smoothness assumption, we have the closure conditions

$$\boldsymbol{n}_i(0) = \boldsymbol{n}_i(\ell_i), \qquad \boldsymbol{n}_i'(0) = \boldsymbol{n}_i'(\ell_i), \qquad \boldsymbol{n}_i''(0) = \boldsymbol{n}_i''(\ell_i), \qquad \text{and} \qquad \boldsymbol{n}_i'''(0) = \boldsymbol{n}_i'''(\ell_i), \tag{3}$$

where a prime denotes differentiation with respect to s on $\mathcal{C}_i$, $i = 1, 2$. To ensure that each loop $\mathcal{C}_i$, $i = 1, 2$, conforms to $\mathcal{S}$ and is inextensible, we stipulate that

$$|\boldsymbol{n}_i| = 1 \qquad \text{and} \qquad |\boldsymbol{n}_i'| = 1. \tag{4}$$

From (2), the vector curvature $\boldsymbol{\kappa}_i$ of each loop $\mathcal{C}_i$, $i = 1, 2$, is given by

$$\boldsymbol{\kappa}_i = \frac{1}{R}\boldsymbol{n}_i''. \tag{5}$$

It is convenient to decompose the vector curvatures into geodesic and normal components. To achieve this, we adopt the convention that the curvature of $\mathcal{S}$ is negative, in which case each loop $\mathcal{C}_i$, $i = 1, 2$, has normal curvature $-1/R$ and its vector curvature $\boldsymbol{\kappa}_i$ can be expressed as

$$\boldsymbol{\kappa}_i = \frac{1}{R}(\mathbf{1} - \boldsymbol{n}_i \otimes \boldsymbol{n}_i)\boldsymbol{n}_i'' - \frac{\boldsymbol{n}_i}{R}, \tag{6}$$

where $\mathbf{1}$ denotes the identity tensor and the tensor product $\boldsymbol{a}\otimes\boldsymbol{b}$ of two vectors $\boldsymbol{a}$ and $\boldsymbol{b}$ is defined such that $(\boldsymbol{a} \otimes \boldsymbol{b})\boldsymbol{c} = (\boldsymbol{b} \cdot \boldsymbol{c})\boldsymbol{a}$ for any vector $\boldsymbol{c}$. Differentiating $(4)_1$ with respect to arclength, we see that on $\mathcal{C}_i$, $i = 1, 2$,

$$\boldsymbol{n}_i' \cdot \boldsymbol{n}_i = 0. \tag{7}$$

By (4) and (7), the triad $\{\boldsymbol{n}_i', \boldsymbol{n}_i, \boldsymbol{n}_i' \times \boldsymbol{n}_i\}$ provides an orthonormal basis — its Darboux frame — on $\mathcal{C}_i$, $i = 1, 2$. Defining $\boldsymbol{t}_i$ and $\boldsymbol{g}_i$ on $\mathcal{C}_i$, $i = 1, 2$, by

$$\boldsymbol{t}_i = \boldsymbol{n}_i' \qquad \text{and} \qquad \boldsymbol{g}_i = \boldsymbol{t}_i \times \boldsymbol{n}_i, \tag{8}$$

we thus recognize from (6) that $\boldsymbol{t}_i'$ can be expressed as

$$\boldsymbol{t}_i' = \boldsymbol{n}_i'' = -\boldsymbol{n}_i - k_i\boldsymbol{g}_i, \tag{9}$$

where k_i determined according to

$$k_i = -\boldsymbol{n}_i'' \cdot \boldsymbol{g}_i = -\boldsymbol{t}_i' \cdot \boldsymbol{g}_i = \boldsymbol{g}_i' \cdot \boldsymbol{t}_i \tag{10}$$

is the dimensionless geodesic curvature of $\mathcal{C}_i$, $i = 1, 2$. Additionally, since $\boldsymbol{g}_i \cdot \boldsymbol{t}_i = 0$ on $\mathcal{C}_i$, $i = 1, 2$, we see from (10) that

$$\boldsymbol{g}_i' = k_i\boldsymbol{t}_i. \tag{11}$$

Since $\boldsymbol{g}_i' \cdot \boldsymbol{n}_i = (\boldsymbol{g}_i \cdot \boldsymbol{n}_i)' - \boldsymbol{g}_i \cdot \boldsymbol{n}_i' = \boldsymbol{g}_i \cdot \boldsymbol{t}_i = 0$ and the geodesic torsion of $\mathcal{C}_i$, $i = 1, 2$, is $\boldsymbol{g}_i' \cdot \boldsymbol{n}_i/R$, (11) is consistent with the established fact that the geodesic torsion of a curve on a sphere must vanish. When augmented by given choices $\boldsymbol{t}_i(0)$, $\boldsymbol{n}_i(0)$, and $\boldsymbol{g}_i(0)$ of $\boldsymbol{t}_i$, $\boldsymbol{n}_i$, and $\boldsymbol{g}_i$, we may integrate the first-order system of differential equations

$$\boldsymbol{t}_i' = -k_i\boldsymbol{g}_i - \boldsymbol{n}_i, \qquad \boldsymbol{n}_i' = \boldsymbol{t}_i, \qquad \boldsymbol{g}_i' = k_i\boldsymbol{t}_i, \tag{12}$$

to uniquely determine $\mathcal{C}_i$, $i = 1, 2$, on $\mathcal{S}$.

2.2. Energetics

We assume that the total energy $\mathcal{E}$ of the system consisting of the loops $\mathcal{C}_1$ and $\mathcal{C}_2$ can be expressed as a sum,

$$\mathcal{E} = \mathcal{E}_{\mathrm{B}} + \mathcal{E}_{\mathrm{S}} + \mathcal{E}_{\mathrm{I}}, \tag{13}$$

of contributions $\mathcal{E}_{\mathrm{B}}$, $\mathcal{E}_{\mathrm{S}}$, and $\mathcal{E}_{\mathrm{I}}$ that account respectively for bending energy, intraloop interaction energy, and interloop interaction energy. For simplicity, we stipulate that the extent to which $\mathcal{C}_i$, $i = 1, 2$, resists bending is characterized by a single constant bending modulus $\mu_i > 0$, so that $\mathcal{E}_{\mathrm{B}}$ has the particular form

$$\mathcal{E}_{\mathrm{B}}[\boldsymbol{n}_1, \boldsymbol{n}_2] = \frac{\mu_1 R}{2}\int_0^{\ell_1} |\boldsymbol{\kappa}_1(s)|^2 \,\mathrm{d}s + \frac{\mu_2 R}{2}\int_0^{\ell_2} |\boldsymbol{\kappa}_2(s)|^2 \,\mathrm{d}s. \tag{14}$$

It is natural to decompose $\mathcal{E}_{\mathrm{B}}$ into terms associated with the geodesic and normal components of the vector curvature $\boldsymbol{\kappa}_i$ of each loop $\mathcal{C}_i$, $i = 1, 2$. With reference to (6) and (9), this leads to the representation

$$\begin{aligned}\mathcal{E}_{\mathrm{B}}[\boldsymbol{n}_1, \boldsymbol{n}_2] &= \frac{\mu_1 R}{2}\int_0^{\ell_1}\left|\boldsymbol{\kappa}_1(s) + \frac{1}{R}\boldsymbol{n}_1(s)\right|^2 \mathrm{d}s + \frac{\mu_2 R}{2}\int_0^{\ell_2}\left|\boldsymbol{\kappa}_2(s) + \frac{1}{R}\boldsymbol{n}_2(s)\right|^2 \mathrm{d}s - \frac{\mu_1\ell_1 + \mu_2\ell_2}{2R}\\ &= \frac{\mu_1}{2R}\int_0^{\ell_1} k_1^2(s)\,\mathrm{d}s + \frac{\mu_2}{2R}\int_0^{\ell_2} k_2^2(s)\,\mathrm{d}s - \frac{\mu_1\ell_1 + \mu_2\ell_2}{2R},\end{aligned} \tag{15}$$

where the term $-(\mu_1\ell_1 + \mu_2\ell_2)/2R$, being a constant, is of no consequence. Furthermore, we stipulate that $\mathcal{E}_{\mathrm{S}}$ has the form

$$\mathcal{E}_{\mathrm{S}}[\boldsymbol{n}_1, \boldsymbol{n}_2] = \frac{A_{11}R^2}{2}\int_0^{\ell_1}\int_0^{\ell_1} f_{11}(|\boldsymbol{n}_1(s) - \boldsymbol{n}_1(\bar{s})|)\,\mathrm{d}\bar{s}\,\mathrm{d}s + \frac{A_{22}R^2}{2}\int_0^{\ell_2}\int_0^{\ell_2} f_{22}(|\boldsymbol{n}_2(s) - \boldsymbol{n}_2(\bar{s})|)\,\mathrm{d}\bar{s}\,\mathrm{d}s, \tag{16}$$

and that $\mathcal{E}_{\mathrm{I}}$ has the form

$$\mathcal{E}_{\mathrm{I}}[\boldsymbol{n}_1, \boldsymbol{n}_2] = \frac{A_{12}R^2}{2}\int_0^{\ell_1}\int_0^{\ell_2} f_{12}(|\boldsymbol{n}_1(s) - \boldsymbol{n}_2(\bar{s})|)\,\mathrm{d}\bar{s}\,\mathrm{d}s, \tag{17}$$

where $A_{11} \geq 0$, $A_{22} \geq 0$, and $A_{12} \geq 0$ are constants with dimensions of energy per unit area, f_{ii} is the dimensionless intraloop interaction energy density for loop $i = 1, 2$ and f_{12} is the dimensionless interloop interaction energy density between the loops. For brevity, we refer to f_{ii}, $i = 1, 2$, as the intraloop potentials and to f_{12} as the interloop potential. These potentials may also depend explicitly on s and $\bar{s}$ (through, for instance, the difference $|s - \bar{s}|$, as would be the case, for example, if the loops were not charged uniformly. However, we suppress any such dependence until further notice.

Our focus is on situations where the intraloop and interloop interaction potentials are repulsive. Consistent with this, we restrict attention to configurations of the system in which contact between the points of a single loop or between points of the two loops cannot occur. This obviates any need to introduce unilateral constraints that would otherwise be necessary to eliminate the passage of either loop through itself or of one loop through the other.

2.3. Dimensionless parameters

We choose a scaling in which lengths are measured relative to the radius R of the sphere $\mathcal{S}$ to which the loops $\mathcal{C}_1$ and $\mathcal{C}_2$ are confined and energies are measured relative to the bending energy μ_1/R that would be stored in $\mathcal{C}_1$ if it were of length $2\pi R$ and coincident with a great circle of $\mathcal{S}$. On this basis, we identify two dimensionless measures,

$$\ell_1 = \frac{L_1}{R} > 0 \qquad \text{and} \qquad \ell_2 = \frac{L_2}{R} > 0, \tag{18}$$

of the length and four dimensionless measures,

$$\nu = \frac{\mu_2}{\mu_1} > 0, \qquad \zeta_1 = \frac{A_{11}R^3}{\mu_1} \geq 0, \qquad \zeta_2 = \frac{A_{22}R^3}{\mu_1} \geq 0, \qquad \text{and} \qquad \chi = \frac{A_{12}R^3}{\mu_1} \geq 0, \tag{19}$$

of energy. Moreover, we define the dimensionless total energy $\mathcal{F}$ of the system of two loops $\mathcal{C}_1$ and $\mathcal{C}_2$ by

$$\mathcal{F} = \frac{R\mathcal{E}}{\mu_1} = \mathcal{F}_{\mathrm{B}} + \mathcal{F}_{\mathrm{S}} + \mathcal{F}_{\mathrm{I}}, \tag{20}$$

where the dimensionless counterparts, $\mathcal{F}_{\mathrm{B}}$, $\mathcal{F}_{\mathrm{S}}$, and $\mathcal{F}_{\mathrm{I}}$, of the bending energy, intraloop interaction energy, and interloop interaction energy are

$$\mathcal{F}_{\mathrm{B}}[\boldsymbol{n}_1, \boldsymbol{n}_2] = \frac{1}{2}\int_0^{\ell_1} k_1^2\,\mathrm{d}s + \frac{\nu}{2}\int_0^{\ell_2} k_2^2\,\mathrm{d}s, \tag{21a}$$

$$\mathcal{F}_{\mathrm{S}}[\boldsymbol{n}_1, \boldsymbol{n}_2] = \frac{\zeta_1}{2}\int_0^{\ell_1}\int_0^{\ell_1} f_{11}(|\boldsymbol{n}_1(s) - \boldsymbol{n}_1(\bar{s})|)\,\mathrm{d}\bar{s}\,\mathrm{d}s + \frac{\zeta_2}{2}\int_0^{\ell_2}\int_0^{\ell_2} f_{22}(|\boldsymbol{n}_2(s) - \boldsymbol{n}_2(\bar{s})|)\,\mathrm{d}\bar{s}\,\mathrm{d}s, \tag{21b}$$

and

$$\mathcal{F}_{\mathrm{I}}[\boldsymbol{n}_1, \boldsymbol{n}_2] = \frac{\chi}{2}\int_0^{\ell_1}\int_0^{\ell_2} f_{12}(|\boldsymbol{n}_1(s) - \boldsymbol{n}_2(\bar{s})|)\,\mathrm{d}\bar{s}\,\mathrm{d}s. \tag{21c}$$

2.4. First and second variation conditions

Following the classical presentations of elastic stability theory provided by Timoshenko and Gere (1962), Ericksen (1966), and Koiter (1970), we focus on obtaining equilibrium configurations of $\mathcal{C}_1$ and $\mathcal{C}_2$, as characterized by $\boldsymbol{n}_1$ and $\boldsymbol{n}_2$, that are stable in the sense that the first variation condition

$$\delta\mathcal{F}[\boldsymbol{n}_1, \boldsymbol{n}_2](\boldsymbol{u}_1, \boldsymbol{u}_2) = 0 \tag{22}$$

and the second variation condition

$$\delta^2\mathcal{F}[\boldsymbol{n}_1,\boldsymbol{n}_2](\boldsymbol{u}_1,\boldsymbol{u}_2)\geq 0, \tag{23}$$

are both required to hold for all variations $\boldsymbol{u}_1=\delta\boldsymbol{n}_1$ and $\boldsymbol{u}_2=\delta\boldsymbol{n}_2$ of $\boldsymbol{n}_1$ and $\boldsymbol{n}_2$ that, consistent with the constraints (4), satisfy

$$\boldsymbol{n}_i\cdot\boldsymbol{u}_i=0 \qquad \text{and} \qquad \boldsymbol{n}_i'\cdot\boldsymbol{u}_i'=0, \qquad i=1,2. \tag{24}$$

In so doing, we assume that the variation $\boldsymbol{u}_i$ depends periodically on arclength on $\mathcal{C}_i$, $i=1,2$. Moreover, we emphasize that $\boldsymbol{n}_1$ and $\boldsymbol{n}_2$ in (23) must satisfy (22).

In Appendix A, we show that the first variation condition (22) yields coupled Euler–Lagrange equations for $\boldsymbol{n}_1$ and $\boldsymbol{n}_2$ of the form

$$\left.\begin{aligned}(\boldsymbol{n}_1'''+\lambda_1\boldsymbol{n}_1')'+\Lambda_1\boldsymbol{n}_1&=\zeta_1\boldsymbol{\varphi}_{11}[\boldsymbol{n}_1,\boldsymbol{n}_1]+\chi\boldsymbol{\varphi}_{12}[\boldsymbol{n}_1,\boldsymbol{n}_2],\\ \nu(\boldsymbol{n}_2'''+\lambda_2\boldsymbol{n}_2')'+\Lambda_2\boldsymbol{n}_2&=\zeta_2\boldsymbol{\varphi}_{22}[\boldsymbol{n}_2,\boldsymbol{n}_2]+\chi\boldsymbol{\varphi}_{21}[\boldsymbol{n}_2,\boldsymbol{n}_1],\end{aligned}\right\} \tag{25}$$

where $\boldsymbol{\varphi}_{11}$, $\boldsymbol{\varphi}_{12}$, $\boldsymbol{\varphi}_{21}$, and $\boldsymbol{\varphi}_{22}$ are defined through

$$\boldsymbol{\varphi}_{ij}[\boldsymbol{n}_i,\boldsymbol{n}_j]=-\int_0^{\ell_j}\boldsymbol{f}_{ij}(\boldsymbol{n}_i-\boldsymbol{n}_j(\bar{s}))\,\mathrm{d}\bar{s}, \qquad i,j=1,2, \tag{26}$$

with

$$\boldsymbol{f}_{ij}(\boldsymbol{\varrho})=\frac{\mathrm{d}f_{ij}(\varrho)}{\mathrm{d}\varrho}\Big|_{\varrho=|\boldsymbol{\varrho}|}\frac{\boldsymbol{\varrho}}{|\boldsymbol{\varrho}|}, \qquad f_{21}=f_{12}, \tag{27}$$

and where Λ_i and λ_i are Lagrange multiplier fields needed to maintain $(4)_1$ and $(4)_2$. Whereas $(25)_1$ holds on $\mathcal{C}_1$, $(25)_2$ holds on $\mathcal{C}_2$.

For $i=1,2$, $-\zeta_i\boldsymbol{\varphi}_{ii}$ is the (dimensionless) force acting on the element $\mathrm{d}s$ of $\mathcal{C}_i$ at arclength s against repulsion by all the remaining elements of $\mathcal{C}_i$. Similarly, for $i,j=1,2$ but $i\neq j$, $-\chi\boldsymbol{\varphi}_{ij}$ is the (dimensionless) force acting on the element $\mathrm{d}s$ of $\mathcal{C}_i$ at arclength s against repulsion by all the remaining elements of $\mathcal{C}_j$. For $i=1,2$, we refer to $-(\lambda_i\boldsymbol{n}_i''+\lambda_i'\boldsymbol{n}_i')$ as the dimensionless reactive tension that acts to prevent elongation or contraction of $\mathcal{C}_i$. Also, for $i=1,2$, we refer to $-\Lambda\boldsymbol{n}_i$ as the dimensionless adhesive reaction which serves to ensure that $\mathcal{C}_i$ remains in contact with $\mathcal{S}$. Precedents for modeling adhesion through the introduction of Lagrange multipliers appear in the works of Guven and Vázquez-Montejo (2012), Guven et al. (2014), and Bischofs et al. (2009).

In Appendix A, we also show that the second variation condition (23) takes the form

$$\begin{aligned}&\int_0^{\ell_1}(|\boldsymbol{u}_1''|^2-\lambda_1|\boldsymbol{u}_1'|^2+(\lambda_1'\boldsymbol{u}_1'+\Lambda_1\boldsymbol{u}_1-\zeta_1\boldsymbol{\vartheta}_{11}[\boldsymbol{n}_1,\boldsymbol{n}_1](\boldsymbol{u}_1,\boldsymbol{u}_1)-\chi\boldsymbol{\vartheta}_{12}[\boldsymbol{n}_1,\boldsymbol{n}_2](\boldsymbol{u}_1,\boldsymbol{u}_2))\cdot\boldsymbol{u}_1)\,\mathrm{d}s\\ &+\int_0^{\ell_2}(\nu(|\boldsymbol{u}_2''|^2-\lambda_2|\boldsymbol{u}_2'|^2)+(\nu\lambda_2'\boldsymbol{u}_2'+\Lambda_2\boldsymbol{u}_2-\zeta_2\boldsymbol{\vartheta}_{22}[\boldsymbol{n}_2,\boldsymbol{n}_2](\boldsymbol{u}_2,\boldsymbol{u}_2)-\chi\boldsymbol{\vartheta}_{21}[\boldsymbol{n}_2,\boldsymbol{n}_1](\boldsymbol{u}_2,\boldsymbol{u}_1))\cdot\boldsymbol{u}_2)\,\mathrm{d}s\geq 0,\end{aligned} \tag{28}$$

where $\boldsymbol{\vartheta}_{11}$, $\boldsymbol{\vartheta}_{12}$, $\boldsymbol{\vartheta}_{21}$, and $\boldsymbol{\vartheta}_{22}$ are defined according to

$$\boldsymbol{\vartheta}_{ij}[\boldsymbol{n}_i,\boldsymbol{n}_j](\boldsymbol{u}_i,\boldsymbol{u}_j)=-\int_0^{\ell_j}\boldsymbol{F}_{ij}(\boldsymbol{n}_i-\boldsymbol{n}_j(\bar{s}))(\boldsymbol{u}_i-\boldsymbol{u}_j(\bar{s}))\,\mathrm{d}\bar{s}, \qquad i,j=1,2, \tag{29}$$

with

$$\boldsymbol{F}_{ij}(\boldsymbol{\varrho})=\frac{1}{\varrho}\Big(\frac{\mathrm{d}f_{ij}(\varrho)}{\mathrm{d}\varrho}\mathbf{1}+\frac{\mathrm{d}}{\mathrm{d}\varrho}\Big(\frac{1}{\varrho}\frac{\mathrm{d}f_{ij}(\varrho)}{\mathrm{d}\varrho}\Big)\boldsymbol{\varrho}\otimes\boldsymbol{\varrho}\Big)\Big|_{\varrho=|\boldsymbol{\varrho}|}. \tag{30}$$

3. Application

3.1. Simplifying assumptions

To acquire some understanding of how the dimensionless measures of bending energy $\mathcal{F}_{\mathrm{B}}$, intraloop interaction energy $\mathcal{F}_{\mathrm{S}}$, and interloop interaction energy $\mathcal{F}_{\mathrm{I}}$ defined in (21) combine to influence equilibrium configurations of the system of two loops, we consider a particular situation where the loops $\mathcal{C}_1$ and $\mathcal{C}_2$ are geometrically and physically indistinguishable in the sense that they are of equal length and have the bending moduli and intraloop interaction parameters:

$$L_1=L_2=L>0, \qquad \mu_1=\mu_2=\mu>0, \qquad \text{and} \qquad A_{11}=A_{22}=A\geq 0. \tag{31}$$

Our simplifying assumptions in (31) are based on modeling practices that exist in the literature. For example, Messina et al. (2003) and Messina et al. (2004) in Monte Carlo simulations of adsorption of polyelectrolytes onto charged sphere and Messina (2003) in a study of the adsorption of polyelectrolytes onto a charged cylinder, assumed the polyelectrolytes to be of the same length and to have equal charge density.

With (31), the problem formulated in Section 2 reduces to one involving only a single dimensionless measure of length, namely

$$a = \frac{L}{2\pi R} > 0, \tag{32}$$

and two dimensionless measures of energy, namely

$$\zeta = \frac{A_{11}R^3}{\mu} = \frac{A_{22}R^3}{\mu} = \frac{AR^3}{\mu} \geq 0 \qquad \text{and} \qquad \chi = \frac{A_{12}R^3}{\mu} \geq 0. \tag{33}$$

We refer to ζ and χ as the intraloop and interloop interaction parameters, respectively.

To guarantee the existence of a trivial (equilibrium) solution in which $\mathcal{C}_1$ and $\mathcal{C}_2$ are circular and lie in parallel planes, we stipulate that

$$0 < a < 1. \tag{34}$$

The condition (34) is violated for loops $\mathcal{C}_1$ and $\mathcal{C}_2$ that are longer than the great circle of the sphere. If such a violation occurs, the inextensible loops $\mathcal{C}_1$ and $\mathcal{C}_2$ cannot adopt circular configurations and it becomes necessary to use numerical methods to obtain equilibrium solutions and associated stability criteria. This is beyond the scope of the present work, in which we have sought to rely on analytical methods.

As a first step toward modeling of charged entities, it is a common practice to restrict attention to Coulombic interactions and to assume that the charge density is uniform. For example, in a study of suspensions of charged rod-like particles, Weyerich et al. (1990) assumed that each rod is endowed with identical uniform charge density. Ciftja et al. (2014) highlighted the importance of models that consider uniformly charged bodies in their study of electrostatic interactions of a system of two identical uniformly charged rods. Furthermore, Scheele and Lauffer (1967) found that Tobacco mosaic virus which infects a wide variety of plants can be well approximated as uniformly charged. Additionally, in studies of phase transitions in suspensions of the Tobacco mosaic virus, Fraden et al. (1989), Fraden et al. (1993), and Graf and Löwen (1999), modeled the virus as a rigid, uniformly charged rod.

For simplicity, we also confine attention to situations in which $\mathcal{C}_1$ and $\mathcal{C}_2$ are uniformly charged, the primary outcome of it is that

$$f_{ij} = f, \qquad i, j = 1, 2, \tag{35}$$

where f is of the simple form

$$f(\varrho) = \frac{1}{\varrho}. \tag{36}$$

Secondarily, applying (35) and (36) to (27) and (30), we see that

$$\boldsymbol{f}_{ij} = \boldsymbol{f} \qquad \text{and} \qquad \boldsymbol{F}_{ij} = \boldsymbol{F}, \qquad i, j = 1, 2, \tag{37}$$

where $\boldsymbol{f}$ and $\boldsymbol{F}$ are given by

$$\boldsymbol{f}(\boldsymbol{\varrho}) = -\frac{\boldsymbol{\varrho}}{\varrho^3} \qquad \text{and} \qquad \boldsymbol{F}(\boldsymbol{\varrho}) = -\frac{1}{\varrho^3}\left(\mathbf{1} - \frac{3\boldsymbol{\varrho}\otimes\boldsymbol{\varrho}}{\varrho^2}\right), \qquad \varrho = |\boldsymbol{\varrho}|. \tag{38}$$

For the interaction potential (36), the dimensionless interaction parameters ζ and χ defined in (33) are related to the prefactors of the Coulombic interaction and are given by

$$\zeta = \frac{q^2R^3}{4\pi\epsilon_0\epsilon\mu} \qquad \text{and} \qquad \chi = \frac{q^2R^3}{4\pi\epsilon_0\epsilon_{12}\mu}, \tag{39}$$

where q is the linear charge density of the loops $\mathcal{C}_1$ and $\mathcal{C}_2$, R is the radius of the sphere $\mathcal{S}$, μ is the bending rigidity defined in (31), ϵ_0 is the vacuum permittivity, ϵ is dielectric permittivity for intraloop interactions, and ϵ_{12} is the dielectric permittivity for interloop interactions. We consider a general case in which the dielectric permittivities for intraloop and interloop interactions are allowed to differ. The resulting interaction parameters ζ and χ generally differ. The special case of $\epsilon = \epsilon_{12}$ or, equivalently, $\chi = \zeta$ of equal interaction parameters is discussed in Section 3.7.

For the specialization (35)–(36), the dimensionless intraloop interaction energy (21b) and dimensionless interloop interaction energy (21c) penalize situations in which either loop intersects itself and both loops intersect, respectively, and, thus, serve purposes analogous to that of the energy functional in O'Hara (1991), which diverges when a curve intersects itself and which O'Hara (1992, 1994) subsequently interpreted as the potential energy of an electrically charged loop, the Coulomb force of which is proportional to inverse of the cube of the distance between points on the curve.

3.2. Mollification of the dimensionless intraloop interaction energy

For (37)–(38), the integrands of (26) and (29) diverge if the variable of integration coincides with the arclength at which $\boldsymbol{\varphi}_{ii}[\boldsymbol{n}_i, \boldsymbol{n}_i]$ and $\boldsymbol{\vartheta}_{ii}[\boldsymbol{n}_i, \boldsymbol{n}_i](\boldsymbol{u}_i, \boldsymbol{u}_i)$, $i = 1, 2$, are evaluated. We interpret such divergences as physically unwarranted consequences of the specialization (35)–(36). To avoid divergence of this kind, we introduce a mollifier M with the properties

$$M(|\eta|) > 0 \qquad \text{and} \qquad M(|\eta|) \sim \eta^4 \qquad \text{as} \qquad \eta \to 0, \tag{40}$$

and replace the self potential by a regularized self potential $\tilde{f}$ of the form

$$\tilde{f}\Big(|\boldsymbol{n}_i(s)-\boldsymbol{n}_i(\bar{s})|,\frac{|\bar{s}-s|}{2a}\Big)=M\Big(\frac{|\bar{s}-s|}{2a}\Big)\frac{1}{|\boldsymbol{n}_i(s)-\boldsymbol{n}_i(\bar{s})|},\qquad i=1,2. \tag{41}$$

Since the variable of integration coincides with the arclength at which $\boldsymbol{\varphi}_{ij}[\boldsymbol{n}_i,\,\boldsymbol{n}_j]$ and $\boldsymbol{\vartheta}_{ij}[\boldsymbol{n}_i,\,\boldsymbol{n}_j](\boldsymbol{u}_i,\,\boldsymbol{u}_j)$, $i,j=1,2,\ i\neq j$, is evaluated only if $\mathcal{C}_1$ and $\mathcal{C}_2$ intersect and such intersections are penalized as described above, there is no analogous need to regularize the interloop interaction potential.

3.3. Regularized Euler–Lagrange equations and second variation condition

Granted that $\mathcal{C}_1$ and $\mathcal{C}_2$ are of equal length, have the same bending moduli and intraloop interaction parameters, and are uniformly charged, and that the intraloop potential is regularized in accord with (41), the equilibrium conditions (25) are replaced by

$$\left.\begin{aligned}(\boldsymbol{n}_1'''+\lambda_1\boldsymbol{n}_1')'+\Lambda_1\boldsymbol{n}_1&=\zeta\,\tilde{\boldsymbol{\varphi}}[\boldsymbol{n}_1,\boldsymbol{n}_1]+\chi\,\boldsymbol{\varphi}[\boldsymbol{n}_1,\boldsymbol{n}_2],\\(\boldsymbol{n}_2'''+\lambda_2\boldsymbol{n}_2')'+\Lambda_2\boldsymbol{n}_2&=\zeta\,\tilde{\boldsymbol{\varphi}}[\boldsymbol{n}_2,\boldsymbol{n}_2]+\chi\,\boldsymbol{\varphi}[\boldsymbol{n}_2,\boldsymbol{n}_1],\end{aligned}\right\} \tag{42}$$

where $\tilde{\boldsymbol{\varphi}}$ and $\boldsymbol{\varphi}$ are given by

$$\tilde{\boldsymbol{\varphi}}[\boldsymbol{n}_i,\boldsymbol{n}_j](s)=\int_0^{2\pi a}M\Big(\frac{|\bar{s}-s|}{2a}\Big)\frac{\boldsymbol{n}_i(s)-\boldsymbol{n}_i(\bar{s})}{|\boldsymbol{n}_i(s)-\boldsymbol{n}_i(\bar{s})|^3}\,\mathrm{d}\bar{s},\qquad i=1,2, \tag{43a}$$

and

$$\boldsymbol{\varphi}[\boldsymbol{n}_i,\boldsymbol{n}_j](s)=\int_0^{2\pi a}\frac{\boldsymbol{n}_i(s)-\boldsymbol{n}_j(\bar{s})}{|\boldsymbol{n}_i(s)-\boldsymbol{n}_j(\bar{s})|^3}\,\mathrm{d}\bar{s},\qquad i,j=1,2,\qquad i\neq j. \tag{43b}$$

Similarly, the second variation condition (28) is replaced by

$$\begin{aligned}&\int_0^{2\pi a}(|\boldsymbol{u}_1''|^2-\lambda_1|\boldsymbol{u}_1'|^2+(\lambda_1'\boldsymbol{u}_1'+\Lambda_1\boldsymbol{u}_1-\zeta\,\tilde{\boldsymbol{\vartheta}}[\boldsymbol{n}_1,\boldsymbol{n}_1](\boldsymbol{u}_1,\boldsymbol{u}_1)-\chi\,\boldsymbol{\vartheta}[\boldsymbol{n}_1,\boldsymbol{n}_2](\boldsymbol{u}_1,\boldsymbol{u}_2))\cdot\boldsymbol{u}_1)\,\mathrm{d}s\\&+\int_0^{2\pi a}((|\boldsymbol{u}_2''|^2-\lambda_2|\boldsymbol{u}_2'|^2)+(\lambda_2'\boldsymbol{u}_2'+\Lambda_2\boldsymbol{u}_2-\zeta\,\tilde{\boldsymbol{\vartheta}}[\boldsymbol{n}_2,\boldsymbol{n}_2](\boldsymbol{u}_2,\boldsymbol{u}_2)-\chi\,\boldsymbol{\vartheta}[\boldsymbol{n}_2,\boldsymbol{n}_1](\boldsymbol{u}_2,\boldsymbol{u}_1))\cdot\boldsymbol{u}_2)\,\mathrm{d}s\geq 0,\end{aligned} \tag{44}$$

where $\tilde{\boldsymbol{\vartheta}}$ and $\boldsymbol{\vartheta}$ are defined by

$$\begin{aligned}&\tilde{\boldsymbol{\vartheta}}[\boldsymbol{n}_i,\boldsymbol{n}_i](\boldsymbol{u}_i,\boldsymbol{u}_i)(s)\\&\quad=\int_0^{2\pi a}M\Big(\frac{|\bar{s}-s|}{2a}\Big)\Big(\mathbf{1}-\frac{3(\boldsymbol{n}_i(s)-\boldsymbol{n}_i(\bar{s}))\otimes(\boldsymbol{n}_i(s)-\boldsymbol{n}_i(\bar{s}))}{|\boldsymbol{n}_i(s)-\boldsymbol{n}_i(\bar{s})|^2}\Big)\frac{\boldsymbol{u}_i(s)-\boldsymbol{u}_i(\bar{s})}{|\boldsymbol{n}_i(s)-\boldsymbol{n}_i(\bar{s})|^3}\,\mathrm{d}\bar{s},\qquad i=1,2,\end{aligned} \tag{45a}$$

and

$$\begin{aligned}&\boldsymbol{\vartheta}[\boldsymbol{n}_i,\boldsymbol{n}_j](\boldsymbol{u}_i,\boldsymbol{u}_j)(s)\\&\quad=\int_0^{2\pi a}\Big(\mathbf{1}-\frac{3(\boldsymbol{n}_i(s)-\boldsymbol{n}_j(\bar{s}))\otimes(\boldsymbol{n}_i(s)-\boldsymbol{n}_j(\bar{s}))}{|\boldsymbol{n}_i(s)-\boldsymbol{n}_j(\bar{s})|^2}\Big)\frac{\boldsymbol{u}_i(s)-\boldsymbol{u}_j(\bar{s})}{|\boldsymbol{n}_i(s)-\boldsymbol{n}_j(\bar{s})|^3}\,\mathrm{d}\bar{s},\qquad i,j=1,2,\qquad i\neq j.\end{aligned} \tag{45b}$$

3.4. Trivial solution

Consider an equatorial plane $\mathcal{P}$ of the sphere $\mathcal{S}$ upon which the loops $\mathcal{C}_1$ and $\mathcal{C}_2$ are confined, as shown in Fig. 2. Let $\{\boldsymbol{\imath},\,\boldsymbol{\jmath},\,\boldsymbol{k}\}$ be a positively-oriented orthonormal basis with $\boldsymbol{k}$ directed upward along the polar axis $\mathcal{A}$ of $\mathcal{S}$. Then, $\boldsymbol{e}$ defined by

$$\boldsymbol{e}(s)=\Big(\cos\frac{s}{a}\Big)\boldsymbol{\imath}+\Big(\sin\frac{s}{a}\Big)\boldsymbol{\jmath},\qquad 0\leq s\leq 2\pi a, \tag{46}$$

represents the restriction to the equatorial great circle of the outward unit normal to $\mathcal{S}$. We suppose that the loops are circles — denoted by $\mathcal{C}_1^*$ and $\mathcal{C}_2^*$ — of radius Ra that reside in planes parallel to and separated from $\mathcal{P}$ by the distance $R\sqrt{1-a^2}$. The total energy of this configuration does not change on fixing one loop and rotating the other loop by an arbitrary angle about $\mathcal{A}$. We may choose the quantities $\boldsymbol{n}_1^*$ and $\boldsymbol{n}_2^*$ that parametrize $\mathcal{C}_1^*$ and $\mathcal{C}_2^*$ to be of the form

$$\boldsymbol{n}_1^*=\boldsymbol{n}_0\qquad\text{and}\qquad\boldsymbol{n}_2^*=\boldsymbol{K}\boldsymbol{n}_0, \tag{47}$$

where $\boldsymbol{n}_0$ is defined such that

$$\boldsymbol{n}_0(s)=a\boldsymbol{e}(s)+\sqrt{1-a^2}\boldsymbol{k},\qquad 0\leq s\leq 2\pi a, \tag{48}$$

and $\boldsymbol{K}$ defined by

$$\boldsymbol{K}=1-2\boldsymbol{k}\otimes\boldsymbol{k}, \tag{49}$$

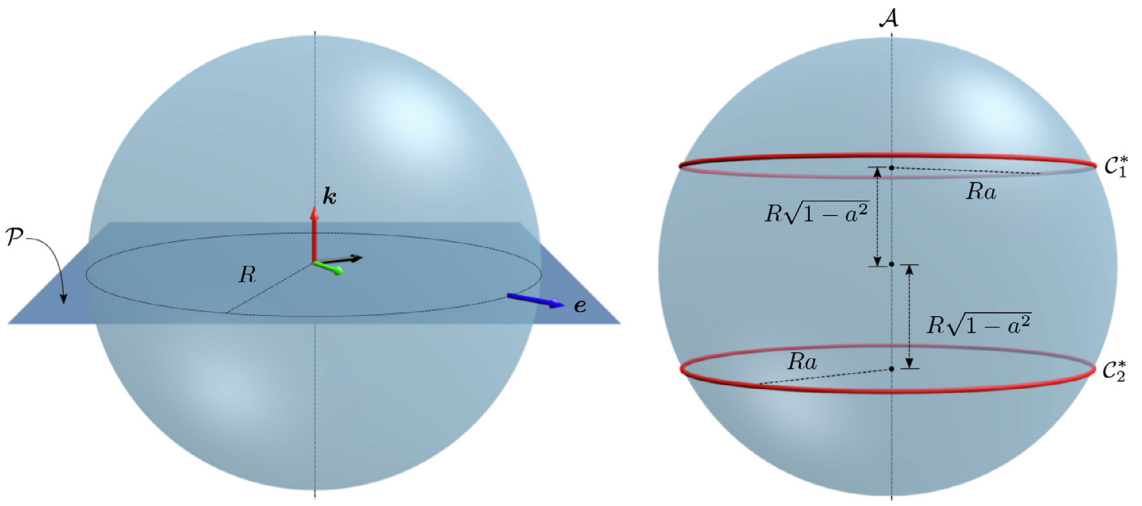

Fig. 2. Circular loops $\mathcal{C}_1$ and $\mathcal{C}_2$ of dimensionless length $2\pi a$, with $0 < a < 1$, situated on opposing planes parallel to an equatorial plane of a sphere $\mathcal{S}$, of radius R, at respective altitudes $R\sqrt{1-a^2}$ and $-R\sqrt{1-a^2}$. The vector field $\boldsymbol{e}$ describes the restriction to the equatorial great circle of the outward unit normal to $\mathcal{S}$ and $\boldsymbol{k}$ is the unit vector along the polar axis $\mathcal{A}$.

is an orthogonal tensor that transforms any vector by reflecting it across $\mathcal{P}$. The elementary properties of $\boldsymbol{K}$ that are useful for further calculations are

$$|\boldsymbol{K}\boldsymbol{m}| = |\boldsymbol{m}|, \qquad \boldsymbol{K}^{\mathrm{T}} = \boldsymbol{K}, \qquad \text{and} \qquad \boldsymbol{K}^2 = \boldsymbol{1}. \tag{50}$$

We substitute the particular choices (47) of $\boldsymbol{n}_1^*$ and $\boldsymbol{n}_2^*$ in the equilibrium equations (42) and make simplifications by applying $\boldsymbol{K}$ to second of the equations obtained and invoke (50), giving

$$\left.\begin{aligned} (\boldsymbol{n}_0''' + \lambda_1^* \boldsymbol{n}_0')' + \Lambda_1^* \boldsymbol{n}_0 &= \zeta\, \tilde{\boldsymbol{\varphi}}[\boldsymbol{n}_0, \boldsymbol{n}_0] + \chi\, \boldsymbol{\varphi}[\boldsymbol{n}_0, \boldsymbol{K}\boldsymbol{n}_0], \\ (\boldsymbol{n}_0''' + \lambda_2^* \boldsymbol{n}_0')' + \Lambda_2^* \boldsymbol{n}_0 &= \zeta\, \boldsymbol{K}\tilde{\boldsymbol{\varphi}}[\boldsymbol{K}\boldsymbol{n}_0, \boldsymbol{K}\boldsymbol{n}_0] + \chi\, \boldsymbol{K}\boldsymbol{\varphi}[\boldsymbol{K}\boldsymbol{n}_0, \boldsymbol{n}_0], \end{aligned}\right\} \tag{51}$$

where Λ_i^* and λ_i^* are as yet undetermined Lagrange multipliers needed to ensure that each circular loop $\mathcal{C}_i^*$, $i = 1, 2$, is configured consistent with the constraints $(4)_1$ and $(4)_2$, respectively. Using (43a) and (50), we see that

$$\boldsymbol{K}\tilde{\boldsymbol{\varphi}}[\boldsymbol{K}\boldsymbol{n}_0, \boldsymbol{K}\boldsymbol{n}_0](s) = \int_0^{2\pi a} M\Big(\frac{|\bar{s} - s|}{2a}\Big) \frac{\boldsymbol{K}^2(\boldsymbol{n}_0 - \boldsymbol{n}_0(\bar{s}))}{|\boldsymbol{K}(\boldsymbol{n}_0 - \boldsymbol{n}_0(\bar{s}))|}\, \mathrm{d}\bar{s} = \tilde{\boldsymbol{\varphi}}[\boldsymbol{n}_0, \boldsymbol{n}_0](s). \tag{52}$$

Similarly, using (43b) and (50), we see that

$$\boldsymbol{K}\boldsymbol{\varphi}[\boldsymbol{K}\boldsymbol{n}_0, \boldsymbol{n}_0](s) = \int_0^{2\pi a} \frac{\boldsymbol{K}(\boldsymbol{K}\boldsymbol{n}_0 - \boldsymbol{n}_0(\bar{s}))}{|\boldsymbol{K}(\boldsymbol{n}_0 - \boldsymbol{K}\boldsymbol{n}_0(\bar{s}))|}\, \mathrm{d}\bar{s} = \int_0^{2\pi a} \frac{\boldsymbol{n}_0 - \boldsymbol{K}\boldsymbol{n}_0(\bar{s})}{|\boldsymbol{n}_0 - \boldsymbol{K}\boldsymbol{n}_0(\bar{s})|} = \boldsymbol{\varphi}[\boldsymbol{n}_0, \boldsymbol{K}\boldsymbol{n}_0](s). \tag{53}$$

Using (52) and (53) in $(51)_2$ and subtracting the resulting equation from $(51)_1$, we obtain the condition

$$\lambda_1^* \boldsymbol{n}_0'' + (\lambda_1^*)' \boldsymbol{n}_0' + \Lambda_1^* \boldsymbol{n}_0 = \lambda_1^* \boldsymbol{n}_0'' + (\lambda_2^*)' \boldsymbol{n}_0' + \Lambda_2^* \boldsymbol{n}_0. \tag{54}$$

Dotting each term of (54) with $\boldsymbol{k}$ and using the consequences $\boldsymbol{k} \cdot \boldsymbol{n}_0' = 0$ and $\boldsymbol{k} \cdot \boldsymbol{n}_0'' = 0$ of (48), we find that

$$\Lambda_1^* = \Lambda_2^* = \Lambda. \tag{55}$$

Similarly, dotting each term of (54) with $\boldsymbol{n}_0''$, using the identities $\boldsymbol{n}_0 \cdot \boldsymbol{n}_0'' = -1$ and $\boldsymbol{n}_0' \cdot \boldsymbol{n}_0'' = 0$, which arise from differentiating $(4)_1$ twice and using $(4)_2$ and differentiating $(4)_2$, respectively, we find that $\lambda_1^* |\boldsymbol{n}_0''|^2 - \Lambda_1^* = \lambda_2^* |\boldsymbol{n}_0''|^2 - \Lambda_2^*$ and, thus, by (55), that

$$\lambda_1^* = \lambda_2^* = \lambda. \tag{56}$$

In view of (53), (55), and (56), the equilibrium conditions $(51)_1$ and $(51)_2$ are equivalent. We may thus use either of these conditions to determine Λ and λ. Using (55) and (56) in the left-hand side of $(51)_1$ while using the expression

$$k = \frac{\sqrt{1-a^2}}{a}, \tag{57}$$

the dimensionless geodesic curvature of $\mathcal{C}_1^*$, we obtain the identity

$$\boldsymbol{n}_0''' + \lambda \boldsymbol{n}_0'' + \Lambda \boldsymbol{n}_0 = \lambda' \boldsymbol{t}_0 + \Big(\Lambda - \lambda + \frac{1}{a^2}\Big)\boldsymbol{n}_0 - \frac{\sqrt{1-a^2}}{a}\Big(\lambda - \frac{1}{a^2}\Big)\boldsymbol{g}_0, \tag{58}$$

where $\boldsymbol{t}_0$ and $\boldsymbol{g}_0$ given by

$$\boldsymbol{t}_0(s) = -\left(\sin\frac{s}{a}\right)\boldsymbol{\imath} + \left(\cos\frac{s}{a}\right)\boldsymbol{\jmath}, \qquad \boldsymbol{g}_0(s) = \sqrt{1-a^2}\boldsymbol{e}(s) - a\boldsymbol{k}, \qquad 0 \le s \le 2\pi a, \tag{59}$$

denote the tangential and geodesic elements of the Darboux frame for $\mathcal{C}_1^*$.

With the change of variables $\eta = |\bar{s}-s|/2a$, we find that the terms on the right-hand side of $(51)_1$ can be represented as

$$\begin{aligned}\zeta\tilde{\boldsymbol{\varphi}}[\boldsymbol{n}_0,\boldsymbol{n}_0] + \chi\boldsymbol{\varphi}[\boldsymbol{n}_0,\boldsymbol{K}\boldsymbol{n}_0] = &\left(\frac{\zeta}{2}\int_0^\pi M(\eta)\csc\eta\,\mathrm{d}\eta + \frac{a\chi}{2}\int_0^\pi \frac{\mathrm{d}\eta}{\sqrt{1-a^2\cos^2\eta}}\right)\boldsymbol{n}_0\\ &+\left(\frac{\zeta}{2}\int_0^\pi M(\eta)\csc\eta\,\mathrm{d}\eta - \frac{a^3\chi}{2}\int_0^\pi \frac{\cos^2\eta\,\mathrm{d}\eta}{\sqrt[3]{1-a^2\cos^2\eta}}\right)\boldsymbol{g}_0.\end{aligned} \tag{60}$$

Using (58) and (60) in $(51)_1$, we thus arrive at a reduced system for Λ and λ:

$$\left.\begin{aligned}\lambda' &= 0,\\ \Lambda - \lambda + \frac{1}{a^2} - \frac{\zeta}{2}\int_0^\pi M(\eta)\csc\eta\,\mathrm{d}\eta - \frac{a\chi}{2}\int_0^\pi \frac{\mathrm{d}\eta}{\sqrt{1-a^2\cos^2\eta}} &= 0,\\ \lambda - \frac{1}{a^2} + \frac{\zeta}{2}\int_0^\pi M(\eta)\csc\eta\,\mathrm{d}\eta - \frac{a^3\chi}{2}\int_0^\pi \frac{\cos^2\eta\,\mathrm{d}\eta}{\sqrt[3]{1-a^2\cos^2\eta}} &= 0.\end{aligned}\right\} \tag{61}$$

Eliminating λ between $(61)_2$ and $(61)_3$, we find that Λ is uniform and given by

$$\Lambda = \frac{a\chi}{2}\int_0^\pi \frac{\mathrm{d}\eta}{\sqrt[3]{1-a^2\cos^2\eta}}. \tag{62}$$

The reactions needed to ensure that the loops adhere to $\mathcal{S}$ are therefore equal and are given by $\mu\Lambda/R^2$. From (62), we see that the adhesive reaction depends only on the common dimensionless radius a of the loops and the dimensionless measure χ of the magnitude of the repulsive interaction between the loops relative to their bending stiffness. Moreover, from (62), we see that the ratio Λ/χ depends only on a and find that

$$\frac{\Lambda}{\chi} \sim a \quad \text{as} \quad a \downarrow 0, \qquad \frac{\Lambda}{\chi} \sim \frac{1}{1-a} \quad \text{as} \quad a \uparrow 1, \qquad \text{and} \qquad \frac{\mathrm{d}}{\mathrm{d}a}\left(\frac{\Lambda}{\chi}\right) > 0 \quad \text{for} \quad 0 < a < 1, \tag{63}$$

from which we infer that the magnitude of the adhesive reaction increases monotonically with a for $0 < a < 1$. If the loops and the sphere cannot sustain the adhesive reaction required to ensure $(4)_1$, detachment will occur. Such events are beyond the scope of the present work, which relies on the fact that all the points of the loops remain in contact of the sphere via the kinematic constraint $(4)_1$.

Additionally, from $(61)_1$ we find that λ is uniform and, in accord with $(61)_3$, is given by

$$\lambda = \frac{1}{a^2} - \frac{\zeta}{2}\int_0^\pi M(\eta)\csc\eta\,\mathrm{d}\eta + \frac{a^3\chi}{2}\int_0^\pi \frac{\cos^2\eta\,\mathrm{d}\eta}{\sqrt[3]{1-a^2\cos^2\eta}}. \tag{64}$$

The reactions needed to ensure that the lengths of the loops are preserved pointwise are equal and are given by $\mu\lambda/R^2$. From (64), we see that the tensile reaction encompasses several competing effects. The first term, $1/a^2$ on the right-hand side of (64) is the contribution to the reaction associated with ensuring that the action of bending a straight segments of length $2\pi Ra$ into a circular loop of radius Ra involves neither local elongation nor local contraction. Since the integral in the second term on the right-hand side of (64) is independent of a, that term simply produces a uniform reaction proportional to the dimensionless measure ζ of the repulsive intraloop interactions of the loops relative to their bending stiffness. The final term on the right-hand side of (64) depends only on a and χ and, thus, is analogous to the only term on the right-hand side of (62). To explore the properties of the associated reaction, we therefore consider the reduced multiplier

$$\tilde{\lambda} = \lambda - \frac{1}{a^2} + \frac{\zeta}{2}\int_0^\pi M(\eta)\csc\eta\,\mathrm{d}\eta = \frac{a^3\chi}{2}\int_0^\pi \frac{\cos^2\eta\,\mathrm{d}\eta}{\sqrt[3]{1-a^2\cos^2\eta}}. \tag{65}$$

Emulating the reasoning leading to (63), we find that

$$\frac{\tilde{\lambda}}{\chi} \sim a^3 \quad \text{as} \quad a \downarrow 0, \qquad \frac{\tilde{\lambda}}{\chi} \sim \frac{1}{1-a} \quad \text{as} \quad a \uparrow 1, \qquad \text{and} \qquad \frac{\mathrm{d}}{\mathrm{d}a}\left(\frac{\tilde{\lambda}}{\chi}\right) > 0 \quad \text{for} \quad 0 < a < 1, \tag{66}$$

from which we infer the magnitude of the reaction needed to ensure that the lengths of the loops are preserved pointwise increases monotonically with a.

Plots of Λ/χ and $\tilde{\lambda}/\chi$ versus a are provided in Fig. 3. These confirm our qualitative observations. For $a \to 0$, the distance between loops is maximized, meaning that the repulsive interaction between them diminishes on passing to that limit. Consequently, Λ and $\tilde{\lambda}$ both vanish as $a \to 0$. Since $\lambda \sim 1/a^2$ in this regime, the tensile reaction is dominated by the bending resistance of the loops. For $a \to 1$, $\Lambda \sim (1-a)^{-1}$ and $\lambda \sim (1-a)^{-1}$, from which we conclude that, on passing to that limit, the reactions are dominated by interactions between the loops.

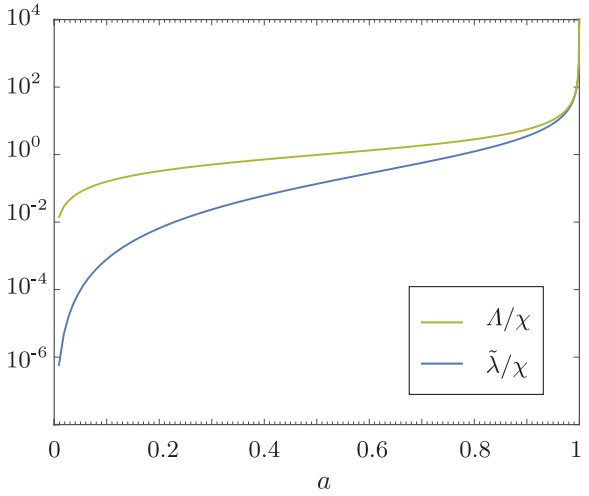

Fig. 3. Plots of the Lagrange multiplier Λ/χ and reduced multiplier $\tilde{\lambda}/\chi$ versus a, where Λ given in (62) and $\tilde{\lambda}$ given in (65) are the lagrange multipliers for adhesive constraint $(4)_1$ and inextensibility constraint $(4)_2$ at the trivial equilibrium solution that is parameterized by (47)-(49), a is dimensionless radius of the loops, defined in (32), and χ is dimensionless interloop interaction parameter defined in $(33)_2$.

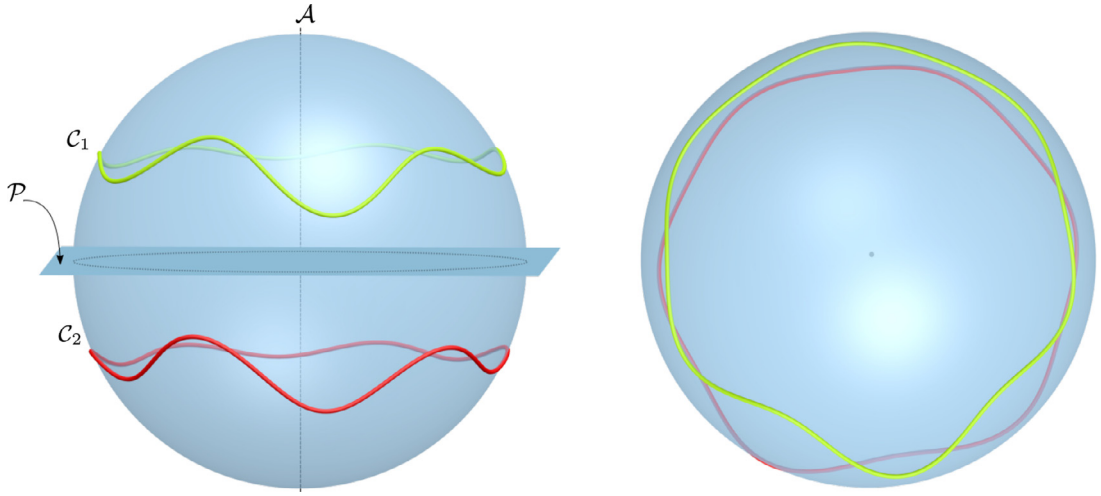

Fig. 4. Side view and top view of schematic of perturbed configurations $\mathcal{C}_1$ and $\mathcal{C}_2$ that are parameterized by $\boldsymbol{n}_1 = \boldsymbol{n}_0 + \boldsymbol{u}_1$ and $\boldsymbol{n}_2 = \boldsymbol{K}\boldsymbol{n}_0 + \boldsymbol{u}_2$, where $\boldsymbol{u}_1$ and $\boldsymbol{u}_2$ are admissible perturbatons that follow the restriction (67) and $\boldsymbol{n}_0$ and $\boldsymbol{K}$ are defined by (48) and (49). Due to (67), $\mathcal{C}_1$ and $\mathcal{C}_2$ are rotated with respect to each other about polar axis $\mathcal{A}$ such that dimensionless interloop interaction energy defined by (21c) is least compared to that for any other rotation between $\mathcal{C}_1$ and $\mathcal{C}_2$.

3.5. Stability analysis of the trivial solution

The relations (47)–(48), (55)–(56), and (62)–(64) defining $\boldsymbol{n}_i^*$, Λ_i, and λ_i, $i = 1, 2$, determine a trivial solution to the problem formulated in Section 3 for each combination of the dimensionless radius a of the loops and the dimensionless measures ζ and χ of the repulsive intraloop interaction energy and interloop interactions satisfying $0 < a < 1$, $\zeta \geq 0$, and $\chi \geq 0$. We next explore the stability of the resulting family of solutions for different combinations of a, ζ, and χ.

We consider perturbations $\boldsymbol{u}_i$ of the unit orientation field $\boldsymbol{n}_i^*$ that parameterize $\mathcal{C}_i^*$, $i = 1, 2$, that obey

$$\boldsymbol{u}_1 = \boldsymbol{v} \qquad \text{and} \qquad \boldsymbol{u}_2 = -\boldsymbol{K}\boldsymbol{v}, \qquad |\boldsymbol{v}| \ll 1, \tag{67}$$

and, thus, recalling the definition (49) of $\boldsymbol{K}$, differ only by a rotation of π about the polar axis $\mathcal{A}$. The assumption leading to (67) is motivated by the observation that, among all possible rotations about $\mathcal{A}$, a rotation by π yields perturbed configurations $\mathcal{C}_1$ and $\mathcal{C}_2$ which minimize the dimensionless interloop interaction energy. A schematic of the loops $\mathcal{C}_1$ and $\mathcal{C}_2$ parameterized by $\boldsymbol{n}_1 = \boldsymbol{n}_0 + \boldsymbol{v}$ and $\boldsymbol{n}_2 = \boldsymbol{K}(\boldsymbol{n}_0 - \boldsymbol{v})$, with $\boldsymbol{v}$ being composed of a superimposition of modes $n = 2 \ldots 6$, is provided in Fig. 4.

Because (67) does not represent all admissible perturbations of the trivial solution, we only expect to obtain an upper bound for the critical parameter $\chi > 0$ corresponding to each choice of $0 < a < 1$ and $\zeta \geq 0$. In mechanics, there is ample

precedent for considering restricted classes of perturbations. A well-known example is Biot's 1963 work on the instability of the surface of an elastic half-space. In deriving the critical compression load, Biot performed linear bifurcation analysis restricted to planar sinusoidal perturbations. As such, the critical load obtained by Biot can be regarded as an upper bound of the exact critical load which could be derived by considering all admissible three dimensional perturbations. The particular class of perturbations considered by Biot has subsequently been used in many studies, including a recent stability analysis of the wrinkling mode experienced by a compressed half-space of neoHookean material conducted by Cao and Hutchinson (2011). Very recently, Chen et al. (2018) used the energy based stability criterion to determine the complete set of stability conditions for a half-space composed of an incompressible neoHookean material. One of their key findings that that the stability region obtained by their analysis, which accounts for all admissible perturbations, coincides with the stability condition found by Biot (1963).

From the consequences $\boldsymbol{n}_2^* \cdot \boldsymbol{u}_2 = -\boldsymbol{K}\boldsymbol{n}_0 \cdot \boldsymbol{K}\boldsymbol{v} = -\boldsymbol{n}_0 \cdot \boldsymbol{v}$, and $\boldsymbol{n}_2^{*\prime} \cdot \boldsymbol{u}_2' = -\boldsymbol{K}\boldsymbol{n}_0' \cdot \boldsymbol{K}\boldsymbol{v}' = -\boldsymbol{n}_0' \cdot \boldsymbol{v}'$ of $(50)_{2,3}$ and (67), we find that for the admissibility requirements (24) to hold, the perturbation $\boldsymbol{v}$ must be restricted according to

$$\boldsymbol{n}_0 \cdot \boldsymbol{v} = 0 \qquad \text{and} \qquad \boldsymbol{n}_0' \cdot \boldsymbol{v}' = 0. \tag{68}$$

Using the expressions (47) and (67) for $\boldsymbol{n}_i$ and $\boldsymbol{u}_i$, $i = 1, 2$, the stability condition (44), and recalling from (55) and (56) that the Lagrange multipliers required to ensure that the constraints are maintained in the trivial equilibrium configuration obey $\Lambda_1^* = \Lambda_2^* = \Lambda$ and $\lambda_1^* = \lambda_2^* = \lambda$ with Λ and λ being uniform, calculations in Appendix B show that the trivial solution is stable only if the inequality

$$\int_0^{2\pi a} (|\boldsymbol{v}''|^2 - \lambda|\boldsymbol{v}'|^2 + \Lambda|\boldsymbol{v}|^2 - \zeta\, \tilde{\boldsymbol{\vartheta}}[\boldsymbol{n}_0, \boldsymbol{n}_0](\boldsymbol{v}, \boldsymbol{v}) \cdot \boldsymbol{v} - \chi\, \boldsymbol{\vartheta}[\boldsymbol{n}_0, \boldsymbol{K}\boldsymbol{n}_0](\boldsymbol{v}, -\boldsymbol{K}\boldsymbol{v}) \cdot \boldsymbol{v})\, \mathrm{d}s \geq 0 \tag{69}$$

holds for all $\boldsymbol{v}$ consistent with (68). Moreover, granted that $\boldsymbol{v}$ admits an orthogonal decomposition of the form

$$\boldsymbol{v} = \sum_{n=2}^{\infty} \boldsymbol{v}_n, \qquad \text{with} \qquad \int_0^{2\pi a} \boldsymbol{v}_m \cdot \boldsymbol{v}_n\, \mathrm{d}s \propto \delta_{mn}, \tag{70}$$

where δ_{mn} denotes the Kronecker symbol, further calculations in Appendix B show that (69) reduces to the requirement that the inequality

$$\int_0^{2\pi a} (|\boldsymbol{v}_n''|^2 - \lambda|\boldsymbol{v}_n'|^2 + \Lambda|\boldsymbol{v}_n|^2 - \zeta\, \tilde{\boldsymbol{\vartheta}}[\boldsymbol{n}_0, \boldsymbol{n}_0](\boldsymbol{v}_n, \boldsymbol{v}_n) \cdot \boldsymbol{v}_n - \chi\, \boldsymbol{\vartheta}[\boldsymbol{n}_0, \boldsymbol{K}\boldsymbol{n}_0](\boldsymbol{v}_n, -\boldsymbol{K}\boldsymbol{v}_n) \cdot \boldsymbol{v}_n)\, \mathrm{d}s \geq 0 \tag{71}$$

holds for each mode $n \geq 2$. Referring to (29) and (45a)–(45b), we confirm that the nonlocal contributions to (71) depend linearly on $\boldsymbol{v}_n$. Recognizing that each mode $\boldsymbol{v}_n$, $n \geq 2$, can be represented by arclength dependent polar and azimuthal angles θ_n and ψ_n through

$$\boldsymbol{v}_n = \sqrt{1-a^2}\,\theta_n \boldsymbol{e} - a\theta_n \boldsymbol{k} + a\psi_n \boldsymbol{k} \times \boldsymbol{e}, \tag{72}$$

we see from (48) and (72) that

$$\boldsymbol{n}_0 \cdot \boldsymbol{v}_n = (a\boldsymbol{e} + \sqrt{1-a^2}\boldsymbol{k}) \cdot (\sqrt{1-a^2}\,\theta_n \boldsymbol{e} - a\theta_n \boldsymbol{k} + a\psi_n \boldsymbol{k} \times \boldsymbol{e}) = 0 \tag{73}$$

and, thus, that the constraint (68) needed to ensure that the variations do not cause the loops to separate from $\mathcal{S}$ is maintained for all choices of the angles θ_n and ψ_n needed to fully determine the form of the representation (72) for $\boldsymbol{v}_n$. Differentiating (48) and (72) with respect to arclength and invoking the consequences

$$\boldsymbol{e} \cdot \boldsymbol{e}' = 0, \qquad \boldsymbol{k} \cdot \boldsymbol{e}' = 0, \qquad \boldsymbol{k} \times \boldsymbol{e} = a\boldsymbol{e}', \qquad \text{and} \qquad a\boldsymbol{k} \times \boldsymbol{e}' = -\boldsymbol{e} \tag{74}$$

of (46), we next see that

$$\boldsymbol{n}_0' \cdot \boldsymbol{v}_n' = a\boldsymbol{e}' \cdot (\sqrt{1-a^2}(\theta_n' \boldsymbol{e} + \theta_n \boldsymbol{e}') - a\theta_n' \boldsymbol{k} + a^2 \psi_n' \boldsymbol{e}' - \psi_n \boldsymbol{e}) = a(\sqrt{1-a^2}\,\theta_n + a^2 \psi_n')|\boldsymbol{e}'|^2 \tag{75}$$

and, thus, that constraint $(68)_2$ needed to ensure that the variations do not cause local changes in the lengths of the loops is maintained only if the angles θ_n and ψ_n obey the relation

$$\sqrt{1-a^2}\,\theta_n + a^2 \psi_n' = 0. \tag{76}$$

Using (76) to eliminate θ_n from (72), we next find that $\boldsymbol{v}_n$ has a reduced representation of the form

$$\boldsymbol{v}_n = -a^2 \psi_n' \left(\boldsymbol{e} - \frac{a}{\sqrt{1-a^2}} \boldsymbol{k} \right) + a\psi_n \boldsymbol{k} \times \boldsymbol{e}. \tag{77}$$

Using the definitions (45a), (45b), (48), (77) of $\tilde{\boldsymbol{\vartheta}}$, $\boldsymbol{\vartheta}$, $\boldsymbol{n}_0$, and $\boldsymbol{v}_n$ in (71) and assuming that ψ_n is given by

$$\psi_n(s) = c_n \cos\frac{ns}{a} + d_n \sin\frac{ns}{a}, \tag{78}$$

calculations in Appendix B show that the stability condition (71) for each mode $n \geq 2$ reduces to

$$\chi \leq \alpha_n(a)\zeta + \beta_n(a), \tag{79}$$

where α_n and β_n are defined in (B.35) and satisfy the inequalities

$$\alpha_n(a) > 0 \qquad \text{and} \qquad \beta_n(a) > 0. \tag{80}$$

The restrictions in (80) ensure that for given a and $n \geq 2$, there exists a combination of the interaction parameters ζ and χ such that the trivial equilibrium configuration is unstable.

For each mode $n \geq 2$ and each a, the line

$$\mathcal{L}_n(a) = \{(\zeta, \chi) : \zeta \geq 0, \chi = \alpha_n(a)\zeta + \beta_n(a)\} \tag{81}$$

generated by replacing the inequality of (79) with an equality determines the critical combinations of ζ and χ at which the trivial configuration becomes unstable when subjected to a perturbation involving mode n. From the inequalities in (80), we see that the slope and χ-intercept of $\mathcal{L}_n(a)$ must be positive. Since the χ-intercept of $\mathcal{L}_n(a)$ is positive, the critical value of χ at $\zeta = 0$ must be positive, from which we infer that a finite interloop repulsion is needed to overcome the resistance of the loops to bending and, consequently, to destabilize the trivial configuration. Furthermore, since the slope of $\mathcal{L}_n(a)$ is positive for each mode $n > 2$, we infer that the value of the dimensionless interloop interaction parameter χ at which the trivial solution becomes unstable to perturbations of each mode $n \geq 2$ increases monotonically as the dimensionless intraloop interaction parameter ζ increases. This is because the dimensionless bending energy and the intraloop interaction energy both penalize noncircular configurations of the loops.

As a consequence of the previous observations, we conclude that the stability lines $\mathcal{L}_m(a)$ and $\mathcal{L}_n(a)$ corresponding to two distinct modes m and n intersect in the first quadrant of the (ζ, χ)-plane if and only if $\alpha_n > \alpha_m$ and $\beta_n < \beta_m$, meaning that $\mathcal{L}_n$ has slope greater than that of $\mathcal{L}_m(a)$ and χ-intercept less than that of $\mathcal{L}_m(a)$. Taking into consideration that the family $\{\mathcal{L}_n(a) : n \geq 2\}$ of lines determined by (81) may intersect at one or more points, we conclude that the trivial equilibrium configuration involving two loops of radius a is linearly stable only if ζ and χ lie on or below the lower envelope

$$\mathcal{L}(a) = \{(\zeta, \chi) : \zeta \geq 0, \chi = \min_{n \geq 2}(\alpha_n(a)\zeta + \beta_n(a))\} \tag{82}$$

of that family. Since the trivial equilibrium configuration for loops of dimensionless radius a is linearly unstable for any combination of ζ and χ that lies above $\mathcal{L}(a)$, we refer to $\mathcal{L}(a)$ as the stability curve for that a.

3.6. Stability results for a particular mollification of the dimensionless self potential

For illustrative purposes, we take the mollifier M described in Subsection 3.2 to be of the particular form

$$M(\eta) = \left(\frac{\sin\eta}{\sin\eta + e^{-7\sin\eta}}\right)^4 \tag{83}$$

used previously by Hoffman and Manning (2009) to calculate the intraloop interaction energy of a charged rod. This choice is consistent with the provision (40) needed to ensure regularization of the intraloop interaction energy up to its second variation. Granted the choice (83), we find that there exists a critical value $a_c \approx 0.74$ of a such that the stability curve $\mathcal{L}(a)$ is polygonal for $0 < a < a_c$ but is the single line $\mathcal{L}(a) = \mathcal{L}_2(a)$ for $a_c \leq a < 1$. We next consider these alternatives separately.

3.6.1. Polygonal stability curve: $0 < a < a_c$

For $0 < a < a_c$ and each mode $n \geq 2$, let $(\zeta_n(a), \alpha_n(a)\zeta_n(a) + \beta_n(a))$ denote point at which the lines $\mathcal{L}_n(a)$ and $\mathcal{L}_{n+1}(a)$ intersect. Then the polygonal stability curve $\mathcal{L}(a)$ consists of the line segments

$$\{(\zeta, \chi) : 0 \leq \zeta \leq \zeta_2(a), \chi = \alpha_2(a)\zeta + \beta_2(a)\} \tag{84}$$

and

$$\{(\zeta, \chi) : \zeta_{n-1}(a) \leq \zeta \leq \zeta_n(a), \chi = \alpha_n(a)\zeta + \beta_n(a)\}, \qquad n > 2. \tag{85}$$

The mode $n \geq 2$ with respect to which the trivial equilibrium configuration first becomes linearly unstable therefore varies with the value of the intraloop interaction parameter $\zeta > 0$. For this case, the stability curve for a representative value $a = 0.6$ of a is shown in Fig. 5.

3.6.2. Straight stability curve: $a_c \leq a < 1$

For $a_c \leq a < 1$, we find that $\alpha_2(a) < \alpha_n(a)$ and $\beta_2(a) < \beta_n(a)$ for all $n > 2$. Thus, $\mathcal{L}_2(a)$ lies below $\mathcal{L}_n(a)$ for each $n \geq 3$ and $\mathcal{L}(a) = \mathcal{L}_2(a)$. Regardless of the value of $\zeta \geq 0$, we thus see that the trivial equilibrium configuration for loops of dimensionless radius $a_c \leq a < 1$ first becomes linearly unstable when subjected to perturbations involving only mode $n = 2$ and the corresponding value of χ at which that occurs is $\chi = \alpha_2(a)\zeta + \beta_2(a)$. A stability curve for the representative value $a = 0.9$ of a is shown in Fig. 5.

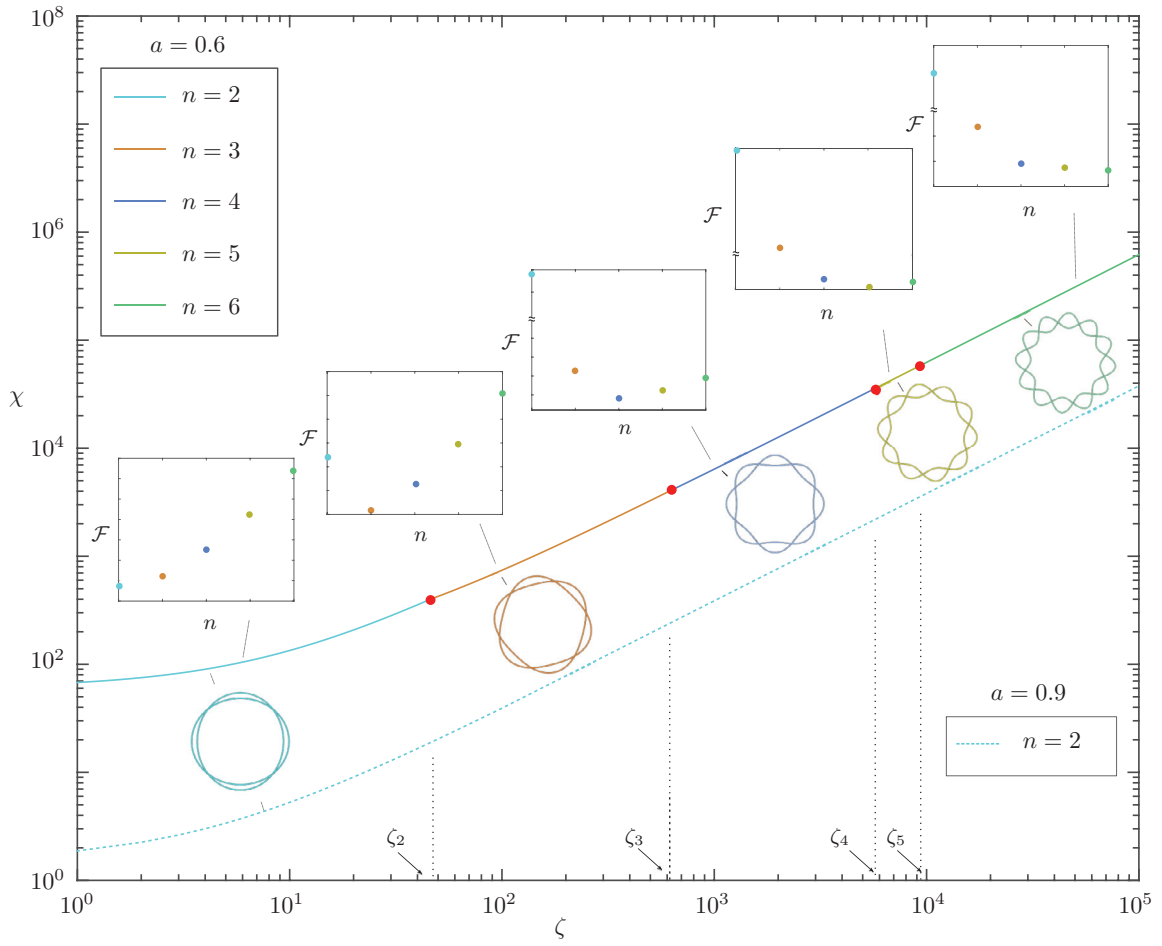

Fig. 5. Stability plot (ζ, χ) on logarithmic scales of ζ and χ for $a = 0.6\,(< a_c)$ and $a = 0.9\,(a \geq a_c)$, where a is dimensionless radius defined in (32), ζ and χ are dimensionless intraloop and interloop interaction parameters defined in (33) and a_c is the critical value of a at which the stability curve that is given by lower envelope $\mathcal{L}(a)$ defined in (82) transitions from a polygonal curve to a straight line. For $a = 0.6$, $\mathcal{L}(a)$ is constituted by modes $n = 2, 3, 4, 5$, and 6 for ζ in intervals 0 and ζ_2, ζ_2 and ζ_3, ζ_3 and ζ_4, ζ_4 and ζ_5, and ζ_5 and 10^5, respectively. Dominant eigenshapes and their dimensionless energies (20) in these intervals of ζ are shown. For $a = 0.9$, $\mathcal{L}(a)$ is a straight line constituted only by mode $n = 2$ for all the values of $\zeta \geq 0$. For each a, the trivial solution is stable below the corresponding stability curve.

3.6.3. Discussion of cross-over behavior

The presence of a crossover between polygonal and straight stability curves can be explained by comparing the total energy of the loops perturbed in different modes. The dimensionless bending and intraloop interaction energies of a loop with dimensionless radius a subject to a perturbation involving only mode n increase and decrease monotonically with n, respectively. However, the dimensionless interloop interaction energy depends nontrivially on the dimensionless vertical gap $2\sqrt{1-a^2}$ between the loops and the mode n. Below a certain critical value of a, we find that the dimensionless interloop interaction energy decreases with n, in which case the total dimensionless energy for mode $n = 2$ may exceed that for some higher mode $n > 2$. In that connection, we see from Fig. 5 that, for $a = 0.6$, in the interval $\zeta_{n-1} < \zeta < \zeta_n$, $n = 2, \ldots, 6$, the total dimensionless energy of the loops is minimized if they are perturbed by mode n. Consistent with that observation, the stability curve consists of line segments corresponding to different modes. Also, for a exceeding the aforementioned threshold, the dimensionless interloop interaction energy increases with n and exhibits a dependence on n that is qualitatively identical to that of the dimensionless bending energy. Consequently, as a approaches a_c, the instability is dominated by repulsive interactions between the loops and the total dimensionless energy is minimized if the loops are subjected to perturbations involving only mode $n = 2$. Under these circumstances, the stability curve is simply the straight line $\mathcal{L}_2(a)$ associated with that mode.

From Fig. 5, we see that, for any admissible value of ζ, the corresponding critical value of χ for $a = 0.9$ is below that for $a = 0.6$. This observation is consistent with the understanding that, as a increases, the dimensionless vertical gap $2\sqrt{1-a^2}$ between the loops decreases, resulting in a concommitant increase in the repulsion between the loops. The value of χ that is required to destabilize the trivial configuration therefore decreases as a increases. A stability plot for $0.01 \leq a \leq 0.98$ is provided in Fig. B.9 of Appendix B.

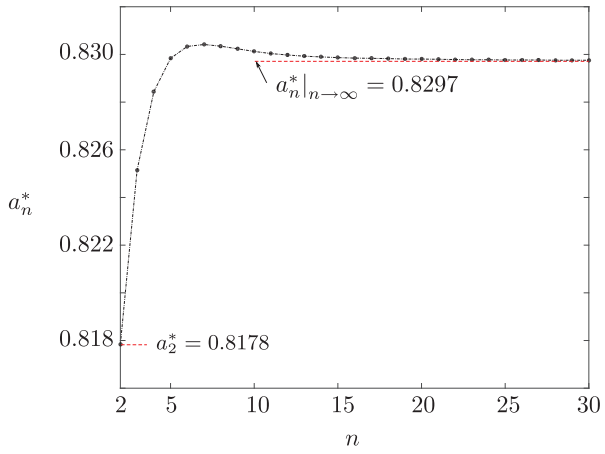

Fig. 6. Plot of n vs a_n^*, where n is mode number and a_n^* is the asymptotic value of a as $\zeta \to \infty$ in (88), where a is the dimensionless radius defined in (32) and ζ is the dimensionless intraloop interaction parameter defined in $(33)_1$. a_n^* is obtained by solving $\alpha_n(a_n^*) = 1$, where α_n is defined in $(B.35)_1$. For a given n, if a is in the interval $0 < a \le a_n^*$, then, $\alpha_n(a) \ge 1$ and therefore the stability condition (86) is satisfied for all values of $\zeta \ge 0$ if the trivial solution (47)–(49) is perturbed by mode n. With $a_n^* > a_2^*$ for all $n > 2$, (86) is satisfied for all $\zeta \ge 0$ and $n \ge 2$ if $0 < a \le a_2^*$.

3.7. Stability results for $\chi = \zeta$

If the interloop and intraloop interaction parameters χ and ζ are equal, we may replace χ by ζ in the stability criterion (79), giving

$$\beta_n(a) + (\alpha_n(a) - 1)\zeta \ge 0, \qquad n \ge 2. \tag{86}$$

For any admissible value of a, the trivial solution is unstable with respect to a perturbation of mode $n \ge 2$ if there exists a critical value of ζ for which (86) is satisfied as an equality. Recalling from $(80)_2$ that $\beta_n(a) > 0$ for all a, we see from (86) that no such critical value exists if α_n satisfies $\alpha_n(a) > 1$. This finding exposes a fundamental difference between the stability of the trivial solution for the alternative cases $\chi = \zeta$ and $\chi \ne \zeta$. For $\chi = \zeta$, the critical value of ζ is purely geometrical in the sense that, for each mode n, it is completely determined by the dimensionless radius a of the loops. This allows for the possibility that no such critical value exists for some combination of those parameters. Consistent with arguments provided after (80), it is always possible to find a combination of ζ and χ with $\chi \ne \zeta$ such that the stability condition (79) is violated regardless of the values of a and n.

We next show that for each $n \ge 2$, there exist a value of a such that $\alpha_n(a) > 1$. Using $(B.38)_1$ and $(B.41)_1$ of B.5, we find that

$$\lim_{a \downarrow 0} \alpha_n(a) \to \infty \qquad \text{and} \qquad \lim_{a \uparrow 1} \alpha_n(a) \to 0, \tag{87}$$

for each $n \ge 2$. Since α_n depends continuously on its argument for each $n \ge 2$, we thus infer that there exists a value a_n^* of a such that $\alpha_n(a) \ge 1$ for each $n \ge 2$ and $0 < a \le a_n^*$. In particular, for the choice (83) of the mollifier M, we find numerically that $a_2^* = 0.8178 < a_n^*$ for all $n > 2$. It thus follows that the trivial solution is stable for $0 < a \le a_2^*$ and for all admissible values of ζ. A plot of n versus a_n^* is shown in Fig. 6.

For each mode $n \ge 2$ and each $a_2^* < a < 1$, the curve

$$\mathcal{L}_n^* = \left\{ (\zeta, a) : a_2^* < a < 1, \zeta = \frac{\beta_n(a)}{1 - \alpha_n(a)} \right\} \tag{88}$$

in the (ζ, a)-plane, generated by replacing the inequality of (86) with an equality determines the critical combinations of $\zeta \ge 0$ and $a_2^* < a < 1$ at which the trivial configuration becomes unstable when subjected to perturbation involving only mode n.

Taking into consideration that the family $\{\mathcal{L}_n^* : n \ge 2\}$ of curves determined by (88) may intersect at one or more points, we conclude that for loops of radius $a_2^* < a < 1$ the trivial equilibrium configuration is linearly stable only if ζ lies on or below the lower envelope

$$\mathcal{L}^* = \left\{ (\zeta, a) : a_2^* < a < 1, \zeta = \min_{n \ge 2} \frac{\beta_n(a)}{1 - \alpha_n(a)} \right\}. \tag{89}$$

of that family. Since the trivial equilibrium configuration for loops that are linearly unstable for any combination of $\zeta \ge 0$ and $a_2^* < a < 1$ that lies above $\mathcal{L}^*$, we refer to $\mathcal{L}^*$ as the stability curve for the relevant value of a. Granted the particular choice (83) of the mollifier M, we find numerically that $\mathcal{L}^*$ consists only of the curve $\mathcal{L}_2^*$ given by (88).

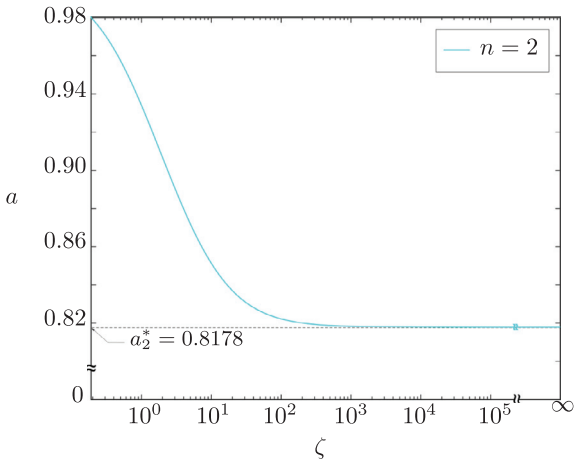

Fig. 7. Stable combinations of (ζ, a) for $\chi = \zeta$ lie on or below the stability curve that satisfies (88), where a is dimensionless radius defined in (32), ζ and χ are dimensionless intraloop and interloop interaction parameters defined in (33). For $0 < a \leq a_2^*$, where a_2^* is asymptotic value of a in (88) as $\zeta \to \infty$ and $n = 2$, the trivial solution is stable for all values of $\zeta \geq 0$.

Since $a_2^* > a_c$, consistent with discussion in Section 3.6.3, the total dimensionless energy of the loops is minimized if subjected to a perturbation involving only mode $n = 2$. Therefore, the trivial solution becomes first unstable if subjected to a perturbation involving only that mode and $\mathcal{L}^* = \mathcal{L}_2^*$, as shown in Fig. 7.

3.8. Bifurcation from the trivial solution

In our setting, the implicit function theorem (as stated, for example, by Golubitsky et al. (2012) and Chen (2001)) ensures that the dimensionless boundary-value problem consisting of (4) and (42) has a nontrivial solution branch that bifurcates from the trivial solution branch characterized by (47) and (62)–(64) only if the boundary-value problem obtained by linearizing (4) and (42) about (47) and (62)–(64) has a nontrivial solution. To explore the existence of such nontrivial solutions for combinations of the dimensionless radius a, dimensionless intraloop interaction parameter ζ, and dimensionless interloop interaction parameter χ, we proceed as in Subsection 3.5 and take $\boldsymbol{n}_1$ and $\boldsymbol{n}_2$ to be given by

$$\boldsymbol{n}_1 = \boldsymbol{n}_0 + \boldsymbol{\nu} \qquad \text{and} \qquad \boldsymbol{n}_2 = \boldsymbol{K}(\boldsymbol{n}_0 - \boldsymbol{\nu}), \qquad |\boldsymbol{\nu}| \ll 1, \tag{90}$$

where $\boldsymbol{n}_0$ is defined in (48) and where $\boldsymbol{\nu}$ satisfies the admissibility conditions (68). Furthermore, we assume that the Lagrange multipliers Λ_i and λ_i, $i = 1, 2$, are given by

$$\Lambda_i = \Lambda + \Sigma_i \qquad \text{and} \qquad \lambda_i = \Lambda + \sigma_i, \qquad |\Sigma_i| \ll 1, \qquad |\sigma_i| \ll 1, \qquad i = 1, 2, \tag{91}$$

where Λ and λ are given by (62) and (64), respectively. Substituting (90) and (91) into the equilibrium conditions (42), neglecting terms of quadratic and higher order in $\boldsymbol{\nu}$, Σ_i, and σ_i, $i = 1, 2$, and their various derivatives, we obtain linearized equations of equilibrium in the form

$$\left.\begin{aligned} &\boldsymbol{\nu}'''' + \lambda\boldsymbol{\nu}'' + \Lambda\boldsymbol{\nu} + \sigma_1'\boldsymbol{n}_0' + \sigma_1\boldsymbol{n}_0'' + \Sigma_1\boldsymbol{n}_0 = \zeta\,\tilde{\boldsymbol{\vartheta}}[\boldsymbol{n}_0, \boldsymbol{n}_0](\boldsymbol{\nu}, \boldsymbol{\nu}) + \chi\,\boldsymbol{\vartheta}[\boldsymbol{n}_0, \boldsymbol{K}\boldsymbol{n}_0](\boldsymbol{\nu}, -\boldsymbol{K}\boldsymbol{\nu}), \\ &\boldsymbol{\nu}'''' + \lambda\boldsymbol{\nu}'' + \Lambda\boldsymbol{\nu} + \sigma_2'\boldsymbol{n}_0' + \sigma_2\boldsymbol{n}_0'' + \Sigma_2\boldsymbol{n}_0 = -\zeta\boldsymbol{K}\tilde{\boldsymbol{\vartheta}}[\boldsymbol{K}\boldsymbol{n}_0, \boldsymbol{K}\boldsymbol{n}_0](-\boldsymbol{K}\boldsymbol{\nu}, -\boldsymbol{K}\boldsymbol{\nu}) - \chi\boldsymbol{K}\boldsymbol{\vartheta}[\boldsymbol{K}\boldsymbol{n}_0, \boldsymbol{n}_0](-\boldsymbol{K}\boldsymbol{\nu}, \boldsymbol{\nu}), \end{aligned}\right\} \tag{92}$$

where $\boldsymbol{\vartheta}$ and $\tilde{\boldsymbol{\vartheta}}$ are defined in (29) and (45a), respectively. Referring to the properties (50) of $\boldsymbol{K}$, we see from (B.3) and (B.5) that

$$\left.\begin{aligned} &-\boldsymbol{K}\tilde{\boldsymbol{\vartheta}}[\boldsymbol{K}\boldsymbol{n}_0, \boldsymbol{K}\boldsymbol{n}_0](-\boldsymbol{K}\boldsymbol{\nu}, -\boldsymbol{K}\boldsymbol{\nu}) = \tilde{\boldsymbol{\vartheta}}[\boldsymbol{n}_0, \boldsymbol{n}_0](\boldsymbol{\nu}, \boldsymbol{\nu}), \\ &-\boldsymbol{K}\boldsymbol{\vartheta}[\boldsymbol{K}\boldsymbol{n}_0, \boldsymbol{n}_0](-\boldsymbol{K}\boldsymbol{\nu}, \boldsymbol{\nu}) = \boldsymbol{\vartheta}[\boldsymbol{n}_0, \boldsymbol{K}\boldsymbol{n}_0](\boldsymbol{\nu}, -\boldsymbol{K}\boldsymbol{\nu}). \end{aligned}\right\} \tag{93}$$

Using (93) to simplify $(92)_2$ and comparing the resulting equation with $(92)_1$, we arrive at the condition

$$\sigma_1'\boldsymbol{n}_0' + \sigma_1\boldsymbol{n}_0'' + \Sigma_1\boldsymbol{n}_0 = \sigma_2'\boldsymbol{n}_0' + \sigma_2\boldsymbol{n}_0'' + \Sigma_2\boldsymbol{n}_0. \tag{94}$$

Applying arguments analogous to those needed to obtain (55) and (56), we see from (94) that

$$\sigma_1 = \sigma_2 = \sigma \qquad \text{and} \qquad \Sigma_1 = \Sigma_2 = \Sigma. \tag{95}$$

From (93) and (95), we find that the linearized equilibrium equations $(92)_{1\text{–}2}$ reduce to a single equation

$$\boldsymbol{\nu}'''' + \lambda\boldsymbol{\nu}'' + \Lambda\boldsymbol{\nu} + \sigma'\boldsymbol{n}_0' + \sigma\boldsymbol{n}_0'' + \Sigma\boldsymbol{n}_0 = \zeta\,\tilde{\boldsymbol{\vartheta}}[\boldsymbol{n}_0, \boldsymbol{n}_0](\boldsymbol{\nu}, \boldsymbol{\nu}) + \chi\,\boldsymbol{\vartheta}[\boldsymbol{n}_0, \boldsymbol{K}\boldsymbol{n}_0](\boldsymbol{\nu}, -\boldsymbol{K}\boldsymbol{\nu}), \tag{96}$$

which must be supplemented by the conditions (68) needed to ensure that $\boldsymbol{v}$ is admissible, which we repeat here for completeness:

$$\boldsymbol{n}_0 \cdot \boldsymbol{v} = 0, \qquad \boldsymbol{n}_0' \cdot \boldsymbol{v}' = 0. \tag{97}$$

Together, (96) and (97) provide a system for determining the increments $\boldsymbol{v}$, Σ, and σ. Consistent with the assumptions in the linear stability analysis detailed in Section 3.5, we assume that $\boldsymbol{v}$ is superimposition of orthogonal functions $\boldsymbol{v}_n$, $n \geq 2$, as defined in (70) and that $\boldsymbol{v}_n$ is given by a single scalar function ψ_n, as indicated in (77). We also assume that Σ and σ admit Fourier decompositions

$$\Sigma = \sum_{n=2}^{\infty} \Omega_n, \qquad \Omega_n(s) = u_n \cos\frac{ns}{a} + v_n \sin\frac{ns}{a}, \tag{98}$$

and

$$\sigma = \sum_{n=2}^{\infty} \omega_n, \qquad \omega_n(s) = p_n \cos\frac{ns}{a} + q_n \sin\frac{ns}{a}. \tag{99}$$

As a convenient consequence of these assumptions, the adhesion constraint and the inextensibility constraint in (97) are trivially satisfied.

Substituting (70), $(98)_1$, and $(99)_1$ in (100), we find that $\boldsymbol{v}_n$ must obey

$$\boldsymbol{v}_n'''' + \lambda \boldsymbol{v}_n'' + \Lambda \boldsymbol{v}_n + \omega_n' \boldsymbol{n}_0' + \omega_n \boldsymbol{n}_0'' + \Omega_n \boldsymbol{n}_0 = \zeta\, \tilde{\boldsymbol{\vartheta}}[\boldsymbol{n}_0, \boldsymbol{n}_0](\boldsymbol{v}_n, \boldsymbol{v}_n) + \chi\, \boldsymbol{\vartheta}[\boldsymbol{n}_0, \boldsymbol{K}\boldsymbol{n}_0](\boldsymbol{v}_n, -\boldsymbol{K}\boldsymbol{v}_n), \tag{100}$$

for each mode $n \geq 2$. Resolving (100) along the directions of $\boldsymbol{e}$, $\boldsymbol{k}$, and $\boldsymbol{k} \times \boldsymbol{e}$, and using the linear independence of the Fourier basis, we obtain, for each mode $n \geq 2$, a homogenous system,

$$\begin{bmatrix} 0 & \Theta_n & -\frac{1}{a} & 0 & a & 0 \\ -\Theta_n & 0 & 0 & -\frac{1}{a} & 0 & a \\ 0 & \Pi_n & 0 & 0 & 1-a^2 & 0 \\ -\Pi_n & 0 & 0 & 0 & 0 & 1-a^2 \\ \Psi_n & 0 & 0 & \frac{n}{a} & 0 & 0 \\ 0 & \Psi_n & -\frac{n}{a} & 0 & 0 & 0 \end{bmatrix} \begin{bmatrix} c_n \\ d_n \\ p_n \\ q_n \\ u_n \\ v_n \end{bmatrix} = \begin{bmatrix} 0 \\ 0 \\ 0 \\ 0 \\ 0 \\ 0 \end{bmatrix}, \tag{101}$$

for the amplitudes c_n, d_n, p_n, q_n, u_n, and v_n, where Θ_n, Π_n, and Ψ_n defined in (C.4) vary with ζ, χ, and a. The boundary-value problem consisting of (4) and (42) has a nontrivial solution if and only if the determinant of the coefficient matrix in (101) vanishes. Referring to Appendix C, where we compute that determinant, we find that the bifurcation points are given by

$$\chi = \alpha_n(a)\zeta + \beta_n(a). \tag{102}$$

The condition (102) for determining the bifurcation points is identical to the condition for marginal stability obtained by replacing the inequality (79) with an equality. In that regard, we observe that the inequality

$$\int_0^{2\pi a} (|\boldsymbol{v}''|^2 - \lambda|\boldsymbol{v}'|^2 + \Lambda|\boldsymbol{v}|^2 - \sigma \boldsymbol{n}_0' \cdot \boldsymbol{v}' + \Sigma \boldsymbol{n}_0 \cdot \boldsymbol{v} - \zeta\, \tilde{\boldsymbol{\vartheta}}[\boldsymbol{n}_0, \boldsymbol{n}_0](\boldsymbol{v}, \boldsymbol{v}) \cdot \boldsymbol{v} - \chi\, \boldsymbol{\vartheta}[\boldsymbol{n}_0, \boldsymbol{K}\boldsymbol{n}_0](\boldsymbol{v}, -\boldsymbol{K}\boldsymbol{v}) \cdot \boldsymbol{v})\, \mathrm{d}s \geq 0, \tag{103}$$

that stems from adding $-\sigma \boldsymbol{n}_0' \cdot \boldsymbol{v}'$ and $\Sigma \boldsymbol{n}_0 \cdot \boldsymbol{v}$, with σ and Σ being given by (95), to the left-hand side of the reduced stability condition (69) is identical to (69). Integrating by parts on the basis of the identities

$$\sigma \boldsymbol{n}_0' \cdot \boldsymbol{v}' = (\sigma \boldsymbol{n}_0' \cdot \boldsymbol{v})' - \sigma' \boldsymbol{n}_0' \cdot \boldsymbol{v} - \sigma \boldsymbol{n}_0'' \cdot \boldsymbol{v}, \qquad |\boldsymbol{v}''| = (\boldsymbol{v}'' \cdot \boldsymbol{v}')' - (\boldsymbol{v}''' \cdot \boldsymbol{v})' + \boldsymbol{v}'''' \cdot \boldsymbol{v}, \qquad \boldsymbol{v}' \cdot \boldsymbol{v}' = (\boldsymbol{v}' \cdot \boldsymbol{v})' - \boldsymbol{v}'' \cdot \boldsymbol{v}, \tag{104}$$

we find that (103) is equivalent to

$$\int_0^{2\pi a} (\boldsymbol{v}'''' + \lambda \boldsymbol{v}'' + \Lambda \boldsymbol{v} + \sigma' \boldsymbol{n}_0' + \sigma \boldsymbol{n}_0'' + \Sigma \boldsymbol{n}_0 - \zeta\, \tilde{\boldsymbol{\vartheta}}[\boldsymbol{n}_0, \boldsymbol{n}_0](\boldsymbol{v}, \boldsymbol{v}) - \chi\, \boldsymbol{\vartheta}[\boldsymbol{n}_0, \boldsymbol{K}\boldsymbol{n}_0](\boldsymbol{v}, -\boldsymbol{K}\boldsymbol{v})) \cdot \boldsymbol{v}\, \mathrm{d}s \geq 0. \tag{105}$$

Granted that $\boldsymbol{v}$ satisfies the linearized equilibrium equation (96), the left-hand side of (105) vanishes and, thus, the stability condition holds as an equality. Calculations in Appendix C confirm that the solvability criterion for (101) yields the same condition that, in keeping with the discussion in the paragraph containing (81), determines the critical combinations of ζ and χ at which the trivial configuration becomes unstable when subjected to perturbation involving mode n.

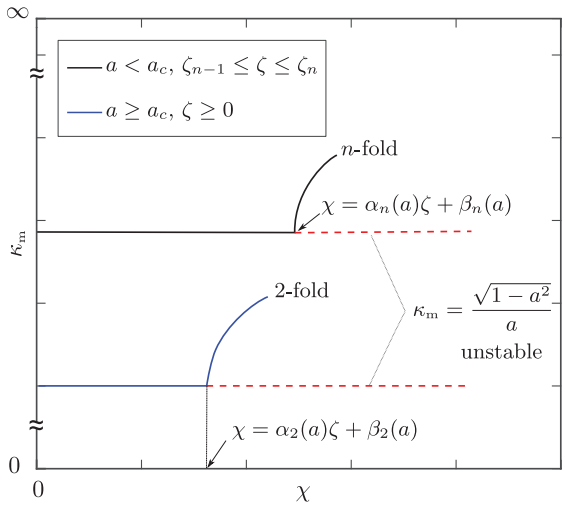

Fig. 8. Schematic of bifurcation diagram in (χ, κ_m)-plane for $a < a_c$ and $a \ge a_c$, where ζ and χ are dimensionless intraloop and interloop interaction parameters defined in (33), a is dimensionless radius defined in (32), κ_m, which depends on a, is the average geodesic curvature of the equilibrium configurations, a_c is value of a at which the lower envelope (stability curve) $\mathcal{L}(a)$ defined in (82) transitions from polygonal to a straight line. For the trivial branch parameterized by (47)–(49), $\kappa_m = \sqrt{1-a^2}/a$ for all $\chi \ge 0$. For given a, κ_m for non-trivial branch increases with χ as explained after (108). For $0 < a < a_c$ and ζ in interval 0 and ζ_2, trivial solution will buckle into mode 2 if χ exceeds the critical value defined in (106) and if ζ is in interval $\zeta_{n-1} < \zeta < \zeta_n$, $n > 2$, trivial solution will buckle into mode n if χ exceeds the critical value defined in (107). For $a_c \le a < 1$ and any given value of $\zeta \ge 0$, the trivial solution first buckles in mode $n = 2$ as χ exceeds the threshold value given by (108).

3.9. Bifurcation results for a particular mollification of the dimensionless self potential

For the choice (83) of M, $0 < a < a_c$ and each mode $n \ge 2$, we find that the bifurcation points (ζ, χ) determined by (102) are given by

$$\{(\zeta, \chi) : 0 \le \zeta \le \zeta_2(a),\ \chi = \alpha_2(a)\zeta + \beta_2(a)\} \tag{106}$$

and

$$\{(\zeta, \chi) : \zeta_{n-1}(a) \le \zeta \le \zeta_n(a),\ \chi = \alpha_n(a)\zeta + \beta_n(a)\}, \qquad n > 2. \tag{107}$$

Thus, the mode $n \ge 2$ for which the trivial equilibrium configuration first buckles varies with the value of ζ. If, in particular, ζ satisfies $\zeta_{n-1}(a) < \zeta < \zeta_n(a)$, then the trivial equilibrium configuration first buckles in response to perturbations involving mode $n \ge 2$ and the corresponding value of χ at which that occurs is $\chi = \alpha_n(a)\zeta + \beta_n(a)$.

For $a_c \le a < 1$, regardless of value of ζ, the trivial configuration first buckles in response to perturbations involving only mode $n = 2$ and the bifurcation points (ζ, χ) for dimensionless radius a are given by

$$\{(\zeta, \chi) : \zeta \ge 0,\ \chi = \alpha_2(a)\zeta + \beta_2(a)\}. \tag{108}$$

In Fig. 8, we present a schematic bifurcation diagram covering both cases $0 < a < a_c$ and $a_c \le a < 1$. The abscissa κ_m of the diagram refers to the average geodesic curvature of the loops in equilibrium. For a trivial solution, $\kappa_m = \sqrt{1-a^2}/a$ for each $0 < a < 1$. For a non-trivial solution, however, κ_m is necessarily greater than $\sqrt{1-a^2}/a$. Moreover, the competition between the repulsive interaction between the loops and the adhesion and the inextensibility constraints generates more undulations as χ increases. Although the bending energy increases with κ_m, for large values of χ, the interloop interaction energy decreases, leading to a total energy less than that of the trivial solution.

3.10. Bifurcation analysis for $\chi = \zeta$

Recalling from Section 3.7 that, for $\chi = \zeta$, the trivial solution is stable for all admissible values of ζ if $0 < a \le a_2^*$, we see that a nontrivial solution branch cannot exist for $0 < a \le a_2^*$. Hence, a stable bifurcation to a nontrivial solution branch can occur only for $a_2^* < a < 1$. To explore that possibility, we substitute $\chi = \zeta$ in (102), take the mollifier M to be of the particular form (83), and use numerical methods to find that the bifurcation points are given by

$$\left\{(\zeta, a) : a_2^* < a < 1, \zeta = \frac{\beta_2(a)}{1 - \alpha_2(a)}\right\}. \tag{109}$$

On the basis of these findings, we see that, for $\chi = \zeta$ and $a_2^* < a < 1$, the trivial solution first buckles if subjected to a perturbation by mode $n = 2$.

4. Summary and discussion

We used a variational approach to study the equilibrium configuration and stability behavior of two closed, inextensible, interacting loops endowed with bending energy and constrained to a lie on a sphere. This amounts to an extension of works by Langer and Singer (1984) and Arroyo et al. (2003, 2004, 2006, 2010) to a setting where the loops are additionally endowed with interaction potentials and is inspired by relevance in novel technological applications such as synthesis of thin organic films (Sukhorukov et al., 1998) and in biology where charged filament like structures adhering to a curved surface is commonplace, as exemplified by the confinement of DNA molecules onto histone-octamer (Nelson et al., 2008, Chapter 24), and charged apolipoproteins on HDL surfaces (Gursky, 2013; Huang et al., 2011; Mei and Atkinson, 2011; Silva et al., 2008; 2007).

After deriving equilibrium equations and stability condition for loops interacting with themselves and with each other through general distance-dependent potentials, we applied our framework to situations in which the loops have identical lengths, bending stiffnesses, and uniform, positive charge densities. As a consequence of the latter simplification, all interactions are Coulombic. For this application, there is a trivial solution in which the loops are parallel and circular. The stability of that solution depends on the dimensionless ratio $0<a<1$ of the radius of the circular loops to the radius of the sphere, the dimensionless intraloop interaction parameter $\zeta\geq 0$, and the dimensionless interloop interaction parameter $\chi\geq 0$. From Figs. 5 and B.9, it is evident that for any admissible value of ζ, increasing a diminishes the range of stable values of χ and favors instability. This occurs because as a increases, the vertical gap between the loops decreases, increasing the repulsive effects between the loops. The value of χ required to destabilize the trivial equilibrium configuration therefore diminishes. Also, for any admissible value of a, increasing ζ increases the range of stable values of χ and favors stability. This occurs because as ζ increases, intraloop repulsion combines with the resistance to bending to stabilize circular configurations. The value of χ required to overcome intraloop interaction therefore increases. Having determined the stable combinations of the parameters a, ζ, and χ, we learn that, consistent with intuitive expectations, the bending energy and the intraloop interaction energy are stabilizing but the interloop repulsion is destabilizing. We also establish the existence of a critical value $a_c\approx 0.74$ of a such that for $0<a<a_c$, the mode $n\geq 2$ with respect to which the trivial solution first becomes unstable varies with ζ. However, if $a_c\leq a<1$, the trivial solution first becomes unstable if perturbed by mode $n=2$ for all admissible values of ζ. We attribute this change in the dominant mode to a switch in the behavior of interloop interaction energy with mode number n which occurs as the vertical gap between the two circular loops decreases. If a is below certain a threshold, or, analogously, if the vertical gap is above a certain threshold, the interloop interaction energy of the loops decreases monotonically with n. Therefore, the competition between the repulsive interloop interaction and the bending resistance determines the dominant mode of instability. If, however, the vertical gap is below that threshold level, the interloop interaction energy increases monotonically with n, in which case the first unstable mode $n=2$ is favored not only by the bending energy but also by the interloop interaction energy. We thus see that the qualitative behavior of two charged elastic loops confined to a sphere differs substantially from that of a purely elastic loop confined to a sphere. Whereas a purely elastic loop confined to a sphere always buckles when subjected to perturbations involving only mode $n=2$, the buckling behavior of two charged elastic loops confined to a sphere is more complex and the dominant buckling mode depends on the vertical gap between the loops and the charge densities of the loops.

We also conducted a linear bifurcation analysis and found the bifurcation points at which the trivial solution first becomes unstable and the loops adopt noncircular configurations. A schematic of the bifurcation diagram is provided in Fig. 8. Although the bifurcation analysis performed here is inadequate for predicting the final shapes of any buckled solution, we conjecture that, consistent with many other problems in structural mechanics, the shape of the buckled solution should be dominated by the first unstable mode. We also explored what occurs if $\chi=\zeta$ and found that for $0<a\leq a_2^*$, the trivial solution is stable for all admissible values of intraloop interaction parameter ζ. Here, a_2^* denotes the asymptotic value of a as $\zeta\to\infty$ at which the trivial solution becomes unstable if perturbed by mode $n=2$. For $0<a\leq a_2^*$, the vertical gap between the loops is large enough to ensure that interloop repulsion cannot overcome effects associated with bending resistance and intraloop repulsion. However, for $a_2^*<a<1$, the trivial solution is first destabilized if perturbed by mode $n=2$. This behavior is in qualitative agreement with classical results for stability of a purely elastic loop.

We have examined the stability of the class of trivial solutions, which exist only if $0<a<1$. In future work, we plan to consider all possible choices of $a>0$ and to use numerical methods to construct nontrivial solutions and to study their stability. We further plan to investigate whether the bifurcation branches from the nontrivial solution branch are continuous or disconnected. In the latter case, a finite perturbation would be required to induce buckling. Another possible extension of the present work would be to conduct a stability analysis of trivial solutions that allows for arbitrary independent perturbations of the loops. If successful, such an analysis would provide the exact threshold for the critical parameter χ and settle the issue of whether or not an analysis based on the restricted class (67) of perturbations suffices to determine that threshold.

We have provided results for the specialized case when the interaction potentials are Coloumbic and the loops that are uniformly charged. We anticipate that it might be beneficial to study the system for Lennard–Jones-type potentials and to consider nonuniformly charged loops. We anticipate that nonuniform charge distribution might generate perturbations that induce buckling modes, serving much as imperfections do in conventional studies of buckling and postbuckling.

In this work, we impose the kinematic constraint $(4)_1$ to ensure that the loops adhere to the sphere. If the loops and the sphere cannot sustain the adhesive reaction that is required to satisfy $(4)_1$, then detachment will occur. Our purpose has not

been to model situations where the loops detach from the sphere. To do that, it would be necessary to relax the kinematic constraint $(4)_1$ and to reparameterize the loops in a way that allows for detachment. To avoid unphysical situations in which the loops penetrate the sphere, we would also need to impose a pointwise, unilateral constraint on the loops. To provide a flavor for how this would be achieved, let the each loop $\mathcal{C}_i$, $i = 1, 2$, be parameterized by

$$\mathcal{C}_i = \{\boldsymbol{r} : \boldsymbol{r} = R\boldsymbol{d}_i(s), 0 \leq s \leq \ell_i\}, \tag{110}$$

where, as before, s represents the dimensionless arclength on each loop, $\boldsymbol{d}_i$ is three-times continuously differentiable, ℓ_i is the dimensionless length of the loop defined in (18), and R is the radius of the sphere $\mathcal{S}$. As consequences of the assumed smoothness, we would have the closure conditions

$$\boldsymbol{d}_i(0) = \boldsymbol{d}_i(\ell_i), \qquad \boldsymbol{d}_i'(0) = \boldsymbol{d}_i'(\ell_i), \qquad \boldsymbol{d}_i''(0) = \boldsymbol{d}_i''(\ell_i), \qquad \text{and} \qquad \boldsymbol{d}_i'''(0) = \boldsymbol{d}_i'''(\ell_i), \qquad i = 1, 2, \tag{111}$$

where a prime denotes differentiation with respect to arclength. To ensure that the loops do not penetrate $\mathcal{S}$ and are inextensible, we would stipulate that

$$|\boldsymbol{d}_i| \geq 1 \qquad \text{and} \qquad |\boldsymbol{d}_i'| = 1. \tag{112}$$

It would also be necessary to penalize any detachment with a sphere-loop adhesion energy term. A simple way to incorporate that effect would be to consider an energy density proportional to square of the shortest distance between the loops and the sphere, in which case the dimensionless sphere-loop adhesion energy would take the form

$$\mathcal{F}_{\text{adh}}[\boldsymbol{d}_1, \boldsymbol{d}_2] = \frac{\gamma_1}{2}\int_0^{\ell_1}(|\boldsymbol{d}_1| - 1)^2\,\mathrm{d}s + \frac{\gamma_2}{2}\int_0^{\ell_2}(|\boldsymbol{d}_2| - 1)^2\,\mathrm{d}s, \tag{113}$$

where γ_1 and γ_2 represent dimensionless measures of adhesive energy. The total dimensionless energy functional in (20) would then be replaced by

$$\hat{\mathcal{F}} = \mathcal{F}_{\text{B}} + \mathcal{F}_{\text{S}} + \mathcal{F}_{\text{I}} + \mathcal{F}_{\text{adh}}, \tag{114}$$

where $\mathcal{F}_{\text{B}}$, $\mathcal{F}_{\text{S}}$, and $\mathcal{F}_{\text{I}}$ are as defined in (21).

In view of the Karush–Kuhn–Tucker (Karush, 1939; Kuhn and Tucker, 1951) condition for constrained optimization, an extremizer of the total energy functional $\hat{\mathcal{F}}$ subjected to (112) would be given by solving the optimality conditions

$$\left.\begin{aligned}(\boldsymbol{d}_1''' + \tilde{\lambda}_1\boldsymbol{d}_1')' - \tilde{\Lambda}_1\boldsymbol{d}_1 + \gamma_1\boldsymbol{d}_1\left(1 - \frac{1}{|\boldsymbol{d}_1|}\right) - \zeta_1\boldsymbol{\varphi}_{11}[\boldsymbol{d}_1, \boldsymbol{d}_1] - \chi\boldsymbol{\varphi}_{12}[\boldsymbol{d}_1, \boldsymbol{d}_2] = \boldsymbol{0},\\ \nu(\boldsymbol{d}_2''' + \tilde{\lambda}_2\boldsymbol{d}_2')' - \tilde{\Lambda}_2\boldsymbol{d}_2 + \gamma_2\boldsymbol{d}_2\left(1 - \frac{1}{|\boldsymbol{d}_2|}\right) - \zeta_2\boldsymbol{\varphi}_{22}[\boldsymbol{d}_2, \boldsymbol{d}_2] - \chi\boldsymbol{\varphi}_{21}[\boldsymbol{d}_2, \boldsymbol{d}_1] = \boldsymbol{0},\end{aligned}\right\} \tag{115}$$

together with the feasibility conditions

$$1 - |\boldsymbol{d}_1|^2 \leq 0, \qquad 1 - |\boldsymbol{d}_2|^2 \leq 0, \qquad |\boldsymbol{d}_1'|^2 - 1 = 0, \qquad \text{and} \qquad |\boldsymbol{d}_1'|^2 - 1 = 0, \tag{116}$$

which result from (112), the non-negativity conditions

$$\tilde{\Lambda}_1 \geq 0 \quad \text{and} \quad \tilde{\Lambda}_2 \geq 0, \tag{117}$$

and the complementarity conditions

$$\tilde{\Lambda}_1(1 - |\boldsymbol{d}_1|^2) = 0 \quad \text{and} \quad \tilde{\Lambda}_1(1 - |\boldsymbol{d}_1|^2) = 0 \tag{118}$$

for $\boldsymbol{d}_1$, $\boldsymbol{d}_2$, $\tilde{\lambda}_1$, $\tilde{\lambda}_2$, $\tilde{\Lambda}_1$, and $\tilde{\Lambda}_2$. Here, ν, ζ_1, ζ_2, χ are the dimensionless parameters defined in (19), γ_1 and γ_2 are the dimensionless sphere-loop adhesion constants, $\boldsymbol{\varphi}_{11}$, $\boldsymbol{\varphi}_{22}$, and $\boldsymbol{\varphi}_{12}$ are defined in (26), and $\tilde{\Lambda}_i$ and $\tilde{\lambda}_i$, $i = 1, 2$, are the Kuhn–Tucker–Karush multipliers that respectively ensure that $(112)_1$ and $(112)_2$ hold.

As $|\boldsymbol{d}_i| \to 1$, $i = 1, 2$, the optimality conditions in (115) become

$$\left.\begin{aligned}(\boldsymbol{d}_1''' + \tilde{\lambda}_1\boldsymbol{d}_1')' - \tilde{\Lambda}_1\boldsymbol{d}_1 = \zeta_1\boldsymbol{\varphi}_{11}[\boldsymbol{d}_1, \boldsymbol{d}_1] + \chi\boldsymbol{\varphi}_{12}[\boldsymbol{d}_1, \boldsymbol{d}_2],\\ \nu(\boldsymbol{d}_2''' + \tilde{\lambda}_2\boldsymbol{d}_2')' - \tilde{\Lambda}_2\boldsymbol{d}_2 = \zeta_2\boldsymbol{\varphi}_{22}[\boldsymbol{d}_2, \boldsymbol{d}_2] + \chi\boldsymbol{\varphi}_{21}[\boldsymbol{d}_2, \boldsymbol{d}_1],\end{aligned}\right\} \tag{119}$$

which by replacing $\tilde{\Lambda}_1$ with $-\Lambda_1$ and $\tilde{\Lambda}_2$ with $-\Lambda_2$, is identical to (25). This demonstrates how the constrained approach taken in this work arises as a limit of perfect adhesion from a model that accounts for adhesive energy.

Declaration of Competing Interest

All authors have participated in (a) conception and design, or analysis and interpretation of the data; (b) drafting the article or revising it critically for important intellectual content; and (c) approval of the final version.

Acknowledgements

The authors gratefully acknowledge support from the Okinawa Institute of Science and Technology Graduate University with subsidy funding from the Cabinet Office, Government of Japan. They also thank Steven Aird for editorial advice.

Appendix A. Detailed derivations of the first and second variation conditions

A.1. Preliminary identities

The first variations of the adhesion constraint $\boldsymbol{n}_i \cdot \boldsymbol{n}_i = 1$ and the inextensibility constraint $\boldsymbol{n}_i' \cdot \boldsymbol{n}_i' = 1$ give

$$\boldsymbol{n}_i \cdot \boldsymbol{u}_i = 0 \qquad \text{and} \qquad \boldsymbol{n}_i' \cdot \boldsymbol{u}_i' = 0, \tag{A.1}$$

respectively. Differentiating the constraint $\boldsymbol{n}_i \cdot \boldsymbol{n}_i = 1$ twice with respect to the dimensionless arc length s gives

$$\boldsymbol{n}_i'' \cdot \boldsymbol{n}_i + \boldsymbol{n}_i' \cdot \boldsymbol{n}_i' = 0, \tag{A.2}$$

which, using the inextensibility constraint $\boldsymbol{n}_i' \cdot \boldsymbol{n}_i' = 1$, gives

$$\boldsymbol{n}_i'' \cdot \boldsymbol{n}_i = -1. \tag{A.3}$$

The first variation of (A.3) gives

$$\boldsymbol{n}_i'' \cdot \boldsymbol{u}_i + \boldsymbol{n}_i \cdot \boldsymbol{u}_i'' = 0. \tag{A.4}$$

A.2. Bending energy

Following (6) and using (A.3), the dimensionless geodesic curvature can be expressed as

$$\kappa_i = |(\mathbf{1} - \boldsymbol{n}_i \otimes \boldsymbol{n}_i)\boldsymbol{n}_i''| = |\boldsymbol{n}_i'' + \boldsymbol{n}_i|. \tag{A.5}$$

Using (A.4) and (A.5), the first variation of κ_i^2 is given by

$$\delta\kappa_i^2 = 2\boldsymbol{n}_i'' \cdot \boldsymbol{u}_i''. \tag{A.6}$$

The first variation of $\mathcal{F}_{\mathrm{B}}$ defined in (21a), using (A.6), is given by

$$\begin{aligned}\delta\mathcal{F}_{\mathrm{B}}[\boldsymbol{n}_1, \boldsymbol{n}_2] = {} & \int_0^{\ell_1} ((\boldsymbol{n}_1''' + \lambda_1\boldsymbol{n}_1)' + \Lambda_1\boldsymbol{n}_1) \cdot \boldsymbol{u}_1 \,\mathrm{d}s + \nu \int_0^{\ell_2} ((\boldsymbol{n}_2''' + \lambda_2\boldsymbol{n}_2)' + \Lambda_2\boldsymbol{n}_2) \cdot \boldsymbol{u}_2 \,\mathrm{d}s \\ & + \boldsymbol{n}_1'' \cdot \boldsymbol{u}_1'|_0^{\ell_1} - (\boldsymbol{n}_1''' + \lambda_1\boldsymbol{n}_1) \cdot \boldsymbol{u}_1|_0^{\ell_1} + \nu\boldsymbol{n}_2'' \cdot \boldsymbol{u}_2'|_0^{\ell_2} - \nu(\boldsymbol{n}_2''' + \lambda_2\boldsymbol{n}_2) \cdot \boldsymbol{u}_2|_0^{\ell_2},\end{aligned} \tag{A.7}$$

where the Lagrange multipliers Λ_i and λ_i, $i = 1, 2$, are required to ensure to maintain the constraints $(A.1)_1$ and $(A.1)_2$, respectively.

A.3. Intra-loop and Inter-loop interaction energy

The first variation of the dimensionless intraloop interaction energy density for $\mathcal{C}_i$, $i = 1, 2$, defined in (21b) is given by

$$\begin{aligned}\delta \int_0^{\ell_i}\int_0^{\ell_i} f_{ii}(|\boldsymbol{n}_i(s) - \boldsymbol{n}_i(\bar{s})|) \,\mathrm{d}\bar{s}\,\mathrm{d}s &= \int_0^{\ell_i}\int_0^{\ell_i} \left(\frac{\mathrm{d}f_{ii}(\varrho)}{\mathrm{d}\varrho}\frac{\boldsymbol{\varrho}}{\varrho} \cdot (\boldsymbol{u}_i(s) - \boldsymbol{u}_i(\bar{s}))\right)\Big|_{\substack{\boldsymbol{\varrho}=\boldsymbol{n}_i(s)-\boldsymbol{n}_i(\bar{s}),\\ \varrho=|\boldsymbol{\varrho}|}} \mathrm{d}\bar{s}\,\mathrm{d}s \\ &= 2\int_0^{\ell_i}\int_0^{\ell_i} \left(\frac{\mathrm{d}f_{ii}(\varrho)}{\mathrm{d}\varrho}\frac{\boldsymbol{\varrho}}{\varrho} \cdot \boldsymbol{u}_i(s)\right)\Big|_{\substack{\boldsymbol{\varrho}=\boldsymbol{n}_i(s)-\boldsymbol{n}_i(\bar{s}),\\ \varrho=|\boldsymbol{\varrho}|}} \mathrm{d}\bar{s}\,\mathrm{d}s.\end{aligned} \tag{A.8}$$

The first variation of the dimensionless interloop interaction energy density between the curve $\mathcal{C}_1$ and $\mathcal{C}_2$ defined in (21c) is given by

$$\begin{aligned}\delta \int_0^{\ell_1}\int_0^{\ell_2} f_{12}(|\boldsymbol{n}_1(s) - \boldsymbol{n}_2(\bar{s})|) \,\mathrm{d}\bar{s}\,\mathrm{d}s &= \int_0^{\ell_1}\int_0^{\ell_2} \left(\frac{\mathrm{d}f_{12}(\varrho)}{\mathrm{d}\varrho}\frac{\boldsymbol{\varrho}}{\varrho} \cdot (\boldsymbol{u}_1(s) - \boldsymbol{u}_2(\bar{s}))\right)\Big|_{\substack{\boldsymbol{\varrho}=\boldsymbol{n}_1(s)-\boldsymbol{n}_2(\bar{s}),\\ \varrho=|\boldsymbol{\varrho}|}} \mathrm{d}\bar{s}\,\mathrm{d}s \\ &= \int_0^{\ell_1}\int_0^{\ell_2} \left(\frac{\mathrm{d}f_{12}(\varrho)}{\mathrm{d}\varrho}\frac{\boldsymbol{\varrho}}{\varrho} \cdot \boldsymbol{u}_1(s)\right)\Big|_{\substack{\boldsymbol{\varrho}=\boldsymbol{n}_1(s)-\boldsymbol{n}_2(\bar{s}),\\ \varrho=|\boldsymbol{\varrho}|}} \mathrm{d}\bar{s}\,\mathrm{d}s \\ &\quad + \int_0^{\ell_2}\int_0^{\ell_1} \left(\frac{\mathrm{d}f_{12}(\varrho)}{\mathrm{d}\varrho}\frac{\boldsymbol{\varrho}}{\varrho} \cdot \boldsymbol{u}_2(s)\right)\Big|_{\substack{\boldsymbol{\varrho}=\boldsymbol{n}_2(s)-\boldsymbol{n}_1(\bar{s}),\\ \varrho=|\boldsymbol{\varrho}|}} \mathrm{d}\bar{s}\,\mathrm{d}s.\end{aligned} \tag{A.9}$$

Using the definition (26) of $\boldsymbol{\varphi}_{ij}$, (A.8) and (A.9) can be written as

$$\delta\mathcal{F}_{\mathrm{S}}[\boldsymbol{n}_1,\boldsymbol{n}_2] = -\zeta_1\int_0^{\ell_1}\boldsymbol{\varphi}_{11}[\boldsymbol{n}_1,\boldsymbol{n}_1]\cdot\boldsymbol{u}_1\,\mathrm{d}s - \zeta_2\int_0^{\ell_2}\boldsymbol{\varphi}_{22}[\boldsymbol{n}_2,\boldsymbol{n}_2]\cdot\boldsymbol{u}_2\,\mathrm{d}s \tag{A.10}$$

and

$$\delta\mathcal{F}_{\mathrm{I}}[\boldsymbol{n}_1,\boldsymbol{n}_2] = -\chi\int_0^{\ell_1}\boldsymbol{\varphi}_{12}[\boldsymbol{n}_1,\boldsymbol{n}_2]\cdot\boldsymbol{u}_1\,\mathrm{d}s - \chi\int_0^{\ell_2}\boldsymbol{\varphi}_{21}[\boldsymbol{n}_2,\boldsymbol{n}_1]\cdot\boldsymbol{u}_2\,\mathrm{d}s, \tag{A.11}$$

respectively.

A.4. First variation condition

On combining (A.7), (A.10), and (A.11), it follows that the first variation of the total dimensionless energy functional $\mathcal{F}$ defined in (20) is given by

$$\begin{aligned}\delta\mathcal{F}[\boldsymbol{n}_1,\boldsymbol{n}_2](\boldsymbol{u}_1,\boldsymbol{u}_2) = &\int_0^{\ell_1}((\boldsymbol{n}_1'''+\lambda_1\boldsymbol{n}_1')' + \Lambda_1\boldsymbol{n}_1 - \zeta_1\boldsymbol{\varphi}_{11}[\boldsymbol{n}_1,\boldsymbol{n}_1] - \chi\boldsymbol{\varphi}_{12}[\boldsymbol{n}_1,\boldsymbol{n}_2])\cdot\boldsymbol{u}_1\,\mathrm{d}s\\ &+\int_0^{\ell_2}(\nu(\boldsymbol{n}_2'''+\lambda_2\boldsymbol{n}_2')' + \Lambda_2\boldsymbol{n}_2 - \zeta_2\boldsymbol{\varphi}_{22}[\boldsymbol{n}_2,\boldsymbol{n}_2] - \chi\boldsymbol{\varphi}_{21}[\boldsymbol{n}_2,\boldsymbol{n}_1])\cdot\boldsymbol{u}_2\,\mathrm{d}s\\ &+\boldsymbol{n}_1''\cdot\boldsymbol{u}_1'|_0^{\ell_1} - (\boldsymbol{n}_1'''+\lambda_1\boldsymbol{n}_1')\cdot\boldsymbol{u}_1|_0^{\ell_1} + \nu\boldsymbol{n}_2''\cdot\boldsymbol{u}_2'|_0^{\ell_2} - \nu(\boldsymbol{n}_2'''+\lambda_2\boldsymbol{n}_2')\cdot\boldsymbol{u}_2|_0^{\ell_2}.\end{aligned} \tag{A.12}$$

Applying the fundamental theorem of the calculus of variations to (A.12) yields equilibrium conditions in the form of a coupled pair of Euler–Lagrange equations, namely

$$\left.\begin{aligned}(\boldsymbol{n}_1'''+\lambda_1\boldsymbol{n}_1')' + \Lambda_1\boldsymbol{n}_1 &= \zeta_1\boldsymbol{\varphi}_{11}[\boldsymbol{n}_1,\boldsymbol{n}_1] + \chi\boldsymbol{\varphi}_{12}[\boldsymbol{n}_1,\boldsymbol{n}_2],\\ \nu(\boldsymbol{n}_2'''+\lambda_2\boldsymbol{n}_2')' + \Lambda_2\boldsymbol{n}_2 &= \zeta_2\boldsymbol{\varphi}_{22}[\boldsymbol{n}_2,\boldsymbol{n}_2] + \chi\boldsymbol{\varphi}_{21}[\boldsymbol{n}_2,\boldsymbol{n}_1],\end{aligned}\right\} \tag{A.13}$$

and the boundary conditions

$$\boldsymbol{n}_1''\cdot\boldsymbol{u}_1'|_0^{\ell_1} - (\boldsymbol{n}_1'''+\lambda_1\boldsymbol{n}_1')\cdot\boldsymbol{u}_1|_0^{\ell_1} + \nu\boldsymbol{n}_2''\cdot\boldsymbol{u}_2'|_0^{\ell_2} - \nu(\boldsymbol{n}_2'''+\lambda_2\boldsymbol{n}_2')\cdot\boldsymbol{u}_2|_0^{\ell_2} = 0. \tag{A.14}$$

For smooth closed curves (loops), the closure conditions (3) and the ancillary requirements

$$\boldsymbol{u}_i(0) = \boldsymbol{u}_i(\ell_i) \qquad \text{and} \qquad \boldsymbol{u}_i'(0) = \boldsymbol{u}_i'(\ell_i), \tag{A.15}$$

on the variations in the boundary conditions (A.14) yields $\lambda_i(0) = \lambda_i(\ell_i)$, $i = 1, 2$, which is a consistent consequence of the periodicity condition of a smoothly closed curve.

A.5. Second variation condition for loops

The second variation of the energy functional $\mathcal{F}$ is given by

$$\begin{aligned}\delta^2\mathcal{F}[\boldsymbol{n}_1,\boldsymbol{n}_2](\boldsymbol{u}_1,\boldsymbol{u}_2) = &\int_0^{\ell_1}((\boldsymbol{n}_1'''+\lambda_1\boldsymbol{n}_1')' + \Lambda_1\boldsymbol{n}_1 - \zeta_1\boldsymbol{\varphi}_{11}[\boldsymbol{n}_1,\boldsymbol{n}_1] - \chi\boldsymbol{\varphi}_{12}[\boldsymbol{n}_1,\boldsymbol{n}_2])\cdot\delta\boldsymbol{u}_1\,\mathrm{d}s\\ &+\int_0^{\ell_2}(\nu(\boldsymbol{n}_2'''+\lambda_2\boldsymbol{n}_2')' + \Lambda_2\boldsymbol{n}_2 - \zeta_2\boldsymbol{\varphi}_{22}[\boldsymbol{n}_2,\boldsymbol{n}_2] - \chi\boldsymbol{\varphi}_{21}[\boldsymbol{n}_2,\boldsymbol{n}_1])\cdot\delta\boldsymbol{u}_2\,\mathrm{d}s\\ &+\int_0^{2\pi a}(|\boldsymbol{u}_1''|^2 - \lambda_1|\boldsymbol{u}_1'|^2 + (\lambda_1'\boldsymbol{u}_1' + \Lambda_1\boldsymbol{u}_1 - \zeta\boldsymbol{\vartheta}_{11}[\boldsymbol{n}_1,\boldsymbol{n}_1](\boldsymbol{u}_1,\boldsymbol{u}_1) - \chi\boldsymbol{\vartheta}_{12}[\boldsymbol{n}_1,\boldsymbol{n}_2](\boldsymbol{u}_1,\boldsymbol{u}_2))\cdot\boldsymbol{u}_1)\,\mathrm{d}s\\ &+\int_0^{2\pi a}((|\boldsymbol{u}_2''|^2 - \lambda_2|\boldsymbol{u}_2'|^2) + (\lambda_2'\boldsymbol{u}_2' + \Lambda_2\boldsymbol{u}_2 - \zeta\boldsymbol{\vartheta}_{22}[\boldsymbol{n}_2,\boldsymbol{n}_2](\boldsymbol{u}_2,\boldsymbol{u}_2) - \chi\boldsymbol{\vartheta}_{21}[\boldsymbol{n}_2,\boldsymbol{n}_1](\boldsymbol{u}_2,\boldsymbol{u}_1))\cdot\boldsymbol{u}_2)\,\mathrm{d}s,\end{aligned} \tag{A.16}$$

where $\boldsymbol{\vartheta}_{11}$, $\boldsymbol{\vartheta}_{12}$, $\boldsymbol{\vartheta}_{21}$, and $\boldsymbol{\vartheta}_{22}$ are defined according to (29). Using (A.13) in (A.16) gives

$$\begin{aligned}\delta^2\mathcal{F}[\boldsymbol{n}_1,\boldsymbol{n}_2](\boldsymbol{u}_1,\boldsymbol{u}_2) = &\int_0^{2\pi a}(|\boldsymbol{u}_1''|^2 - \lambda_1|\boldsymbol{u}_1'|^2 + (\lambda_1'\boldsymbol{u}_1' + \Lambda_1\boldsymbol{u}_1 - \zeta\boldsymbol{\vartheta}_{11}[\boldsymbol{n}_1,\boldsymbol{n}_1](\boldsymbol{u}_1,\boldsymbol{u}_1) - \chi\boldsymbol{\vartheta}_{12}[\boldsymbol{n}_1,\boldsymbol{n}_2](\boldsymbol{u}_1,\boldsymbol{u}_2))\cdot\boldsymbol{u}_1)\,\mathrm{d}s\\ &+\int_0^{2\pi a}((|\boldsymbol{u}_2''|^2 - \lambda_2|\boldsymbol{u}_2'|^2) + (\lambda_2'\boldsymbol{u}_2' + \Lambda_2\boldsymbol{u}_2 - \zeta\boldsymbol{\vartheta}_{22}[\boldsymbol{n}_2,\boldsymbol{n}_2](\boldsymbol{u}_2,\boldsymbol{u}_2) - \chi\boldsymbol{\vartheta}_{21}[\boldsymbol{n}_2,\boldsymbol{n}_1](\boldsymbol{u}_2,\boldsymbol{u}_1))\cdot\boldsymbol{u}_2)\,\mathrm{d}s.\end{aligned} \tag{A.17}$$

Appendix B. Second variation condition for the specialized case

Substituting $\boldsymbol{n}_1 = \boldsymbol{n}_0$, $\boldsymbol{n}_2 = \boldsymbol{K}\boldsymbol{n}_0$, with $\boldsymbol{n}_0$ and $\boldsymbol{K}$ defined by (48) and (49), $\boldsymbol{u}_1 = \boldsymbol{v}$, $\boldsymbol{u}_2 = -\boldsymbol{K}\boldsymbol{v}$ according to (67), $\Lambda_1 = \Lambda_2 = \Lambda$, and $\lambda_1 = \lambda_2 = \lambda$ defined by (62) and (64), respectively, in (A.17) and replacing $\boldsymbol{\vartheta}_{11}$ and $\boldsymbol{\vartheta}_{22}$ with regularized functional $\tilde{\boldsymbol{\vartheta}}$

defined in (45a) in (A.17), yields a reduced form of second variation expression given by

$$\delta^2\mathcal{F}[\boldsymbol{n}_0,\boldsymbol{K}\boldsymbol{n}_0](\boldsymbol{v},-\boldsymbol{K}\boldsymbol{v}) = \int_0^{2\pi a}(|\boldsymbol{v}''|^2-\lambda|\boldsymbol{v}'|^2+(\Lambda\boldsymbol{v}-\zeta\,\tilde{\boldsymbol{\vartheta}}[\boldsymbol{n}_0,\boldsymbol{n}_0](\boldsymbol{v},\boldsymbol{v})-\chi\,\boldsymbol{\vartheta}[\boldsymbol{n}_0,\boldsymbol{K}\boldsymbol{n}_0](\boldsymbol{v},-\boldsymbol{K}\boldsymbol{v}))\cdot\boldsymbol{v})\,\mathrm{d}s$$
$$+\int_0^{2\pi a}((|\boldsymbol{K}\boldsymbol{v}''|^2-\lambda|\boldsymbol{K}\boldsymbol{v}'|^2)+(-\Lambda\boldsymbol{K}\boldsymbol{v}-\zeta\,\tilde{\boldsymbol{\vartheta}}[\boldsymbol{K}\boldsymbol{n}_0,\boldsymbol{K}\boldsymbol{n}_0](-\boldsymbol{K}\boldsymbol{v},-\boldsymbol{K}\boldsymbol{v})-\chi\,\boldsymbol{\vartheta}[\boldsymbol{K}\boldsymbol{n}_0,\boldsymbol{n}_0](-\boldsymbol{K}\boldsymbol{v},\boldsymbol{v}))\cdot(-\boldsymbol{K}\boldsymbol{v}))\,\mathrm{d}s, \tag{B.1}$$

where using (45a) and (45b),

$$\tilde{\boldsymbol{\vartheta}}[\boldsymbol{n}_0,\boldsymbol{n}_0](\boldsymbol{v},\boldsymbol{v})(s) = \int_0^{2\pi a} M\Big(\frac{|\bar{s}-s|}{2a}\Big)\Big(1-\frac{3(\boldsymbol{n}_0(s)-\boldsymbol{n}_0(\bar{s}))\otimes(\boldsymbol{n}_0(s)-\boldsymbol{n}_0(\bar{s}))}{|\boldsymbol{n}_0(s)-\boldsymbol{n}_0(\bar{s})|^2}\Big)\frac{\boldsymbol{v}(s)-\boldsymbol{v}(\bar{s})}{|\boldsymbol{n}_0(s)-\boldsymbol{n}_0(\bar{s})|^3}\,\mathrm{d}\bar{s}, \tag{B.2}$$

$$\tilde{\boldsymbol{\vartheta}}[\boldsymbol{K}\boldsymbol{n}_0,\boldsymbol{K}\boldsymbol{n}_0](-\boldsymbol{K}\boldsymbol{v},-\boldsymbol{K}\boldsymbol{v})(s)$$
$$= -\boldsymbol{K}\int_0^{2\pi a} M\Big(\frac{|\bar{s}-s|}{2a}\Big)\Big(\mathbf{1}-\frac{3(\boldsymbol{n}_0(s)-\boldsymbol{n}_0(\bar{s}))\otimes(\boldsymbol{n}_0(s)-\boldsymbol{n}_0(\bar{s}))}{|\boldsymbol{n}_0(s)-\boldsymbol{n}_0(\bar{s})|^2}\Big)\frac{\boldsymbol{v}(s)-\boldsymbol{v}(\bar{s})}{|\boldsymbol{n}_0(s)-\boldsymbol{n}_0(\bar{s})|^3}\,\mathrm{d}\bar{s}, \tag{B.3}$$

$$\boldsymbol{\vartheta}[\boldsymbol{n}_0,\boldsymbol{K}\boldsymbol{n}_0](\boldsymbol{v},-\boldsymbol{K}\boldsymbol{v})(s) = \int_0^{2\pi a}\Big(\mathbf{1}-\frac{3(\boldsymbol{n}_0(s)-\boldsymbol{K}\boldsymbol{n}_0(\bar{s}))\otimes(\boldsymbol{n}_0(s)-\boldsymbol{K}\boldsymbol{n}_0(\bar{s}))}{|\boldsymbol{n}_0(s)-\boldsymbol{K}\boldsymbol{n}_0(\bar{s})|^2}\Big)\frac{\boldsymbol{v}(s)+\boldsymbol{K}\boldsymbol{v}(\bar{s})}{|\boldsymbol{n}_0(s)-\boldsymbol{K}\boldsymbol{n}_0(\bar{s})|^3}\,\mathrm{d}\bar{s}, \tag{B.4}$$

and

$$\boldsymbol{\vartheta}[\boldsymbol{K}\boldsymbol{n}_0,\boldsymbol{n}_0](-\boldsymbol{K}\boldsymbol{v},\boldsymbol{v})(s)$$
$$= -\boldsymbol{K}\int_0^{2\pi a}\Big(\mathbf{1}-\frac{3(\boldsymbol{n}_0(s)-\boldsymbol{K}\boldsymbol{n}_0(\bar{s}))\otimes(\boldsymbol{n}_0(s)-\boldsymbol{K}\boldsymbol{n}_0(\bar{s}))}{|\boldsymbol{n}_0(s)-\boldsymbol{K}\boldsymbol{n}_0(\bar{s})|^2}\Big)\frac{\boldsymbol{v}(s)+\boldsymbol{K}\boldsymbol{v}(\bar{s})}{|\boldsymbol{n}_0(s)-\boldsymbol{K}\boldsymbol{n}_0(\bar{s})|^3}\,\mathrm{d}\bar{s}, \tag{B.5}$$

respectively, and the elementary properties of $\boldsymbol{K}$ defined in (50) have been used to obtain (B.3) and (B.5). Reduced expression (B.1) can be further simplified as follows. The first three terms in second integral of (B.1) simplify to

$$|-\boldsymbol{K}\boldsymbol{v}''|^2=|\boldsymbol{v}''|^2,\quad |-\boldsymbol{K}\boldsymbol{v}'|^2=|\boldsymbol{v}'|^2,\quad\text{and}\quad |-\boldsymbol{K}\boldsymbol{v}|^2=|\boldsymbol{v}|^2. \tag{B.6}$$

From (B.2) and (B.3), it follows that

$$\tilde{\boldsymbol{\vartheta}}[\boldsymbol{K}\boldsymbol{n}_0,\boldsymbol{K}\boldsymbol{n}_0](-\boldsymbol{K}\boldsymbol{v},-\boldsymbol{K}\boldsymbol{v})\cdot(-\boldsymbol{K}\boldsymbol{v}) = \tilde{\boldsymbol{\vartheta}}[\boldsymbol{n}_0,\boldsymbol{n}_0](\boldsymbol{v},\boldsymbol{v})\cdot\boldsymbol{v}. \tag{B.7}$$

From (B.4) and (B.5), it follows similarly that

$$\boldsymbol{\vartheta}[\boldsymbol{K}\boldsymbol{n}_0,\boldsymbol{n}_0](-\boldsymbol{K}\boldsymbol{v},\boldsymbol{v})\cdot(-\boldsymbol{K}\boldsymbol{v}) = \boldsymbol{\vartheta}[\boldsymbol{n}_0,\boldsymbol{K}\boldsymbol{n}_0](\boldsymbol{v},-\boldsymbol{K}\boldsymbol{v})\cdot\boldsymbol{v}, \tag{B.8}$$

The conditions (B.6), (B.7), and (B.8) imply that the contributions from the bending energy, intraloop interaction energy, and interloop interaction energy, respectively, to the second variation of the total energy from the loops are equal. On using (B.6)–(B.8) in (B.1) and the stability condition (23), it follows that the trivial solution is stable only if

$$\int_0^{2\pi a}(|\boldsymbol{v}''|^2-\lambda|\boldsymbol{v}'|^2+\Lambda|\boldsymbol{v}|^2-\zeta\,\tilde{\boldsymbol{\vartheta}}[\boldsymbol{n}_0,\boldsymbol{n}_0](\boldsymbol{v},\boldsymbol{v})\cdot\boldsymbol{v}-\chi\,\boldsymbol{\vartheta}[\boldsymbol{n}_0,\boldsymbol{K}\boldsymbol{n}_0](\boldsymbol{v},-\boldsymbol{K}\boldsymbol{v})\cdot\boldsymbol{v})\,\mathrm{d}s\geq 0. \tag{B.9}$$

On using the representation (70) of the perturbation $\boldsymbol{v}$, the terms in (B.9) can be written as

$$\left.\begin{aligned}
\int_0^{2\pi a}\Big|\sum_{n=2}^{\infty}\boldsymbol{v}_n''\Big|^2\,\mathrm{d}s &= \sum_{n=2}^{\infty}\int_0^{2\pi a}|\boldsymbol{v}_n''|^2\,\mathrm{d}s,\\
\int_0^{2\pi a}\Big|\sum_{n=2}^{\infty}\boldsymbol{v}_n'\Big|^2\,\mathrm{d}s &= \sum_{n=2}^{\infty}\int_0^{2\pi a}|\boldsymbol{v}_n'|^2\,\mathrm{d}s,\\
\int_0^{2\pi a}\Big|\sum_{n=2}^{\infty}\boldsymbol{v}_n\Big|^2\,\mathrm{d}s &= \sum_{n=2}^{\infty}\int_0^{2\pi a}|\boldsymbol{v}_n|^2\,\mathrm{d}s,\\
\int_0^{2\pi a}\tilde{\boldsymbol{\vartheta}}[\boldsymbol{n}_0,\boldsymbol{n}_0]\Big(\sum_{n=2}^{\infty}\boldsymbol{v}_n,\sum_{m=2}^{\infty}\boldsymbol{v}_m\Big)\cdot\sum_{q=2}^{\infty}\boldsymbol{v}_q\,\mathrm{d}s &= \sum_{n=2}^{\infty}\int_0^{2\pi a}\tilde{\boldsymbol{\vartheta}}[\boldsymbol{n}_0,\boldsymbol{n}_0](\boldsymbol{v}_n,\boldsymbol{v}_n)\cdot\boldsymbol{v}_n\,\mathrm{d}s,\quad\text{and}\\
\int_0^{2\pi a}\boldsymbol{\vartheta}[\boldsymbol{n}_0,\boldsymbol{K}\boldsymbol{n}_0]\Big(\sum_{n=2}^{\infty}\boldsymbol{v}_n,-\boldsymbol{K}\sum_{m=2}^{\infty}\boldsymbol{v}_m\Big)\cdot\sum_{q=2}^{\infty}\boldsymbol{v}_q\,\mathrm{d}s &= \sum_{n=2}^{\infty}\int_0^{2\pi a}\boldsymbol{\vartheta}[\boldsymbol{n}_0,\boldsymbol{K}\boldsymbol{n}_0](\boldsymbol{v}_n,-\boldsymbol{K}\boldsymbol{v}_n)\cdot\boldsymbol{v}_n\,\mathrm{d}s.
\end{aligned}\right\} \tag{B.10}$$

It follows from (B.9), (B.10), and the linear independence of the modes $\boldsymbol{\nu}_n$, $n \geq 2$, that the trivial solution is stable only if

$$\int_0^{2\pi a} (|\boldsymbol{\nu}_n''|^2 - \lambda |\boldsymbol{\nu}_n'|^2 + \Lambda |\boldsymbol{\nu}_n|^2 - \zeta\, \tilde{\boldsymbol{\vartheta}}[\boldsymbol{n}_0, \boldsymbol{n}_0](\boldsymbol{\nu}_n, \boldsymbol{\nu}_n) \cdot \boldsymbol{\nu}_n - \chi\, \boldsymbol{\vartheta}[\boldsymbol{n}_0, \boldsymbol{K}\boldsymbol{n}_0](\boldsymbol{\nu}_n, -\boldsymbol{K}\boldsymbol{\nu}_n) \cdot \boldsymbol{\nu}_n)\, \mathrm{d}s \geq 0 \tag{B.11}$$

holds for all the admissible $\boldsymbol{\nu}_n$, $n \geq 2$.

B.1. Useful relations

On introducing the change of variables $\eta = (\bar{s} - s)/2a$, quantities at arclength $\bar{s}$ can be represented in terms of s and η. Some useful expressions for further calculations include

$$\left.\begin{aligned}
\boldsymbol{e}(\bar{s}) &= \cos 2\eta \boldsymbol{e} + \sin 2\eta \boldsymbol{k} \times \boldsymbol{e},\\
\boldsymbol{n}_0(\bar{s}) &= a \cos 2\eta \boldsymbol{e} + \sqrt{1-a^2}\boldsymbol{k} + a \sin 2\eta \boldsymbol{k} \times \boldsymbol{e},\\
\boldsymbol{\nu}_n(\bar{s}) &= -(a\psi_n(\bar{s}) \sin 2\eta + a^2 \psi_n'(\bar{s}) \cos 2\eta)\boldsymbol{e} + \frac{a^3 \psi_n'(\bar{s})}{\sqrt{1-a^2}}\boldsymbol{k} + (a\psi_n(\bar{s}) \cos 2\eta - a^2 \psi_n'(\bar{s}) \sin 2\eta)\boldsymbol{k} \times \boldsymbol{e},\\
\boldsymbol{K}\boldsymbol{n}_0 &= a\boldsymbol{e} - \sqrt{1-a^2}\boldsymbol{k},\\
\boldsymbol{K}\boldsymbol{n}_0(\bar{s}) &= a \cos 2\eta \boldsymbol{e} - \sqrt{1-a^2}\boldsymbol{k} + a \sin 2\eta \boldsymbol{k} \times \boldsymbol{e},\\
\boldsymbol{K}\boldsymbol{\nu}_n(\bar{s}) &= -(a\psi_n(\bar{s}) \sin 2\eta + a^2 \psi_n'(\bar{s}) \cos 2\eta)\boldsymbol{e} - \frac{a^3 \psi_n'(\bar{s})}{\sqrt{1-a^2}}\boldsymbol{k} + (a\psi_n(\bar{s}) \cos 2\eta - a^2 \psi_n'(\bar{s}) \sin 2\eta)\boldsymbol{k} \times \boldsymbol{e},\\
|\boldsymbol{n}_0 - \boldsymbol{n}_0(\bar{s})| &= 2a|\sin \eta|,\\
|\boldsymbol{n}_0 - \boldsymbol{K}\boldsymbol{n}_0(\bar{s})| &= 2\sqrt{1 - a^2 \cos^2 \eta}.
\end{aligned}\right\} \tag{B.12}$$

B.2. Bending energy terms

Using the representation of $\boldsymbol{\nu}_n$ in terms of ψ_n and ψ_n' as defined in (77) gives

$$\left.\begin{aligned}
\boldsymbol{\nu}_n &= -a^2 \psi_n' \boldsymbol{e} + \frac{a^3 \psi_n'}{\sqrt{1-a^2}}\boldsymbol{k} + a\psi_n \boldsymbol{k} \times \boldsymbol{e},\\
\boldsymbol{\nu}_n' &= -(\psi_n + a^2 \psi_n'')\boldsymbol{e} + \frac{a^3 \psi_n''}{\sqrt{1-a^2}}\boldsymbol{k},\\
\boldsymbol{\nu}_n'' &= -(a^2 \psi_n'''' + \psi_n')\boldsymbol{e} + \frac{a^3 \psi_n''''}{\sqrt{1-a^2}}\boldsymbol{k} - \left(a\psi_n'' + \frac{\psi_n}{a}\right)\boldsymbol{k} \times \boldsymbol{e}.
\end{aligned}\right\} \tag{B.13}$$

Using fourier series representation (78) of ψ_n, a straightforward calculation yields

$$\int_0^{2\pi a} \psi_n^2\, \mathrm{d}s = \pi a (c_n^2 + d_n^2) \qquad \text{and} \qquad \int_0^{2\pi a} \psi_n'^2\, \mathrm{d}s = \frac{\pi n^2}{a}(c_n^2 + d_n^2). \tag{B.14}$$

From (B.13) and (B.14), it follows that

$$\int_0^{2\pi a} |\boldsymbol{\nu}_n''|^2\, \mathrm{d}s = \pi a \left(\frac{(n^2-1)^2(n^2+1)}{a^2} + \frac{n^6}{1-a^2}\right)(c_n^2 + d_n^2), \tag{B.15}$$

$$\int_0^{2\pi a} |\boldsymbol{\nu}_n'|^2\, \mathrm{d}s = \pi a \left((n^2-1)^2 + \frac{a^2 n^4}{1-a^2}\right)(c_n^2 + d_n^2), \tag{B.16}$$

and

$$\int_0^{2\pi a} |\boldsymbol{\nu}_n|^2\, \mathrm{d}s = \pi a \left(a^2 + \frac{a^2 n^2}{1-a^2}\right)(c_n^2 + d_n^2). \tag{B.17}$$

Combining (B.15)–(B.17) gives

$$\begin{aligned}
&\int_0^{2\pi a} (|\boldsymbol{\nu}_n''|^2 - \lambda |\boldsymbol{\nu}_n'|^2 + \Lambda |\boldsymbol{\nu}_n|^2)\, \mathrm{d}s\\
&= \pi a \left(\frac{(n^2-1)^2(n^2+1)}{a^2} + \frac{n^6}{1-a^2} - \lambda\left((n^2-1)^2 + \frac{a^2 n^4}{1-a^2}\right) + \Lambda a^2 \left(1 + \frac{n^2}{1-a^2}\right)\right)(c_n^2 + d_n^2).
\end{aligned} \tag{B.18}$$

B.3. Intraloop interaction terms

With the change of variables $\bar{s} = s + 2a\eta$ and using the expressions (B.12), the components of $\tilde{\boldsymbol{\vartheta}}[\boldsymbol{n}_0, \boldsymbol{n}_0](\boldsymbol{v}_n, \boldsymbol{v}_n)$, defined in (B.2) in the direction $\boldsymbol{e}$, $\boldsymbol{k}$, and $\boldsymbol{k}\times\boldsymbol{e}$ are given by

$$\left.\begin{aligned}
\tilde{\boldsymbol{\vartheta}}[\boldsymbol{n}_0, \boldsymbol{n}_0](\boldsymbol{v}_n, \boldsymbol{v}_n)\cdot\boldsymbol{e} &= -\frac{\psi_n'}{4}\int_0^\pi M(\eta)\csc^3\eta\,\mathrm{d}\eta \\
&\quad + \frac{1}{4a}\int_0^\pi M(\eta)\frac{\psi_n(s+2a\eta)\sin 2\eta + a\psi_n'(s+2a\eta)\cos 2\eta}{\sin^3\eta}\,\mathrm{d}\eta \\
&\quad + \frac{3}{4a}\int_0^\pi M(\eta)\frac{\cos\eta(\psi_n - \psi_n(s+2a\eta)) + a\sin\eta(\psi_n' + \psi_n'(s+2a\eta))}{\sin^2\eta}\,\mathrm{d}\eta, \\
\tilde{\boldsymbol{\vartheta}}[\boldsymbol{n}_0, \boldsymbol{n}_0](\boldsymbol{v}_n, \boldsymbol{v}_n)\cdot\boldsymbol{k} &= \frac{a\psi_n'}{4\sqrt{1-a^2}}\int_0^\pi M(\eta)\csc^3\eta\,\mathrm{d}\eta - \frac{a}{4\sqrt{1-a^2}}\int_0^\pi \frac{\psi_n'(s+2a\eta)}{\sin^3\eta}\,\mathrm{d}\eta, \\
\tilde{\boldsymbol{\vartheta}}[\boldsymbol{n}_0, \boldsymbol{n}_0](\boldsymbol{v}_n, \boldsymbol{v}_n)\cdot\boldsymbol{k}\times\boldsymbol{e} &= \frac{\psi_n}{4a}\int_0^\pi M(\eta)\csc^3\eta\,\mathrm{d}\eta \\
&\quad - \frac{1}{4a}\int_0^\pi M(\eta)\frac{\psi_n(s+2a\eta)\cos 2\eta - a\psi_n'(s+2a\eta)\sin 2\eta}{\sin^3\eta}\,\mathrm{d}\eta \\
&\quad - \frac{1}{4a}\int_0^\pi \frac{\cos\eta[\cos\eta(\psi_n - \psi_n(s+2a\eta)) + a\sin\eta(\psi_n' + \psi_n'(s+2a\eta))]}{\sin^3\eta}\,\mathrm{d}\eta.
\end{aligned}\right\} \tag{B.19}$$

Substituting

$$\psi_n(s+2a\eta) = \cos 2n\eta\,\psi_n(s) + \sin 2n\eta\,\frac{a}{n}\psi_n'(s) \tag{B.20}$$

and

$$\psi_n'(s+2a\eta) = -\sin 2n\eta\,\frac{n}{a}\psi_n(s) + \cos 2n\eta\,\psi_n'(s) \tag{B.21}$$

in the integrals on the right-hand side of $(B.19)_1$, $(B.19)_2$, and $(B.19)_3$, respectively gives

$$\left.\begin{aligned}
\tilde{\boldsymbol{\vartheta}}[\boldsymbol{n}_0, \boldsymbol{n}_0](\boldsymbol{v}_n, \boldsymbol{v}_n)\cdot\boldsymbol{e} &= \frac{1}{4}\left(I_1 + I_3 - I_4 + 3I_5 - \frac{I_2}{n}\right)\psi_n', \\
\tilde{\boldsymbol{\vartheta}}[\boldsymbol{n}_0, \boldsymbol{n}_0](\boldsymbol{v}_n, \boldsymbol{v}_n)\cdot\boldsymbol{k} &= \frac{a}{4\sqrt{1-a^2}}(I_4 - I_3)\psi_n', \\
\tilde{\boldsymbol{\vartheta}}[\boldsymbol{n}_0, \boldsymbol{n}_0](\boldsymbol{v}_n, \boldsymbol{v}_n)\cdot\boldsymbol{k}\times\boldsymbol{e} &= \frac{1}{4a}(2I_3 - 2I_4 - I_1 + 3I_5 + nI_2)\psi_n,
\end{aligned}\right\} \tag{B.22}$$

where I_1, I_2, I_3, I_4, and I_5 are defined by

$$\left.\begin{aligned}
I_1 &= \int_0^\pi M(\eta)\cos 2n\eta\csc\eta\,\mathrm{d}\eta, \\
I_2 &= \int_0^\pi M(\eta)\sin 2n\eta\cos\eta\csc^2\eta\,\mathrm{d}\eta, \\
I_3 &= \int_0^\pi M(\eta)\cos 2n\eta\csc^3\eta\,\mathrm{d}\eta, \\
I_4 &= \int_0^\pi M(\eta)\csc^3\eta\,\mathrm{d}\eta, \\
I_5 &= \int_0^\pi M(\eta)\csc\eta\,\mathrm{d}\eta.
\end{aligned}\right\} \tag{B.23}$$

From $(B.13)_1$ and (B.22),

$$\begin{aligned}
&\tilde{\boldsymbol{\vartheta}}[\boldsymbol{n}_0, \boldsymbol{n}_0](\boldsymbol{v}_n, \boldsymbol{v}_n)\cdot\boldsymbol{v}_n \\
&= -a^2\psi_n'\tilde{\boldsymbol{\vartheta}}[\boldsymbol{n}_0, \boldsymbol{n}_0](\boldsymbol{v}_n, \boldsymbol{v}_n)\cdot\boldsymbol{e} + \frac{a^3}{\sqrt{1-a^2}}\psi_n'\tilde{\boldsymbol{\vartheta}}[\boldsymbol{n}_0, \boldsymbol{n}_0](\boldsymbol{v}_n, \boldsymbol{v}_n)\cdot\boldsymbol{k} + a\psi_n'\tilde{\boldsymbol{\vartheta}}[\boldsymbol{n}_0, \boldsymbol{n}_0](\boldsymbol{v}_n, \boldsymbol{v}_n)\cdot\boldsymbol{k}\times\boldsymbol{e} \\
&= \frac{-a^2}{4}\left(I_1 + I_3 - I_4 + 3I_5 - \frac{I_2}{n}\right)\psi_n'^2 + \frac{a^4}{4(1-a^2)}(I_4 - I_3)\psi_n'^2 + \frac{1}{4}(2I_3 - 2I_4 - I_1 + 3I_5 + nI_2)\psi_n{}^2.
\end{aligned} \tag{B.24}$$

Using (B.14) and (B.24), it follows that

$$\begin{aligned}
&\int_0^{2\pi a}\tilde{\boldsymbol{\vartheta}}[\boldsymbol{n}_0, \boldsymbol{n}_0](\boldsymbol{v}_n, \boldsymbol{v}_n)\cdot\boldsymbol{v}_n\,\mathrm{d}s \\
&= \frac{\pi a}{4}\left(-\left(I_1 + I_3 - I_4 + 3I_5 - \frac{I_2}{n}\right)n^2 + \frac{a^2(I_4 - I_3)n^2}{1-a^2} + (2I_3 - 2I_4 - I_1 + 3I_5 + nI_2)\right)(c_n^2 + d_n^2).
\end{aligned} \tag{B.25}$$

B.4. Interloop energy terms:

On using (B.12), the components of $\vartheta[\boldsymbol{n}_0, \boldsymbol{K}\boldsymbol{n}_0](\boldsymbol{v}_n, -\boldsymbol{K}\boldsymbol{v}_n)$, defined in (B.4), along the directions $\boldsymbol{e}$, $\boldsymbol{k}$, and $\boldsymbol{k}\times\boldsymbol{e}$ are given by

$$\left.\begin{aligned}
\vartheta[\boldsymbol{n}_0, \boldsymbol{K}\boldsymbol{n}_0](\boldsymbol{v}_n, -\boldsymbol{K}\boldsymbol{v}_n)\cdot\boldsymbol{e} &= -\frac{a^3}{4}\psi_n'\int_0^\pi \frac{1}{\sqrt[3]{1-a^2\cos^2\eta}}\,\mathrm{d}\eta \\
&\quad +\frac{a^2}{4}\int_0^\pi \frac{\psi_n(s+2a\eta)\sin 2\eta - a\psi_n'(s+2a\eta)\cos 2\eta}{\sqrt[3]{1-a^2\cos^2\eta}}\,\mathrm{d}\eta \\
&\quad +\frac{3a^4}{4}\int_0^\pi \frac{\sin^2\eta\cos\eta[\sin\eta(\psi_n+\psi_n(s+2a\eta)) - a\cos\eta(\psi_n'-\psi_n'(s+2a\eta))]}{\sqrt[5]{1-a^2\cos^2\eta}}\,\mathrm{d}\eta, \\
\vartheta[\boldsymbol{n}_0, \boldsymbol{K}\boldsymbol{n}_0](\boldsymbol{v}_n, -\boldsymbol{K}\boldsymbol{v}_n)\cdot\boldsymbol{k} &= \frac{a^4\psi_n'}{4\sqrt{1-a^2}}\int_0^\pi \frac{1}{\sqrt[3]{1-a^2\cos^2\eta}}\,\mathrm{d}\eta - \frac{a^4}{4\sqrt{1-a^2}}\int_0^\pi \frac{\psi_n'(s+2a\eta)}{\sqrt[3]{1-a^2\cos^2\eta}}\,\mathrm{d}\eta \\
&\quad +\frac{3a^3\sqrt{1-a^2}}{4}\int_0^\pi \frac{\cos\eta[\sin\eta(\psi_n+\psi_n(s+2a\eta) - a\cos\eta(\psi_n'-\psi_n'(s+2a\eta))]}{\sqrt[5]{1-a^2\cos^2\eta}}\,\mathrm{d}\eta, \\
\vartheta[\boldsymbol{n}_0, \boldsymbol{K}\boldsymbol{n}_0](\boldsymbol{v}_n, -\boldsymbol{K}\boldsymbol{v}_n)\cdot\boldsymbol{k}\times\boldsymbol{e} &= \frac{a^2}{4}\psi_n\int_0^\pi \frac{1}{\sqrt[3]{1-a^2\cos^2\eta}}\,\mathrm{d}\eta \\
&\quad -\frac{a^2}{4}\int_0^\pi \frac{\psi_n(s+2a\eta)\cos 2\eta + a\psi_n'(s+2a\eta)\sin 2\eta}{\sqrt[3]{1-a^2\cos^2\eta}}\,\mathrm{d}\eta \\
&\quad -\frac{3a^4}{4}\int_0^\pi \frac{\sin\eta\cos^2\eta[\sin\eta(\psi_n+\psi_n(s+2a\eta) - a\cos\eta(\psi_n'-\psi_n'(s+2a\eta))]}{\sqrt[5]{1-a^2\cos^2\eta}}\,\mathrm{d}\eta.
\end{aligned}\right\} \tag{B.26}$$

Using (B.20) and (B.21) in the integrals on the right-hand side of $(B.26)_1$, $(B.26)_2$, and $(B.26)_3$, respectively, gives

$$\left.\begin{aligned}
\vartheta[\boldsymbol{n}_0, \boldsymbol{K}\boldsymbol{n}_0](\boldsymbol{v}_n, -\boldsymbol{K}\boldsymbol{v}_n)\cdot\boldsymbol{e} &= \frac{a^3}{4}\left(-J_1 - \left(J_3 + \frac{J_4}{n}\right) - 6a^2\left(K_2 - \frac{K_3}{2n}\right)\right)\psi_n', \\
\vartheta[\boldsymbol{n}_0, \boldsymbol{K}\boldsymbol{n}_0](\boldsymbol{v}_n, -\boldsymbol{K}\boldsymbol{v}_n)\cdot\boldsymbol{k} &= \frac{a^4}{4\sqrt{1-a^2}}\left(J_1 - J_2 - 6(1-a^2)\left(K_1 - \frac{K_3+K_4}{2n}\right)\right)\psi_n', \\
\vartheta[\boldsymbol{n}_0, \boldsymbol{K}\boldsymbol{n}_0](\boldsymbol{v}_n, -\boldsymbol{K}\boldsymbol{v}_n)\cdot\boldsymbol{k}\times\boldsymbol{e} &= \frac{a^2}{4}\left(J_1 + J_3 + nJ_4 - 6a^2\left(K_5 - K_2 - \frac{nK_4}{2}\right)\right)\psi_n,
\end{aligned}\right\} \tag{B.27}$$

where J_1, J_2, J_3, J_4, and J_5 are defined by

$$\left.\begin{aligned}
J_1 &= \int_0^\pi \frac{1}{\sqrt[3]{1-a^2\cos^2\eta}}\,\mathrm{d}\eta, \\
J_2 &= \int_0^\pi \frac{\cos 2n\eta}{\sqrt[3]{1-a^2\cos^2\eta}}\,\mathrm{d}\eta, \\
J_3 &= \int_0^\pi \frac{\cos 2\eta\cos 2n\eta}{\sqrt[3]{1-a^2\cos^2\eta}}\,\mathrm{d}\eta, \\
J_4 &= \int_0^\pi \frac{\sin 2\eta\sin 2n\eta}{\sqrt[3]{1-a^2\cos^2\eta}}\,\mathrm{d}\eta, \\
J_5 &= \int_0^\pi \frac{\cos^2\eta}{\sqrt[3]{1-a^2\cos^2\eta}}\,\mathrm{d}\eta,
\end{aligned}\right\} \tag{B.28}$$

and K_1, K_2, K_3, K_4, and K_5 are given by

$$\left.\begin{aligned}
K_1 &= \int_0^\pi \frac{\cos^2\eta\sin^2 n\eta}{\sqrt[5]{1-a^2\cos^2\eta}}\,\mathrm{d}\eta, \\
K_2 &= \int_0^\pi \frac{\cos^2\eta\sin^2\eta\sin^2 n\eta}{\sqrt[5]{1-a^2\cos^2\eta}}\,\mathrm{d}\eta, \\
K_3 &= \int_0^\pi \frac{\cos\eta\sin^3\eta\sin 2n\eta}{\sqrt[5]{1-a^2\cos^2\eta}}\,\mathrm{d}\eta, \\
K_4 &= \int_0^\pi \frac{\sin\eta\cos^3\eta\sin 2n\eta}{\sqrt[5]{1-a^2\cos^2\eta}}\,\mathrm{d}\eta, \\
K_5 &= \int_0^\pi \frac{\sin^2\eta\cos^2\eta}{\sqrt[5]{1-a^2\cos^2\eta}}\,\mathrm{d}\eta.
\end{aligned}\right\} \tag{B.29}$$

From (B.13)$_1$ and (B.27),

$$\begin{aligned}\boldsymbol{\vartheta}[\boldsymbol{n}_0, \boldsymbol{K}\boldsymbol{n}_0](\boldsymbol{v}_n, -\boldsymbol{K}\boldsymbol{v}_n)\cdot\boldsymbol{v}_n =& -a^2\psi_n'\boldsymbol{\vartheta}[\boldsymbol{n}_0, \boldsymbol{K}\boldsymbol{n}_0](\boldsymbol{v}_n, -\boldsymbol{K}\boldsymbol{v}_n)\cdot\boldsymbol{e} + \frac{a^3}{\sqrt{1-a^2}}\psi_n'\boldsymbol{\vartheta}[\boldsymbol{n}_0, \boldsymbol{K}\boldsymbol{n}_0](\boldsymbol{v}_n, -\boldsymbol{K}\boldsymbol{v}_n)\cdot\boldsymbol{k}\\ &+ a\psi_n'\boldsymbol{\vartheta}[\boldsymbol{n}_0, \boldsymbol{K}\boldsymbol{n}_0](\boldsymbol{v}_n, -\boldsymbol{K}\boldsymbol{v}_n)\cdot\boldsymbol{k}\times\boldsymbol{e}\\ =&\frac{a^5}{4}\left(J_1+J_3+\frac{J_4}{n}+6a^2\frac{K_2-K_3}{2n}\right)\psi_n'^2\\ &+\frac{a^7}{4(1-a^2)}\left(J_1-J_2-6(1-a^2)\left(K_1-\frac{K_2+k_4}{2n}\right)\right)\psi_n'^2\\ &+\frac{a^3}{4}\left(J_1+J_3+nJ_4-6a^2\left(K_5-K_2-\frac{nK_4}{2}\right)\right)\psi_n^2.\end{aligned} \tag{B.30}$$

Using (B.14) and (B.30) gives

$$\begin{aligned}\int_0^{2\pi a}\boldsymbol{\vartheta}[\boldsymbol{n}_0, \boldsymbol{K}\boldsymbol{n}_0](\boldsymbol{v}_n, -\boldsymbol{K}\boldsymbol{v}_n)\cdot\boldsymbol{v}_n =& \frac{\pi a^4}{4}[J_1+(J_3+J_4/n)+6a^2(K_2-K_3/2n))n^2(c_n^2+d_n^2)\\ &+\frac{\pi a^6}{4(1-a^2)}\left(J_1-J_2-6(1-a^2)\left(K_1-\frac{K_3+K_4}{2n}\right)\right)n^2(c_n^2+d_n^2)\\ &+\frac{\pi a^4}{4}\left(J_1+(J_3+nJ_4)-6a^2\left(K_5-K_2-\frac{nK_4}{2}\right)\right)(c_n^2+d_n^2).\end{aligned} \tag{B.31}$$

With I_5, J_1, and J_5, the expressions (62) and (64) for Λ and λ can be rewritten as

$$\Lambda = \frac{\chi a}{2}J_1 \qquad \text{and} \qquad \lambda = \frac{1}{a^2}-\frac{\zeta}{2}I_5+\frac{\chi a^3}{2}J_5. \tag{B.32}$$

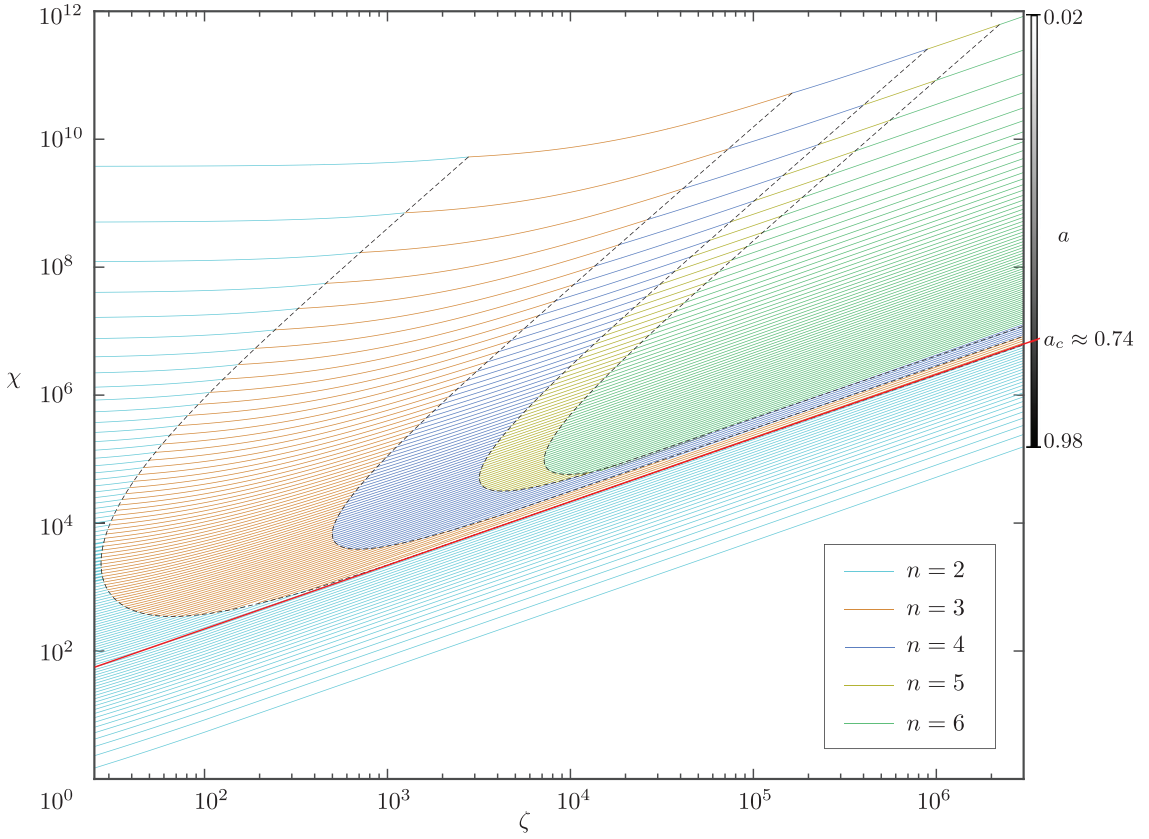

Fig. B.9. Stability curves separating the stable and unstable combinations of intraloop and interloop interaction parameters ζ and χ defined in (33) for values of the dimensionless radius a of the loops defined in (32) ranging from 0.02 to 0.98. Straight line shown in red color corresponds to $a = a_c$ at which the stability curve, given by (84) and (85) transitions from a polygonal curve to a straight line. For each $0 < a < a_c$, the stability curve consists of different colors that correspond to the first mode for which the trivial configuration becomes unstable in different intervals of $\zeta \geq 0$. For $a_c \leq a < 1$, the stability curve is a straight line constituted by mode $n = 2$. For given a, the trivial solution is stable below the corresponding stability curve.

On substituting (B.32) in (B.18) and combining (B.18), (B.25), and (B.31), the reduced stability condition (B.9) can be rewritten as

$$\pi a(\Upsilon_{\mathrm{B}}(n,a)+\zeta\,\Upsilon_{\mathrm{S}}(n,a)-\chi\,\Upsilon_{\mathrm{I}}(n,a))(c_n^2+d_n^2)\geq 0,\quad n\geq 2. \tag{B.33}$$

The condition (B.33) holds for all c_n and d_n if and only if

$$\chi\leq \alpha_n(a)\zeta+\beta_n(a), \tag{B.34}$$

where α_n and β_n are defined by

$$\alpha_n(a)=\frac{\Upsilon_{\mathrm{S}}(n,a)}{\Upsilon_{\mathrm{I}}(n,a)}\quad\text{and}\quad \beta_n(a)=\frac{\Upsilon_{\mathrm{B}}(n,a)}{\Upsilon_{\mathrm{I}}(n,a)}, \tag{B.35}$$

with

$$\left.\begin{aligned}
\Upsilon_{\mathrm{B}}(n,a)&=\frac{n^2(n^2-1)}{a^2(1-a^2)}(n^2-1+a^2),\\
\Upsilon_{\mathrm{S}}(n,a)&=\frac{1}{4}\Big(\frac{2I_5}{1-a^2}n^4+n^2\Big(I_1-I_5+\frac{I_3-I_4}{1-a^2}\Big)-2nI_2+I_1-I_5-2I_3+2I_4\Big),\\
\Upsilon_{\mathrm{I}}(n,a)&=\frac{a^3}{4}\Big(\frac{2J_5}{1-a^2}n^4+n^2\Big(J_3-4J_5+6a^2(K_2-K_1)-\frac{J_1+a^2J_2}{1-a^2}\Big)\\
&\quad+2n(J_4+3a^2K_4)+J_3-J_1+2J_5+6a^2(K_2-K_5)\Big).
\end{aligned}\right\} \tag{B.36}$$

The stability curves for $0.02\leq a\leq 0.98$ are shown in Fig. B.9.

B.5. Asymptotic limits of Υ_B, Υ_S, and Υ_I

As $a\to 0$,

$$\Upsilon_{\mathrm{B}}\sim\frac{1}{a^2},\quad \Upsilon_{\mathrm{S}}\sim 1,\quad\text{and}\quad \Upsilon_{\mathrm{I}}\sim a^3. \tag{B.37}$$

It follows from (B.35) and (B.37) that

$$\alpha_n(a)\sim\frac{1}{a^3}\quad\text{and}\quad\beta_n(a)\sim\frac{1}{a^5}\quad\text{as}\quad a\to 0. \tag{B.38}$$

Further, as $a\to 1$,

$$\Upsilon_{\mathrm{B}}\sim\frac{1}{1-a}\quad\text{and}\quad\Upsilon_{\mathrm{S}}\sim\frac{1}{1-a}. \tag{B.39}$$

It can be shown that each integral in (B.28) behaves as $1/(1-a)$ and each integral in (B.29) behaves as $1/(1-a)^2$ as $a\to 1$. Therefore, using $(B.36)_3$,

$$\Upsilon_{\mathrm{I}}\sim\frac{1}{(1-a)^2}\quad\text{as}\quad a\to 1. \tag{B.40}$$

Furthermore,

$$\alpha_n(a)\to 1-a\quad\text{and}\quad\beta_n(a)\sim 1-a\quad\text{as}\quad a\to 1. \tag{B.41}$$

B.5.1. Asymptotic limit of a_n^*

The limit of a_n^* as $n\to\infty$ is obtained by solving for a_n^* such that

$$\lim_{n\to\infty}\alpha_n(a_n^*)=1, \tag{B.42}$$

which, following $(B.35)_1$ is equivalent to

$$\lim_{n\to\infty}\Upsilon_{\mathrm{S}}(n,a_n^*)=\lim_{n\to\infty}\Upsilon_{\mathrm{I}}(n,a_n^*). \tag{B.43}$$

Bearing in mind that integrals on right hand side of $(B.36)_2$ and $(B.36)_3$, defined by (B.23), (B.28), and (B.29) are bounded as $n\to\infty$,

$$\Upsilon_{\mathrm{S}}(n,a_n^*)\sim\frac{I_5}{2(1-a_n^{*2})}n^4\quad\text{and}\quad\Upsilon_{\mathrm{I}}(n,a_n^*)\sim\frac{a_n^{*3}J_5}{2(1-a_n^{*2})}n^4\quad\text{as}\quad n\to\infty. \tag{B.44}$$

Substituting asymptotic expressions of $\Upsilon_{\mathrm{S}}(n,a_n^*)$ and $\Upsilon_{\mathrm{I}}(n,a_n^*)$ from (B.44) in (B.43), and using definitions $(B.23)_5$ and $(B.28)_5$ gives

$$\int_0^\pi M(\eta)\csc\eta\,\mathrm{d}\eta=a_n^{*3}\int_0^\pi\frac{\cos^2\eta}{\sqrt[3]{1-a_n^{*2}\cos^2\eta}}\,\mathrm{d}\eta. \tag{B.45}$$

For $M(\eta)$ of particular form (83), numerically solving (B.45) yields $a_n^*=0.829710524894442$, with $n\to\infty$.

B.6. Showing that $\alpha_n > 0$ and $\beta_n > 0$

Following the definitions (B.35)$_1$ and (B.35)$_2$ of $\alpha_n(a)$ and $\beta_n(a)$, it suffices to show that the quantities $\Upsilon_B(n,a)$, $\Upsilon_S(n,a)$, and $\Upsilon_I(n,a)$ are strictly positive for $0<a<1$ and $n\geq 2$.

B.6.1. $\Upsilon_B(n,a) > 0$

Note, from (B.36)$_1$, for $0<a<1$ and $n\geq 2$, that $\Upsilon_B(n,a) > 0$.

B.6.2. $\Upsilon_S(n,a) > 0$

On using the definition of the integrals in (B.23), the quantity $\Upsilon_S(n,a)$ defined in (B.36)$_2$ can be written as

$$\begin{aligned}&\Upsilon_S(n,a)\\&=\frac{1}{2}\int_0^\pi M(\eta)\csc^3\eta\left[\frac{n^4\sin^2\eta}{1-a^2}-n^2\sin^2 n\eta\left(\sin^2\eta+\frac{1}{1-a^2}\right)-\frac{\sin 2n\eta\sin 2\eta}{2}n-\sin^2 n\eta(\sin^2\eta-2)\right]\mathrm{d}\eta.\end{aligned}\tag{B.46}$$

A more specific can be obtained by using a particular form (83) of the mollifier M discussed in Section 3.5. Let I_0 be the maximum value of the denominator $\sin\eta+\exp(-7\sin\eta)$ of M, so that

$$M(\eta) > \frac{\sin^4\eta}{I_0^4}.\tag{B.47}$$

By substituting $M(\eta)$ on the right-hand side of (B.46) with $\sin^4\eta/I_0^4$, it can then be deduced that

$$\begin{aligned}&\tilde{\Upsilon}_S(n,a)\\&=\frac{1}{2I_0^4}\int_0^\pi \sin\eta\left(\frac{n^4\sin^2\eta}{1-a^2}-n^2\sin^2 n\eta\left(\sin^2\eta+\frac{1}{1-a^2}\right)-\frac{\sin 2n\eta\sin 2\eta}{2}n-\sin^2 n\eta(\sin^2\eta-2)\right)\mathrm{d}\eta\\&=8n^2(n^2-1)\frac{(4n^2-7)(n^2-1)+a^2(2n^2-7)}{3I_0^4(1-a^2)(9-40n^2+16n^4)}>0,\quad n\geq 2,\quad 0<a<1.\end{aligned}\tag{B.48}$$

Since $\tilde{\Upsilon}_S(n,a) > \Upsilon_S(n,a)$, it follows from (B.48) that

$$\Upsilon_S(n,a) > 0,\qquad n\geq 2,\qquad 0<a<1.\tag{B.49}$$

Although a particular form of M defined in (83) is used to obtain (B.49), similar arguments can be followed to show $\Upsilon_S(n,a) > 0$ for any other mollifier M satisfying (40).

B.6.3. $\Upsilon_I(n,a) > 0$

Substituting the $(J_1,\cdots,J_5)$ and $(K_1,\cdots,K_5)$ from (B.28) and (B.29) in $\Upsilon_I(n,a)$ defined in (B.36)$_3$ gives

$$\begin{aligned}\Upsilon_I(n,a)=&\frac{n^4a^3}{4}\int_0^\pi\frac{2\cos^2\eta(1-a^2\cos^2\eta)}{(1-a^2)\sqrt[5]{1-a^2\cos^2\eta}}\mathrm{d}\eta\\&+\frac{n^2a^3}{4}\int_0^\pi\left(\frac{(\cos 2\eta\cos 2n\eta-4\cos^2\eta(1-a^2)-1-2a^2\cos 2n\eta\cos^2\eta)(1-a^2\cos^2\eta)-6a^2\cos^4\eta\sin^2 n\eta(1-a^2)}{\sqrt[5]{1-a^2\cos^2\eta}}\right)\mathrm{d}\eta\\&+\frac{na^3}{4}\int_0^\pi\frac{\sin 2\eta\sin 2n\eta}{\sqrt[5]{1-a^2\cos^2\eta}}(2-5a^2\cos^2\eta)\,\mathrm{d}\eta\\&+\frac{a^3}{4}\int_0^\pi\frac{2\cos 2\eta\cos^2 n\eta(1-a^2\cos^2\eta)+6a^2\sin^2\eta\cos^2\eta\cos^2 n\eta}{\sqrt[5]{1-a^2\cos^2\eta}}\mathrm{d}\eta.\end{aligned}\tag{B.50}$$

Next, consider the quantity

$$\begin{aligned}\tilde{\Upsilon}_I(n,a)=&\frac{n^4a^3}{4}\int_0^\pi\frac{2\cos^2\eta(1-a^2\cos^2\eta)}{1-a^2}\mathrm{d}\eta\\&+\frac{n^2a^3}{4}\int_0^\pi\left(\left(\cos 2\eta\cos 2n\eta-4\cos^2\eta-\frac{1+a^2\cos 2n\eta}{1-a^2}\right)(1-a^2\cos^2\eta)-6a^2\cos^4\eta\sin^2 n\eta\right)\mathrm{d}\eta\\&+\frac{na^3}{4}\int_0^\pi\sin 2\eta\sin 2n\eta(2-5a^2\cos^2\eta)\,\mathrm{d}\eta\\&+\frac{a^3}{4}\int_0^\pi(2\cos 2\eta\cos^2 n\eta(1-a^2\cos^2\eta)+6a^2\sin^2\eta\cos^2\eta\cos^2 n\eta)\,\mathrm{d}\eta,\end{aligned}\tag{B.51}$$

obtained by replacing $\sqrt[5]{1-a^2\cos^2\eta}$ by unity in the denominator of integrand on right-hand side of (B.50). A calculation then yields

$$\tilde{\Upsilon}_{\rm I}(n,a)=\frac{a^3(n^4(8-6a^2)-n^2(3a^4-23a^2+24)-11a^2(1-a^2))}{32(1-a^2)}. \tag{B.52}$$

The first and second derivatives of $\tilde{\Upsilon}_{\rm I}$ with respect to n are given by

$$\frac{d\tilde{\Upsilon}_{\rm I}}{dn}=\frac{a^3(2n^3(8-6a^2)-n(3a^4-23a^2+24))}{16(1-a^2)} \tag{B.53}$$

and

$$\frac{d^2\tilde{\Upsilon}_{\rm I}}{dn^2}=\frac{a^3(6n^2(8-6a^2)-(3a^4-23a^2+24))}{16(1-a^2)}. \tag{B.54}$$

Since $d^2\tilde{\Upsilon}_{\rm I}/dn^2>0$ for $n\geq 2$ and $0<a<1$, $d\tilde{\Upsilon}_{\rm I}/dn$ increases monotonically with n for $n>2$. Also,

$$\left.\frac{d\tilde{\Upsilon}_{\rm I}}{dn}\right|_{n=2}=\frac{a^3(40-25a^2-3a^4)}{2(1-a^2)}>0, \tag{B.55}$$

from which it follows that $d\tilde{\Upsilon}_{\rm I}/dn>0$ for all $n\geq 2$. Thus, $\tilde{\Upsilon}_{\rm I}(n,a)\geq\tilde{\Upsilon}_{\rm I}(2,a)$ for all $0<a<1$ $n\geq 2$. Next,

$$\tilde{\Upsilon}_{\rm I}(2,a)=\frac{a^3(32-15a^2-a^4)}{32(1-a^2)}>0,\qquad 0<a<1, \tag{B.56}$$

which implies that $\tilde{\Upsilon}_{\rm I}(2,a)>0$ for $0<a<1$. Since $\Upsilon_{\rm I}(n,a)>\tilde{\Upsilon}_{\rm I}(n,a)$, it follows from (B.56) that

$$\Upsilon_{\rm I}(n,a)>0. \tag{B.57}$$

Appendix C. Linear Bifurcation analysis

Differentiating $(B.13)_3$ twice yields and using the identities in (73) gives

$$\boldsymbol{v}_n''''=\Big(-a^2\psi_n''''+2\psi_n''+\frac{3\psi_n'}{a^2}\Big)\boldsymbol{e}+\frac{a^3\psi_n'''''}{\sqrt{1-a^2}}\boldsymbol{k}+\Big(-3a\psi_n''''-\frac{2\psi_n''}{a}+\frac{\psi_n}{a^3}\Big)\boldsymbol{k}\times\boldsymbol{e}. \tag{C.1}$$

On using the Fourier representation (78) of ψ_n in (B.13) and (C.1), the components of first three terms on the left-hand side of the linearized equilibrium equations (100) in the direction $\boldsymbol{e}$, $\boldsymbol{k}$, and $\boldsymbol{k}\times\boldsymbol{e}$ can be written as

$$\left.\begin{aligned}(\boldsymbol{v}_n''''+\lambda\boldsymbol{v}_n''+\Lambda\boldsymbol{v}_n)\cdot\boldsymbol{e}&=\Big(-\frac{(n^2-1)(n^2+3)}{a^2}+\lambda(n^2-1)-\Lambda a^2\Big)\psi_n',\\(\boldsymbol{v}_n''''+\lambda\boldsymbol{v}_n''+\Lambda\boldsymbol{v}_n)\cdot\boldsymbol{k}&=\frac{1}{\sqrt{1-a^2}}\Big(\frac{n^4}{a}-\lambda an^2+\Lambda a^3\Big)\psi_n',\\(\boldsymbol{v}_n''''+\lambda\boldsymbol{v}_n''+\Lambda\boldsymbol{v}_n)\cdot\boldsymbol{k}\times\boldsymbol{e}&=\Big(\frac{-3n^4+2n^2+1+\lambda a^2(n^2-1)}{a^3}+a\Lambda\Big)\psi_n.\end{aligned}\right\} \tag{C.2}$$

The terms $\tilde{\boldsymbol{\vartheta}}[\boldsymbol{n}_0,\boldsymbol{n}_0](\boldsymbol{v}_n,\boldsymbol{v}_n)$ and $\boldsymbol{\vartheta}[\boldsymbol{n}_0,\boldsymbol{K}\boldsymbol{n}_0](\boldsymbol{v}_n,-\boldsymbol{K}\boldsymbol{v}_n)$ on the right-hand side of (100) in the terms of ψ_n and its arclength derivatives are provided in (B.22) and (B.27), respectively.

Resolving the linearized equation (100) along $\boldsymbol{e}$, $\boldsymbol{k}$, and $\boldsymbol{k}\times\boldsymbol{e}$, substituting (C.2), (B.22), and (B.27) in the resulting equations, and substituting the Fourier expansions for ψ_n, ω_n, and Ω_n, provided in (78), $(99)_1$, and $(98)_2$, respectively, yields a system of six linear equations for the unknown amplitudes c_n, d_n, p_n, q_n, u_n, and v_n. That system can be written as

$$\begin{bmatrix}0&\Theta_n&-\frac{1}{a}&0&a&0\\-\Theta_n&0&0&0&0&a\\0&\Pi_n&0&0&1-a^2&0\\-\Pi_n&0&0&0&0&1-a^2\\\Psi_n&0&0&\frac{n}{a}&0&0\\0&\Psi_n&-\frac{n}{a}&0&0&0\end{bmatrix}\begin{bmatrix}c_n\\d_n\\p_n\\q_n\\u_n\\v_n\end{bmatrix}=\begin{bmatrix}0\\0\\0\\0\\0\\0\end{bmatrix}, \tag{C.3}$$

where, recalling the definitions (B.23), (B.28), and (B.29) of $(I_1,\dots,I_5)$, $(J_1,\dots,J_5)$, and $(K_1,\dots,K_5)$, Θ_n, Π_n, and Ψ_n are given by

$$\left.\begin{aligned}
\Theta_n &= -\frac{n(n^2-1)(n^2+2)}{a^3} - \frac{\zeta n}{4a}\left(2n^2I_5 + I_1 + I_3 - I_4 + I_5 - \frac{I_2}{n}\right)\\
&\quad + \frac{n\chi a^2}{4}\left(2n^2J_5 + J_3 - J_1 - 2J_5 + J_4/n + 6a^2\left(K_2 - \frac{K_3}{2n}\right)\right),\\
\Pi_n &= \frac{n^3(n^2-1)}{a^2} + \frac{\zeta n}{4}(2n^2I_5 + I_3 - I_4) + \frac{n\chi a^3}{4}\left(J_1 + J_2 - 2n^2J_5 + 6(1-a^2)\left(K_1 - \frac{K_3+K_4}{2n}\right)\right),\\
\Psi_n &= -\frac{3n^2(n^2-1)}{a^3} - \frac{\zeta}{4a}(2n^2I_5 + nI_2 + I_5 + 2I_3 - 2I_4 - I_1)\\
&\quad + \frac{\chi a^2}{4}(2n^2J_5 - n(J_4 + 3a^2K_4) + J_1 - J_3 - 2J_5 + 6a^2(K_5 - K_2)).
\end{aligned}\right\} \tag{C.4}$$

Equating determinant of the coefficient matrix of the system (C.3) to zero yields

$$\Psi_n - n\Theta_n + \frac{an\Pi_n}{1-a^2} = 0. \tag{C.5}$$

On using the definition of Θ_n, Π_n, and Ψ_n presented in (C.4) and the definition (B.35) of $\alpha_n(a)$ and $\beta_n(a)$ for each $n \geq 2$, it can be shown that (C.5) is equivalent

$$\chi = \alpha_n(a)\zeta + \beta_n(a), \tag{C.6}$$

which is the equality condition in the stability condition (B.34).

References

Arroyo, J., Garay, O., Mencıa, J., 2003. Closed generalized elastic curves in $s^2(1)$. J. Geom. Phys. 48, 339–353.
Arroyo, J., Garay, O., Mencıa, J., 2004. Extremals of curvature energy actions on spherical closed curves. J. Geom. Phys. 51, 101–125.
Arroyo, J., Garay, O., Mencía, J., 2006. Elastic circles in 2-spheres. J. Phys. A Math. Gen. 39, 2307..
Arroyo, J., Garay, O.J., Mencía, J., 2010. Quadratic curvature energies in the 2-sphere. Bull. Aus. Math. Soc. 81, 496–506.
Biot, M.A., 1963. Surface instability of rubber in compression. Appl. Scientif. Res. Section A 12, 168–182.
Bischofs, I.B., Schmidt, S.S., Schwarz, U.S., 2009. Effect of adhesion geometry and rigidity on cellular force distributions. Phys. Rev. Lett. 103, 048101.
Biton, Y.Y., Coleman, B.D., Swigon, D., 2007. On bifurcations of equilibria of intrinsically curved, electrically charged, rod-like structures that model DNA molecules in solution. J. Elast. 87, 187–210.
Cao, Y., Hutchinson, J.W., 2011. From wrinkles to creases in elastomers: the instability and imperfection-sensitivity of wrinkling. Proc. R. Soc. A: Math. Phys. Eng. Sci. 468, 94–115.
Caruso, F., Caruso, R.A., Möhwald, H., 1998. Nanoengineering of inorganic and hybrid hollow spheres by colloidal templating. Science 282, 1111–1114.
Chen, Y.C., 2001. Singularity Theory and Nonlinear Bifurcation Analysis. In: London Mathematical Society Lecture Note Series. Cambridge University Press, pp. 305–344.
Chen, Y.c., Yang, S., Wheeler, L., 2018. Surface instability of elastic half-spaces by using the energy method. Proc. R. Soc. A: Math. Phys. Eng. Sci. 474, 20170854.
Cherstvy, A., Winkler, R., 2011. Polyelectrolyte adsorption onto oppositely charged interfaces: unified approach for plane, cylinder, and sphere. Phys. Chem. Chem. Phys. 13, 11686–11693.
Cherstvy, A.G., Winkler, R.G., 2004. Complexation of semiflexible chains with oppositely charged cylinder. J. Chem. Phys. 120, 9394–9400.
Cherstvy, A.G., Winkler, R.G., 2005. Simple model for overcharging of a sphere by a wrapped oppositely charged asymmetrically neutralized polyelectrolyte: possible effects of helical charge distribution. J. Phys. Chem. B 109, 2962–2969.
Ciftja, O., Paredes, G., Griffin, M., 2014. Mathematical expressions for a system of two identical uniformly charged rods. Phys. Scr. 89, 115803.
Decher, G., 1997. Fuzzy nanoassemblies: toward layered polymeric multicomposites. Science 277, 1232–1237.
Decher, G., Hong, J., 1991. Buildup of ultrathin multilayer films by a self-assembly process: II. consecutively alternating adsorption of anionic and cationic polyelectrolytes on charged surfaces. Berichte der Bunsengesellschaft für physikalische Chemie 95, 1430–1434.
Decher, G., Hong, J., Schmitt, J., 1992. Buildup of ultrathin multilayer films by a self-assembly process: III. consecutively alternating adsorption of anionic and cationic polyelectrolytes on charged surfaces. Thin Solid Films 210, 831–835.
Decher, G., Lehr, B., Lowack, K., Lvov, Y., Schmitt, J., 1994. New nanocomposite films for biosensors: layer-by-layer adsorbed films of polyelectrolytes, proteins or DNA. Biosens. Bioelectron. 9, 677–684.
Dobrynin, A.V., Rubinstein, M., 2005. Theory of polyelectrolytes in solutions and at surfaces. Prog. Polym. Sci. 30, 1049–1118.
Ericksen, J., 1966. A thermo-kinetic view of elastic stability theory. Int. J. Solids Struct. 2, 573–580.
Fraden, S., Maret, G., Caspar, D., 1993. Angular correlations and the isotropic-nematic phase transition in suspensions of tobacco mosaic virus. Phys. Rev. E 48, 2816.
Fraden, S., Maret, G., Caspar, D., Meyer, R.B., 1989. Isotropic-nematic phase transition and angular correlations in isotropic suspensions of tobacco mosaic virus. Phys. Rev. Lett. 63, 2068.
Fukuhara, S., 1988. Energy of a Knot. In: Matsumoto, Y., Mizutani, T., Morita, S. (Eds.), A Fête of Topology. Academic Press, pp. pp.443–451.
Gittins, D.I., Caruso, F., 2001. Tailoring the polyelectrolyte coating of metal nanoparticles. J. Phys. Chem. B 105, 6846–6852.
von Goeler, F., Muthukumar, M., 1994. Adsorption of polyelectrolytes onto curved surfaces. J. Chem. Phys. 100, 7796–7803.
Golubitsky, M., Stewart, I., Schaeffer, D.G., 2012. Singularities and Groups in Bifurcation Theory, 2. Springer Science & Business Media.
Graf, H., Löwen, H., 1999. Phase diagram of tobacco mosaic virus solutions. Phys. Rev. E 59, 1932.
Gursky, O., 2013. Crystal structure of △(185–243) apoa-i suggests a mechanistic framework for the protein adaptation to the changing lipid load in good cholesterol: from flatland to sphereland via double belt, belt buckle, double hairpin and trefoil/tetrafoil. J. Mol. Biol. 425, 1–16.
Guven, J., Valencia, D.M., Vázquez-Montejo, P., 2014. Environmental bias and elastic curves on surfaces. J. Phys. A: Math. Theor. 47. 355–201.
Guven, J., Vázquez-Montejo, P., 2012. Confinement of semiflexible polymers. Phys. Rev. E 85, 026603.
Hermo, R., Mier, C., Mazzotta, M., Tsuji, M., Kimura, S., Gugliucci, A., 2005. Circulating levels of nitrated apolipoprotein a-i are increased in type 2 diabetic patients. Clin. Chem. Lab. Med. 43, 601–606.
Hoang, A., Murphy, A., Coughlan, M., Thomas, M., Forbes, J., O'brien, R., Cooper, M., Chin-Dusting, J., Sviridov, D., 2007. Advanced glycation of apolipoprotein a-i impairs its anti-atherogenic properties. Diabetologia 50, 1770–1779.

Hoffman, K.A., Manning, R.S., 2009. An extended conjugate point theory with application to the stability of planar buckling of an elastic rod subject to a repulsive self-potential. SIAM J. Math. Anal. 41, 465–494.
Hoogeveen, N.G., Cohen Stuart, M.A., Fleer, G.J., Böhmer, M.R., 1996. Formation and stability of multilayers of polyelectrolytes. Langmuir 12, 3675–3681.
Huang, R., Silva, R.G.D., Jerome, W.G., Kontush, A., Chapman, M.J., Curtiss, L.K., Hodges, T.J., Davidson, W.S., 2011. Apolipoprotein a-i structural organization in high-density lipoproteins isolated from human plasma. Nat. Struct. Mol. Biol. 18, 416–422.
Joan, B., Lomonaco, Jr.S.J., 1983. Electrostatic knots. Talk presented at Low Dimensional topology at the joint AMS/CMS meeting held in Vancouver, British Columbia, Canada..
Karush, W., 1939. Minima of functions of several variables with inequalities as side constraints. M.Sc. Dissertation. Department of Mathematics, University of Chicago.
Khovidhunkit, W., Kim, M.S., Memon, R.A., Shigenaga, J.K., Moser, A.H., Feingold, K.R., Grunfeld, C., 2004. Effects of infection and inflammation on lipid and lipoprotein metabolism: mechanisms and consequences to the host. J. Lipid Res. 45, 1169–1196.
Khrapunov, S., Dragan, A., Sivolob, A., Zagariya, A., 1997. Mechanisms of stabilizing nucleosome structure. study of dissociation of histone octamer from DNA. Biochimica et Biophysica Acta (BBA)-Gene Structure and Expression 1351, 213–222.
Koiter, W. T., 1970. Over de stabiliteit van het elastisch evenwicht. Thesis, Technische Hooge School, Delft, The Netherlands. (English translation: National Aeronautics and Space Administration TFF-10, 833, 1967; Technical report AFFDL-TR-705, 1970.).
Kong, C., Muthukumar, M., 1998. Monte carlo study of adsorption of a polyelectrolyte onto charged surfaces. J. Chem. Phys. 109, 1522–1527.
Kontush, A., Chapman, M.J., 2008. Why is HDL functionally deficient in type 2 diabetes? Curr. Diab. Rep. 8, 51–59.
Kuhn, H.W., Tucker, A.W., 1951. Nonlinear Programming. In: In proceedings of the Second Berkeley Symposium on Mathematical Statistics and Probability. University of California Press, Berkeley, California, pp. 481–492. https://projecteuclid.org/euclid.bsmsp/1200500249.
Kusner, R.B., Sullivan, J.M., 1994. Möbius energies for knots and links, surfaces and submainfolds. Geometric topology (Athens, GA, 1993) 570–604. AMS/IP Stud. Adv. Math., 2.1, Amer. Math. Soc., Providence, RI.
Langer, J., Singer, D.A., 1984. The total squared curvature of closed curves. J. Diff. Geom. 20, 1–22.
Luger, K., Mäder, A.W., Richmond, R.K., Sargent, D.F., Richmond, T.J., 1997. Crystal structure of the nucleosome core particle at 2.8 Å resolution. Nature 389, 251–260.
Mei, X., Atkinson, D., 2011. Crystal structure of c-terminal truncated apolipoprotein a-i reveals the assembly of high density lipoprotein (HDL) by dimerization. J. Biol. Chem. 286, 38570–38582.
Messina, R., 2003. Adsorption of oppositely charged polyelectrolytes onto a charged rod. J. Chem. Phys. 119, 8133–8139.
Messina, R., 2009. Electrostatics in soft matter. J. Phys.: Condens. Matter 21, 113102.
Messina, R., Holm, C., Kremer, K., 2003. Polyelectrolyte multilayering on a charged sphere. Langmuir 19, 4473–4482.
Messina, R., Holm, C., Kremer, K., 2004. Polyelectrolyte adsorption and multilayering on charged colloidal particles. J. Polym. Sci., Part B: Polym. Phys. 42, 3557–3570.
Nelson, D.L., Lehninger, A.L., Cox, M.M., 2008. Lehninger principles of biochemistry, seventh ed. Worth Publishers, New York.
Netz, R.R., Andelman, D., 2003. Neutral and charged polymers at interfaces. Phys. Rep. 380, 1–95.
O'Brien, K.D., Chait, A., 2006. Serum amyloid a: the "other" inflammatory protein. Curr. Atheroscler. Rep. 8, 62–68.
O'Hara, J., 1991. Energy of a knot. Topology 30, 241–247.
O'Hara, J., 1992. Family of energy functionals of knots. Topol. Appl. 48, 147–161.
O'Hara, J., 1994. Energy functionals of knots II. Topol. Appl. 56, 45–61.
Scheele, R.B., Lauffer, M.A., 1967. Acid-base titrations of tobacco mosaic virus and tobacco mosaic virus protein. Biochemistry 6, 3076–3081.
Schiessel, H., 2003. The physics of chromatin. J. Phys.: Condens. Matter 15, R699.
Silva, R.G.D., Huang, R., Morris, J., Fang, J., Gracheva, E.O., Ren, G., Kontush, A., Jerome, W.G., Rye, K.A., Davidson, W.S., 2008. Structure of apolipoprotein a-i in spherical high density lipoproteins of different sizes. Proc. Natl. Acad. Sci. U.S.A. 105, 12176–12181.
Silva, R.G.D., Schneeweis, L.A., Krishnan, S.C., Zhang, X., Axelsen, P.H., Davidson, W.S., 2007. The structure of apolipoprotein a-II in discoidal high density lipoproteins. J. Biol. Chem. 282, 9713–9721.
Sukhorukov, G.B., Donath, E., Davis, S., Lichtenfeld, H., Caruso, F., Popov, V.I., Möhwald, H., 1998. Stepwise polyelectrolyte assembly on particle surfaces: a novel approach to colloid design. Polym. Adv. Technol. 9, 759–767.
Timoshenko, S.P., Gere, J.M., 1962. Theory of Elastic Stability, second ed. McGraw-Hill, New York.
Weyerich, B., D'Aguanno, B., Canessa, E., Klein, R., 1990. Structure and dynamics of suspensions of charged rod-like particles. Faraday Discuss Chem. Soc. 90, 245–259.